

CRANFIELD UNIVERSITY

F KRAL

MAPPING SEDIMENT PROPERTIES IN THE MISSISSIPPI RIVER  
DELTA

SCHOOL OF APPLIED SCIENCES  
Geographical Information Management

MSc THESIS  
Academic year: 2009-10

Supervisor: Dr R. Corstanje  
September 2010

CRANFIELD UNIVERSITY

SCHOOL OF APPLIED SCIENCES  
Geographical Information Management

MSc THESIS

Academic Year 2009-2010

F KRAL

Mapping sediment properties in the Mississippi River Delta

Supervisor: Dr R Corstanje

September 2010

This thesis is submitted in partial fulfilment of the requirements  
for the degree of Master of Science

© Cranfield University 2010. All rights reserved. No part of this  
publication may be reproduced without the written permission of the  
copyright owner.

## **Abstract**

Coastal zone of Louisiana, USA, is experiencing high rate of wetland loss since the Mississippi River was isolated from the delta by man made levees. Freshwater diversions reintroduce the river water into coastal marshes in order to balance salinity levels and provide sediments and nutrients for marsh accretion. This study presents the geostatistical analysis of soil moisture (MOIST), bulk density (BD), pH, organic matter content (OM), total phosphorus (TP), total nitrogen (TN), and total carbon (TC) in 0–10 cm and 10–20 cm soil depth in the ponding area of Davis Pond Freshwater Diversion that has been receiving Mississippi River water since 2002. Cores from 139 locations visited in 2007 were analysed by members of the Department of Oceanography and Coastal Sciences, Louisiana State University. In 0–10 cm soil depth, TN, TC, and OM had similar spatial properties and were closely related to BD. Practical range of exponential variogram models fitted to TN, TC, and OM was approximately 3300 m, exponential model of BD had range around 2700 m. Close relationship of these variables is explained by the role of vegetation in marsh ecosystems. Spatial autocorrelation of both TP and pH was weak and interpolated values were associated with high uncertainty. Also relationship between TP or pH and any other variable was weak. Spherical variogram model with 1400 m range was fitted to TP and we infer that processes driving dynamics of TP in Davis Pond act on finer spatial scale than processes affecting TN, TC, and OM. TP was highly variable even at distances shorter than the minimum sampling interval (100 m). Spherical variogram model fitted to pH with 4500 m range indicated that pH was autocorrelated over the longest distances. Maps of soil properties in 0–10 cm soil depth were produced using kriging, but no spatial autocorrelation was detected in 10–20 cm soil depth.

## **Acknowledgements**

The author would like to thank Dr Ron Corstanje from Cranfield University for diligent supervision of this thesis, Dr John R. White and his team from the Department of Oceanography and Coastal Sciences, Louisiana State University, for providing the data set with supplementary material and explanations, Mr Fabio Veronesi for helpful consultations, Dr Ben Marchant for useful recommendations, and at last, but not least, the members of the Department of Water Resources and Environmental Modelling, Czech University of Life Sciences Prague, who indirectly contributed to realization of this thesis.

## List of Contents

<b>Abstract</b> .....	i
<b>Acknowledgements</b> .....	i
<b>List of Contents</b> .....	ii
<b>List of Figures</b> .....	iii
<b>List of Tables</b> .....	v
<b>Notation and Acronyms</b> .....	vi
<i>Notation</i> .....	vi
<i>Acronyms</i> .....	viii
<b>Abstract</b> .....	1
<b>Keywords</b> .....	1
<b>1 Introduction</b> .....	2
<b>2 Literature Review</b> .....	2
2.1 <i>Broad View of the Mississippi River Delta</i> .....	2
2.2 <i>Freshwater Wetlands Biogeochemistry and its Relation to the Measured Variables</i> .....	3
2.3 <i>Geostatistics</i> .....	5
2.3.1 <i>General background</i> .....	5
2.3.2 <i>Geostatistical work flow</i> .....	7
2.3.3 <i>Linear model of coregionalization</i> .....	9
2.4 <i>Moving Window Analysis</i> .....	10
<b>3 Materials and Methods</b> .....	11
3.1 <i>Study Area</i> .....	11
3.2 <i>Sampling and Soil Analysis</i> .....	12
3.3 <i>Statistical Analysis</i> .....	13
<b>4 Results</b> .....	16
<b>5 Discussion</b> .....	26
<b>6 Conclusions</b> .....	30
<b>7 Acknowledgements</b> .....	31
<b>References</b> .....	32
<b>Appendix A Explanatory Data Analysis</b> .....	37
<b>Appendix B Variograms of the Original Variables</b> .....	46
<b>Appendix C Correlation Surfaces</b> .....	49
<b>Appendix D Derivation of Regional Stocks</b> .....	51
<b>Appendix E Indicator Variograms of Variables in the Lower Layer</b> .....	53
<b>Appendix F Mapping Moisture According to Density</b> .....	55
<b>Appendix G R Code</b> .....	56
<b>Appendix H Maps</b> .....	83

## List of Figures

<i>Fig. 1. Example of experimental variogram with fitted spherical model and main features identified: sill, partial sill, range, and nugget (Burrough and McDonnell, 2000, adjusted).....</i>	<i>6</i>
<i>Fig. 2. Daily discharge of Davis Pond Freshwater Diversion before and during the time of soil sampling (Oct 2006 - Aug 2007) (USGS, 2010).....</i>	<i>12</i>
<i>Fig. 3. Overview map of the study area, Davis Pond, Louisiana, USA.....</i>	<i>12</i>
<i>Fig. 4. Experimental autovariograms (dots) and fitted variogram models (lines) of soil properties in 0–10 cm soil depth; (a) total nitrogen, (b) total carbon, (c) bulk density transformed by box-cox transformation with power –0.5, (d) pH, (e) organic matter content, (f) total phosphorus. Model of pH was obtained by residual maximum likelihood method.....</i>	<i>18</i>
<i>Fig. 5. Maps of (a) total carbon (TC), (b) pH, (c) total phosphorus (TP), and (d) bulk density (BD) in 0–10 cm soil depth and associated estimated standard deviations. Gray line is Davis Pond boundary, black crosses are sampling locations.....</i>	<i>19</i>
<i>Fig. 6. Experimental cross-variograms (dots) of pH, bulk density transformed by box-cox transformation with power –0.5 (bxBD), organic matter content (OM), total phosphorus (TP), total nitrogen (TN), and total carbon (TC) in 0–10 cm soil depth and fitted linear model of coregionalization with exponential model of 1100 m range (solid line). Proximity of the exponential model to the hull of perfect correlation (dashed lines) indicates strength of spatial relationship between the involved soil properties: (a) pH and TP, (b) OM and TP, (c) pH and OM, (d) pH and TN, (e) OM and TN, (f) TP and TN, (g) TC and bxBD, (h) pH and TC, (i) OM and TC, (j) TP and TC, (k) TN and TC, (l) pH and bxBD, (m) OM and bxBD, (n) TP and bxBD, (o) TN and bxBD.....</i>	<i>20</i>
<i>Fig. 7. Experimental autovariograms (dots) of soil properties in 0–10 cm soil depth and fitted linear model of coregionalization with exponential model of 1100 m range (line); (a) pH, (b) organic matter content, (c) total phosphorus, (d) total nitrogen, (e) total carbon, (f) bulk density transformed by box-cox transformation with power –0.5.....</i>	<i>21</i>
<i>Fig. 8. Codispersion coefficients (dots) of pH, bulk density transformed by box-cox transformation with power –0.5 (bxBD), organic matter content (OM), total phosphorus (TP), total nitrogen (TN), and total carbon (TC) in 0–10 cm soil depth for lag distances from 300 to 8000 m by 600 m. The dashed line is constant zero; (a) pH and TP, (b) OM and TP, (c) pH and OM, (d) pH and TN, (e) OM and TN, (f) TP and TN, (g) TC and bxBD, (h) pH and TC, (i) OM and TC, (j) TP and TC, (k) TN and TC, (l) pH and bxBD, (m) OM and bxBD, (n) TP and bxBD, (o) TN and bxBD.....</i>	<i>24</i>
<i>Fig. 9. Moving window correlation surfaces of (a) total carbon and pH, and (b) total carbon and total phosphorus in 0–10 cm soil depth.....</i>	<i>25</i>
<i>Fig. 10. Concept of recommended extension of sampling design for future sampling in Davis Pond. Black circles represent the original points, black square is the newly added sampling point.....</i>	<i>30</i>
<i>Fig. A.1. Histograms of moisture (MOIST), bulk density (BD), bulk density transformed by box-cox transformation with power –0.5 (bxBD), pH (PH), organic matter content (OM), total phosphorus (TP), total nitrogen (TN), and total carbon (TC) in 0–10 cm ( _UP, a to h) and 10–20 cm ( _LW, i to o) soil depth with probability density function of normal distribution with mean and standard deviation of the sample superimposed.....</i>	<i>38</i>
<i>Fig. A.2. Normal distribution quantile-quantile plots of soil moisture (MOIST), bulk density (BD), bulk density transformed by box-cox transformation with power –0.5 (bxBD), pH (PH), organic matter content (OM), total phosphorus (TP), total nitrogen (TN), and total carbon (TC) in 0–10 cm ( _UP, a to h) and 10–20 cm ( _LW, i to o) soil depth.....</i>	<i>39</i>

<i>Fig. A.3 (1 of 4). Scatter-grams of soil moisture (MOIST), bulk density (BD), pH (PH), organic matter content (OM), total phosphorus (TP), total nitrogen (TN), and total carbon (TC) in 0–10 cm (_UP) and 10–20 cm (_LW) soil depth. The figure continues on the next page.....</i>	<i>42</i>
<i>Fig. B.1. Experimental variograms of (a) soil moisture, (b) bulk density, (c) pH, (d) organic matter content, (e) total phosphorus, (f) total nitrogen, and (g) total carbon in 0–10 cm soil depth constructed by method of moments (dots) and Hawkins and Cressie estimator (line). Breaks were 0, 200, 400, 500, 600, 1000 to 8000 by 400 m.....</i>	<i>46</i>
<i>Fig. B.2. Experimental variograms of (a) soil moisture, (b) bulk density, (c) pH, (d) organic matter content, (e) total phosphorus, (f) total nitrogen, and (g) total carbon in 10–20 cm soil depth constructed by method of moments (dots) and Hawkins and Cressie estimator (line). Breaks were 0, 200, 400, 500, 600, 1000 to 8000 by 400 m.....</i>	<i>47</i>
<i>Fig. B.3. Experimental variograms of total phosphorus (TP), total nitrogen (TN), and total carbon (TC) in 0–10 cm (UP, a to c) and 10–20 cm (LW, d to f) soil depth constructed by method of moments (dots) and Hawkins and Cressie estimator (line) using mass per volume units. Breaks were 0, 200, 400, 500, 600, 1000 to 8000 by 400 m.....</i>	<i>48</i>
<i>Fig. C.1. Correlation surfaces between organic matter content (OM), bulk density (BD), total carbon (TC), total phosphorus (TP), and total nitrogen (TN) in 0–10 cm soil depth (variables involved in each surface are separated by dot).....</i>	<i>49</i>
<i>Fig. C.2. Correlation surfaces between organic matter content (OM), bulk density (BD), total carbon (TC), total phosphorus (TP), total nitrogen (TN), and pH in 0–10 cm soil depth (variables involved in each surface are separated by dot).....</i>	<i>50</i>
<i>Fig. D.1. Block dimensions and schematic orientation (units are metres).....</i>	<i>51</i>
<i>Fig. E.1. Experimental indicator variograms for the variables in 10–20 cm soil depth. (a) pH, (b) moisture, (c) bulk density, (d) organic matter content, (e) total phosphorus, (f) total nitrogen, (g) total carbon. Breaks were a sequence from 0 to 4500 by 300.....</i>	<i>54</i>
<i>Fig. F.1. Regression line of Moisture = 0.99 – 0.78 Density, R2=0.98.....</i>	<i>55</i>

## List of Tables

<i>Table 1. Distribution of distances between sampling locations.....</i>	<i>13</i>
<i>Table 2. Variables measured at each sampling point, their units and naming convention.....</i>	<i>13</i>
<i>Table 3. Pearson's correlation coefficients between variables in 0–10 cm soil depth in Davis Pond. †.....</i>	<i>17</i>
<i>Table 4. Variogram models used for kriging of soil properties in 0–10 cm soil depth. †.....</i>	<i>18</i>
<i>Table 5. Parameters of linear model of coregionalization of soil properties in 0–10 cm soil depth. Model type is exponential with fixed range of 1100 m. †.....</i>	<i>22</i>
<i>Table 6. Structural codispersion coefficients of each structure and variable in the linear model of coregionalization.....</i>	<i>23</i>
<i>Table A.1. Summary statistics of soil properties obtained from 139 samples. †.....</i>	<i>37</i>
<i>Table A.2. Results of Shapiro-Wilk normality test. †.....</i>	<i>40</i>
<i>Table A.3. Correlation coefficients between soil properties. Lower triangle contains Pearson's product moment correlation coefficients, upper triangle contains Spearman's rank correlation coefficients. †.....</i>	<i>40</i>
<i>Table A.4. Coefficients of determination of polynomial trend surfaces fitted to the original data.....</i>	<i>41</i>
<i>Table D.1. Estimated elements stocks in Davis Pond. †.....</i>	<i>52</i>
<i>Table F.1. Results of linear regression between moisture and bulk density in 0–10 cm soil depth. R<sup>2</sup> = 0.98, F-statistic: 7882 on 1 and 137 degrees of freedom. †.....</i>	<i>55</i>
<i>Table G.1. R scripts used during the analysis.....</i>	<i>56</i>

## Notation and Acronyms

### Notation

$ \cdot $	Absolute value
$\hat{\cdot}$	Estimated value
$(\cdot)^T$	Matrix transposition
$E[\cdot]$	Expectation
$\mu$	Mean
$\text{Var}[\cdot], \sigma^2$	Variance
$n$	Number of points used for estimation, generally number of elements in a set
$\mathbf{x}$	Location vector
$\mathbf{x}_i$	Sampled location
$\mathbf{x}_0$	Unsampled location
$Z$	Stochastic variable
$Z(\mathbf{x})$	Stochastic variable at location $\mathbf{x}$
$z(\mathbf{x}_i)$	Observed value of $Z$ at sampled location $\mathbf{x}_i$
$\hat{Z}(\mathbf{x}_0)$	Estimated value of $Z$ at unsampled location $\mathbf{x}_0$
$\hat{\sigma}_{KR}^2(\mathbf{x})$	Kriging variance at location $\mathbf{x}$
$W$	Set of stochastic variables $\{Z_w, w=1, 2, \dots, t\}$
$Z_w, Z_u, Z_v$	Stochastic variables from a set $W$
$z_u(\mathbf{x}_i), z_v(\mathbf{x}_i)$	Observed values of $Z_u$ and $Z_v$ at location $\mathbf{x}_i$
$\mu_w$	Mean of $Z_w \in W$
$m(\mathbf{x})$	Structural (deterministic) component of $Z(\mathbf{x})$
$\epsilon(\mathbf{x})$	Stochastic spatially autocorrelated component of $Z(\mathbf{x})$
$\epsilon'(\mathbf{x})$	Stochastic spatially uncorrelated component of $Z(\mathbf{x})$
$\mathbf{h},  \mathbf{h} $	Lag (separating) vector, lag (separating) distance
$\text{Cov}, \text{Cov}(\mathbf{h})$	Covariance, autocovariance function
$N(\mathbf{h})$	Number of sampling points separated by $\mathbf{h}$
$\gamma, \gamma(\mathbf{h})$	Semivariance (referred also as variance, semivariogram, or variogram value)
$\hat{\gamma}, \hat{\gamma}(\mathbf{h})$	Semivariance estimated from sampling points
$\gamma_{ij}$	Semivariance for vector separating locations $\mathbf{x}_i$ and $\mathbf{x}_j$ ; $\gamma_{ij} = \gamma(\mathbf{x}_i - \mathbf{x}_j)$



$\gamma_{uv}(\mathbf{h})$	Cross-semivariance between $Z_u$ and $Z_v$
$\hat{\gamma}_{uv}(\mathbf{h})$	Estimated cross-semivariance between $Z_u$ and $Z_v$
$\gamma_{\text{exp}}( \mathbf{h} )$	Exponential variogram model for isotropic case
$\gamma_{\text{sph}}( \mathbf{h} )$	Spherical variogram model for isotropic case
$a$	Range of a variogram model
$c$	Sill of a variogram model
$r$	Distance parameter for the exponential variogram model
$\exp(\cdot)$	Exponential function
$\lambda_i$	Kriging weight for $z(\mathbf{x}_i)$
$\Phi$	Lagrange multiplier
$s$	Index of the variogram structure included in the linear model of coregionalization
$L$	Number of variogram structures included in the linear model of coregionalization minus 1
$t$	Number of variables included in the linear model of coregionalization
$Y_j^s(\mathbf{x})$	Stochastic variable with standard normal distribution corresponding to the $j$ -th variable in $W$ and the $s$ -th variogram structure in the linear model of coregionalization
$a_{wj}^s$	Coefficient of linear combination corresponding to the combination of the $w$ -th and the $j$ -th variable in $W$ and the $s$ -th variogram structure in the linear model of coregionalization
$\delta_{pq}$	Kronecker delta being 1 for $p=q$ and 0 otherwise
$g_s(\mathbf{h})$	The $s$ -th elementary variogram model included in the linear model of coregionalization
$b_{uv}^s$	Element of the $s$ -th coregionalization matrix at position $(u,v)$
$\hat{\gamma}_{CH}(\mathbf{h})$	Hawkins and Cressie variogram estimator
$\hat{\kappa}_{uv}(\mathbf{h})$	Codispersion coefficient between variables $Z_u$ and $Z_v$ for lag vector $\mathbf{h}$
$\rho_{uv}^s$	Structural codispersion coefficient between variables $Z_u$ and $Z_v$ for lag vector $\mathbf{h}$ and the $s$ -th variogram structure; specifically for this study, $s=0$ denotes nugget effect and $s=1$ denotes exponential model with 1100 m range
$\text{hull}[\gamma_{uv}(\mathbf{h})]$	Hull of perfect correlation of cross-variogram of $Z_u$ and $Z_v$
$\rho$	Correlation coefficient
$\rho_w$	Moving window correlation coefficient

### *Acronyms*

BD	Bulk density
BD_LW	Bulk density in 10–20 cm soil depth
BD_UP	Bulk density in 0–10 cm soil depth
bxBD_UP	Bulk density in 0–10 cm soil depth transformed by box-cox transformation with power $-0.5$ .
C	Carbon
LMCR	Linear model of coregionalization
LW	Lower layer, i.e., 10–20 cm soil depth
ML	Maximum likelihood
MOIST	Moisture
MOIST_LW	Moisture in 10–20 cm soil depth
MOIST_UP	Moisture in 0–10 cm soil depth
MSDR	Mean squared deviation ratio
N	Nitrogen
OM	Organic matter content
OM_LW	Organic matter content in 10–20 cm soil depth
OM_UP	Organic matter content in 0–10 cm soil depth
P	Phosphorus
PH	pH
PH_LW	pH in 10–20 cm soil depth
PH_UP	pH in 0–10 cm soil depth
REML	Residual maximum likelihood
SSA	Spatial simulated annealing
TC	Total carbon
TC_LW	Total carbon in 10–20 cm soil depth
TC_UP	Total carbon in 0–10 cm soil depth
TN	Total nitrogen
TN_LW	Total nitrogen in 10–20 cm soil depth
TN_UP	Total nitrogen in 0–10 cm soil depth
TP	Total phosphorus
TP_LW	Total phosphorus in 10–20 cm soil depth
TP_UP	Total phosphorus in 0–10 cm soil depth
UP	Upper layer, i.e., 0–10 cm soil depth

This thesis has been prepared in the format used for scientific papers appearing in journals published by American Society of Agronomy, Crop Science Society of America, and Soil Science Society of America. Additional information is available in the appendices and the paper has extended literature review.

## Mapping Sediment Properties in the Mississippi River Delta

F. Kral<sup>a,b,c</sup> and R. Corstanje<sup>a</sup>

<sup>a</sup> Natural Resources Department, School of Applied Sciences, Cranfield University, College Road, Cranfield, Bedfordshire, MK43 0AL, UK.

<sup>b</sup> Faculty of Environmental Sciences, Czech University of Life Sciences Prague, Kamýcká 129, Prague, 165 21, Czech Republic

<sup>c</sup> Corresponding author (filipking@gmail.com)

### Abstract

Coastal zone of Louisiana, USA, is experiencing high rate of wetland loss since the Mississippi River was isolated from the delta by man made levees. Freshwater diversions reintroduce the river water into coastal marshes in order to balance salinity levels and provide sediments and nutrients for marsh accretion. This study presents the geostatistical analysis of soil moisture (MOIST), bulk density (BD), pH, organic matter content (OM), total phosphorus (TP), total nitrogen (TN), and total carbon (TC) in 0–10 cm and 10–20 cm soil depth in the ponding area of Davis Pond Freshwater Diversion that has been receiving Mississippi River water since 2002. Cores from 139 locations visited in 2007 were analysed by members of the Department of Oceanography and Coastal Sciences, Louisiana State University. In 0–10 cm soil depth, TN, TC, and OM had similar spatial properties and were closely related to BD. Practical range of exponential variogram models fitted to TN, TC, and OM was approximately 3300 m, exponential model of BD had range around 2700 m. Close relationship of these variables is explained by the role of vegetation in marsh ecosystems. Spatial autocorrelation of both TP and pH was weak and interpolated values were associated with high uncertainty. Also relationship between TP or pH and any other variable was weak. Spherical variogram model with 1400 m range was fitted to TP and we infer that processes driving dynamics of TP in Davis Pond act on finer spatial scale than processes affecting TN, TC, and OM. TP was highly variable even at distances shorter than the minimum sampling interval (100 m). Spherical variogram model fitted to pH with 4500 m range indicated that pH was autocorrelated over the longest distances. Maps of soil properties in 0–10 cm soil depth were produced using kriging, but no spatial autocorrelation was detected in 10–20 cm soil depth.

### Keywords

geostatistics, Mississippi Delta, Davis Pond, total phosphorus, total nitrogen, total carbon

## **1 Introduction**

Marshes in southern Louisiana were isolated from the Mississippi River by man made levees in the 20th century. This isolation prevented spring time river water coming into coastal marshes, which resulted in increasing salinity, ecosystem destabilization and consequently rapid increase in wetland loss rate. There are numerous restoration projects that are currently taking place in southern Louisiana to slow down or even reverse the process of marsh deterioration. One of the main ideas behind this effort is to reintroduce fresh river water into the ecosystem to balance salinity and re-establish marsh accretionary processes.

This study focuses on the ponding area of Davis Pond Freshwater Diversion which has been receiving fresh Mississippi River water since 2002. The aim of this study is to describe spatial distribution and relationships of several key variables in this freshwater marsh. Soil sampling was conducted in 2007 by the Department of Oceanography and Coastal Sciences, Louisiana State University. Information about moisture, bulk density, pH, total phosphorus (TP), organic matter content, total nitrogen (TN), and total carbon (TC) from 139 sampling points were made available by Department of Oceanography and Coastal Sciences, Louisiana State University. The specific objectives of this study were to 1) investigate univariate properties of each variable 2) construct experimental variograms and fit variogram models if possible, 3) produce maps showing spatial distribution of the variables, 4) describe the spatial relationships between the variables using geostatistical methods and moving window statistics.

## **2 Literature Review**

### *2.1 Broad View of the Mississippi River Delta*

Mississippi River Delta undergoes substantial changes that affect both the ecological and economic stability of Louisiana, Texas and Mississippi states and consequently the whole United States. The region (both inland and offshore) is important for fisheries, oil and gas supplies, and other resources (Turner and Cahoon, 1987; LNDR, 2005; Lindquist and Summer, 2007; LNDR, 2009). Although land loss and land gain permanently occur during natural delta formation, the land loss rate in Louisiana is high and extensive landscape changes are documented in many studies (Turner and Cahoon, 1987; Evers et al., 1992; USGS, 2003; Barras, 2006; Lindquist and Summer, 2007). Change of coastal marshes into open water is of the major concern. The land loss rate increased rapidly between 1930's and late 1970's, up to about  $104 \text{ km}^2 \text{ year}^{-1}$ , then decreased and was stabilized in 1990's at the average annual rate of  $62 \text{ km}^2 \text{ year}^{-1}$  (Lindquist and Summer, 2007). The increase in the rate of environmental changes in the last century is attributed mainly to anthropogenic activities like building levees along the Mississippi River and dredging of navigational canals (Turner and Cahoon, 1987; Reed, 1989).

In 1930's, levees along the Mississippi River were finished (Turner et Cahoon 1987), which prevented flooding in adjacent areas. This had two major negative effects. The water from spring overbank floods, which used to be crucial source of sediment and nutrients for marshes accretion, could not interact with surrounding landscape any more (Hatton et al., 1983; Evers et al., 1992; Day et al., 2009). Furthermore, the nutrients in the river water that are now led through the river channel directly to the sea cause severe eutrophication, hypoxia, and consequently so called 'dead zones' in the Gulf of Mexico (Turner and Rabalais, 1994; Rabalais et al., 1998; Engle et al., 1999; Dodds, 2006). Not only that marshes can no longer serve as a natural water treatment, they undergo rapid deterioration as the accretion cannot keep pace with sea level rise due to the lack of nutrient and sediment load. Extremely low slope of the Mississippi Delta and often insufficient marsh accretion rates result in submergence of many wetlands although the relative sea level rise is in order of a few centimetres (Turner and Cahoon 1987; Reed, 1989; Evers et al., 1992; DeLaune et al., 2003).

Linear structures like boat canals contribute to intrusion of salt water from the sea further into the coastal zone (Hatton et al., 1983; Turner and Cahoon, 1987). Changes in salinity and hydrologic regime affect wetland soils and plant communities, particularly in the freshwater marshes (Turner and Cahoon, 1987; Mitsch and Gosselink, 2000). Emergent plants in the submerging marshes do not root properly, hence the inorganic sediments and organic debris cannot be fixed in the sparse web of roots and the marsh deteriorates (Evers et al., 1992).

The rapid land loss rate has triggered more than 600 coastal restoration projects of various extent, objectives, and funding since 1970's (Lindquist and Summer, 2007; LDNR, 2009). The projects particularly relevant for this study are the Mississippi River diversions, which reintroduce river water into the delta lobes to support sedimentation processes, thus marsh accretion, and to reduce eutrophication and the amount of sediment deposition in the Gulf of Mexico (DeLaune et al., 2003; DeLaune et al., 2005; Lindquist and Summer 2007; Allison and Meselhe, 2010). Several studies warned that freshwater reintroduction may cause eutrophication of the basin (DeLaune et al., 2003; DeLaune et al., 2005; DeLaune et al., 2008; Turner et al., 2007). Determination of optimal operational regimes of freshwater diversions and evaluation of their effects on biogeochemistry of the receiving ecosystems are subject for recent and ongoing research (DeLaune et al., 2008; Day et al., 2009; Boustany, 2010).

## *2.2 Freshwater Wetlands Biogeochemistry and its Relation to the Measured Variables*

Processes typical for both terrestrial and aquatic ecosystems take place in marshes; the presence and range of aerobic and anaerobic processes is highly determined by hydroperiod of each marsh (Mitsch and Gosselink, 2000). Many studies (DeLaune et al., 2005; Grunwald et al., 2006; Gardner and White, 2010) focus on a specific part of the nutrient cycle or describe specific form of each nutrient, but properties and relationships of agglomerative variables like TP, TC, TN are mentioned sporadically.

Several geostatistical studies of TP, TC, or TN have been conducted elsewhere, such as in The Everglades, Florida (Bruland et al., 2006; Corstanje et al., 2006).

Both phosphorus (P) and nitrogen (N) are major limiting factors for plant and microbial growth in wetlands (Mitsch and Gosselink, 2000; DeBusk et al., 2001). Conley et al. (2009) emphasize that it is also the ratio of bioavailable P and N which affects the primary production. Grunwald and Reddy (2008) identified the main processes affecting P and N in marshes as influx, transformation, resuspension, transport, and chemical precipitation for P, then transport, mineralization, nitrification, denitrification,  $\text{NH}_4^+$  adsorption and desorption,  $\text{NH}_3$  volatilisation, and vegetative assimilation and decay as processes driving distribution of N.

Plants accept P in form of  $\text{H}_2\text{PO}_4^-$ , potentially  $\text{HPO}_4^{2-}$ , and nitrogen as  $\text{NO}_3^-$  or  $\text{NH}_4^+$ . While the bioavailability of P is predominantly driven by interaction of orthophosphates ( $\text{H}_2\text{PO}_4^-$ ,  $\text{HPO}_4^{2-}$ ,  $\text{PO}_4^{3-}$ ) with ions ( $\text{Fe}^{3+}$ ,  $\text{Al}^{3+}$ ,  $\text{Mn}^{2+}$ ,  $\text{Ca}^{2+}$ ) and sorption to soil particles, the bioavailability of N is to large extent determined by the microbial activity and relative rates of nitrification, denitrification, and N fixation. Microbes play important role also in dynamics of the metal ions. Carbon (C) is accepted by plants from the atmosphere as  $\text{CO}_2$ , which is generally abundant, and represents a dominant compound of plant tissues. Dead vegetation parts enter the detrital processing chain typical for marshes to eventually become a resource for bacterial anaerobic processes like fermentation and methanogenesis, or aerobic respiration. Decomposition under anaerobic conditions in waterlogged environment is slow which usually results in accumulation of dead plant tissues in various stages of decomposition as peat (Mitsch and Gosselink, 2000; DeBusk et al., 2001; Kayranli et al., 2010). Both N and C in wetland soils are bounded mainly in complex organic substances and inorganic forms represent just a small fraction, while considerable portion of P in wetlands is inorganic and interactions with mineral sediments through sorption play important role in dynamics of P (Mitsch and Gosselink, 2000, DeBusk et al., 2001; Rivero et al., 2007).

Relationship of pH and the three elements is complex, indirect, and poorly understood. However, there is a reasonable belief that pH alters the concentration of C, N, and P in soil through bacteria and plant growth (Mitsch and Gosselink, 2000; Gutknecht et al., 2006; Grunwald and Reddy, 2008). There are still many interactions of nutrients with biota and effects of other environmental factors in marshes about which very little is known (Mitsch and Gosselink, 2000; Gutknecht et al., 2006).

Soil moisture and bulk density in marshes are naturally negatively correlated. Bulk density is defined as dry weight of soil material per unit volume (Mitsch and Gosselink, 2000), thus a sample with high water content has less space for the solid compound. From the methodical perspective, bulk density was necessary for recalculation between concentration per mass and concentration per volume of soil, utilized for derivation of total stocks of elements in Davis Pond (Appendix D). For TP, TN, and TC, concentrations per mass of soil were the primary units for the geostatistical analysis.

## 2.3 Geostatistics

### 2.3.1 General background

Investigation of spatial relationships by statistical means, geostatistics, has become highly popular since the first theoretical cornerstones and practical techniques were developed in 1960's. Geostatistics has been widely used in soil science (Goovaerts, 1992; Taylor et al., 2003; Carrol and Oliver, 2005) and more specifically in wetland soils they were used in Everglades National Park, Florida, USA (Bruland et al., 2006; Corstanje et al., 2006; Grunwald et al., 2006; Rivero et al., 2007). This paper presents the first geostatistical study of coastal marshes of Louisiana.

Geostatistics relies on the assumption that values of the variable of interest,  $Z$ , in certain region, are an outcome of a random function  $Z(\mathbf{x})$ . The values of  $Z$  at a finite set of locations within the region represent one particular realisation of the random function and constitute the regionalized variable (Clark, 1979; Isaaks and Srivastava, 1989; Cressie, 1993; Burrough and McDonnell, 2000; Webster and Oliver, 2007). A general linear model describing  $Z$  at location  $\mathbf{x}$  can be formulated as:

$$Z(\mathbf{x}) = m(\mathbf{x}) + \epsilon(\mathbf{x}) + \epsilon'(\mathbf{x}) \quad [1]$$

where  $m(\mathbf{x})$  represents the structural (deterministic) component,  $\epsilon(\mathbf{x})$  is the stochastic spatially autocorrelated component, and  $\epsilon'(\mathbf{x})$  represents the stochastic spatially uncorrelated noise with normal distribution with zero mean. Note that in this formulation, the regionalized variable is only the  $\epsilon(\mathbf{x})$  (Burrough and McDonnell, 2000). In a basic case,  $m(\mathbf{x})$  is assumed to be spatially invariant and  $\epsilon'(\mathbf{x})$  can not be separated from  $\epsilon(\mathbf{x})$ , thus the linear model can be written as:

$$Z(\mathbf{x}) = \mu + \epsilon(\mathbf{x}) \quad [2]$$

where  $\mu$  is the unknown spatially invariant mean and  $\epsilon(\mathbf{x})$  is the stochastic component.

The assumption of spatially invariant mean is important for the description of spatial dependency which is generally described by taking the value of  $Z(\mathbf{x})$  as one random variable, value of  $Z(\mathbf{x} + \mathbf{h})$ , where  $\mathbf{h}$  is the lag (separating) vector, as the second variable, and calculating a measure of similarity between these two variables. The assumption of stationarity is necessary to calculate covariance, Cov, between these two considered variables. Assumption of weak (second order) stationarity, the most strict assumption applicable in practice, states that the mean and variance of  $Z(\mathbf{x})$  are invariant across the region and hence the covariance between the considered variables depends only on the lag vector, not on the location of the points within the region:

$$\begin{aligned} \text{Cov}[Z(\mathbf{x}), Z(\mathbf{x} + \mathbf{h})] &= E\{[Z(\mathbf{x}) - \mu][Z(\mathbf{x} + \mathbf{h}) - \mu]\} = \\ &= E\{[Z(\mathbf{x})Z(\mathbf{x} + \mathbf{h}) - \mu^2]\} = \text{Cov}(\mathbf{h}) \end{aligned} \quad [3]$$

The covariance in Eq. [3] is also called autocovariance function of variable  $Z$  and it still requires  $\mu$  to be estimated. To get rid of this requirement, the assumption of intrinsic stationarity has to be accepted. Under intrinsic stationarity, constant mean is still



assumed, but semivariance,  $\gamma(\mathbf{h})$  (Eq. [4]), referred also as semivariogram or variogram value, is used as a measure of similarity to describe spatial dependency.

$$\gamma(\mathbf{h}) = \frac{1}{2} E \{ [Z(\mathbf{x}) - Z(\mathbf{x} + \mathbf{h})]^2 \} \quad [4]$$

The goal of geostatistical analysis is usually kriging, estimation of the value of the studied variable at unsampled location,  $\hat{Z}(\mathbf{x}_o)$ , from values measured at different locations  $z(\mathbf{x}_i)$ ,  $i=1,2,\dots,n$ . However, it is also the variogram or autocovariance function that reveals spatial properties of  $Z$  (Burrough and McDonnell, 2000; Taylor et al., 2003).

Variograms are typically described by three main features. For simplicity, isotropic situation,  $\gamma(\mathbf{h}) = \gamma(|\mathbf{h}|)$ , is considered further. From certain  $|\mathbf{h}|$ , called range, semivariance can reach more or less stable value, sill. Range provides information about the scale of spatial dependency; points further than range from  $\mathbf{x}$  have no influence on the value of  $Z(\mathbf{x})$ . In practice, semivariance often does not approach zero as  $|\mathbf{h}|$  approaches zero, but there is a step increment in semivariance near the origin of the variogram. This step increment is called the nugget effect and expresses the  $\epsilon'(\mathbf{x})$  term in Eq. [1], i.e., the variability for  $|\mathbf{h}|$  shorter than the shortest sampling interval and the variance introduced from measurement errors. Nugget to sill ratio (relative nugget) expresses the strength of spatial autocorrelation and how close does the kriging estimate approach simple averaging of measured values. The higher the relative nugget, the weaker is the spatial autocorrelation and the closer is the kriging estimate to the sample mean (Isaaks and Srivastava, 1989; Rivero et al., 2007; Webster and Oliver, 2007). Note that the variogram model with nugget effect is sometimes expressed as two separate models, e.g., pure nugget and pure spherical model, then sill of the spherical structure is called partial sill of the whole model (Fig. 1).

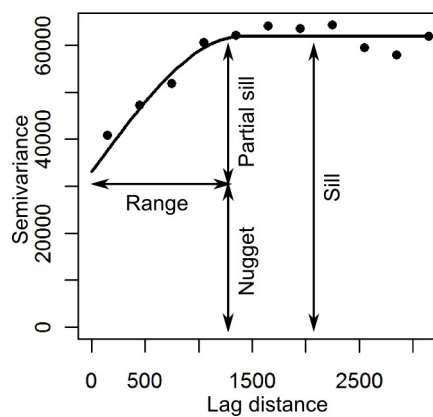


Fig. 1. Example of experimental variogram with fitted spherical model and main features identified: sill, partial sill, range, and nugget (Burrough and McDonnell, 2000, adjusted).

### 2.3.2 Geostatistical work flow

Typical work flow of geostatistical analysis involves 1) explanatory data analysis, 2) construction of experimental variograms, 3) fitting variogram models, 4) kriging and map production.

The distribution of data needs to be investigated and outliers removed during the explanatory data analysis. Although normal distribution is beneficial for geostatistics, non-normality is not an obstacle (Clark, 1979; Cressie, 1993; Lark, 2000; Webster and Oliver, 2007). However, square root or logarithmic transformation are recommended to stabilize variance of samples from highly skewed data. Logit, box-cox, or normal score transformations are other alternatives (Goovaerts, 1999; Burrough and McDonnell, 2000; Webster and Oliver, 2007). Webster and Oliver (2007) state that although the estimated values based on skewed distribution may not be the most accurate, it is still possible to proceed. Whether to transform and which transformation to use is one of the subjective decisions that has to be made by the practitioner. During the explanatory data analysis, data should be examined for presence of trend and a decision whether to remove trend should be made.

Construction of experimental variograms and subsequent fitting of variogram models, is the most critical step (Cressie, 1993; Webster and Oliver, 2007). Classical approach is to estimate  $\gamma(\mathbf{h})$  for certain lag vectors  $\mathbf{h}$  and then fit a continuous function through these estimates to obtain  $\gamma(\mathbf{h})$  defined for any  $\mathbf{h}$ . The original method for semivariance estimation is the Matheron's method of moments:

$$\hat{\gamma}(\mathbf{h}) = \frac{1}{2N(\mathbf{h})} \sum_{i=1}^{N(\mathbf{h})} [z(\mathbf{x}_i) - z(\mathbf{x}_i + \mathbf{h})]^2 \quad [5]$$

where  $N(\mathbf{h})$  denotes the number of points in the data set that are separated just by the vector  $\mathbf{h}$ . Some directional and distance tolerance on  $\mathbf{h}$  must be set if the sampling design is irregular (Isaaks and Srivastava, 1989; Webster and Oliver 2007), which results in a series of breaks of  $|\mathbf{h}|$  for the isotropic situation.

An important detail is that  $N(\mathbf{h})$  must be regarded in weightings for the fitting procedure (Cressie, 1993; Webster and Oliver, 2007). Weighted sum of squares between experimental and modelled semivariogram values is the measure commonly used to asses goodness of fit of different types of models. The choice of the model is again partly a matter of the practitioner's experience and knowledge of the underlying process (Isaaks and Srivastava, 1989). Exponential (Eq. [6]) and spherical (Eq. [7]) variogram models are the most commonly used in soil science (French et al., 1995; Lark, 2000; Bruland et al., 2006; Grunwald et al., 2006; Webster and Oliver, 2007):

$$\gamma_{\text{exp}}(|\mathbf{h}|) = c \{1 - \exp(-|\mathbf{h}|/r)\} \quad [6]$$

$$\gamma_{\text{sph}}(|\mathbf{h}|) = c \left\{ \frac{3|\mathbf{h}|}{2|\mathbf{h}|} - \frac{1}{2} \left( \frac{|\mathbf{h}|}{a} \right)^3 \right\} \quad \text{for } a \leq |\mathbf{h}| \quad ; \quad \gamma_{\text{sph}}(|\mathbf{h}|) = c \quad \text{for } a > |\mathbf{h}| \quad [7]$$

where  $c$  is the sill,  $a$  is the range, and  $r$  is the distance parameter for exponential model (practical range of exponential model is approximately  $3r$ ).

Once the model parameters are known, kriging, referred also as the best linear unbiased estimator (Isaaks and Srivastava, 1989; Burrough and McDonnell, 2000), can be performed. Kriging is linear because the value of the variable at unsampled location  $\hat{Z}(\mathbf{x}_0)$  is a linear combination of observed values at sampled locations  $z(\mathbf{x}_i)$ :

$$\hat{Z}(\mathbf{x}_0) = \sum_1^n \lambda_i z(\mathbf{x}_i) \quad [8]$$

and the question is how to determine the weights  $\lambda_i$  for each of the  $n$  points used for the prediction. Kriging is unbiased as the expected residual (difference between estimated and true value) is 0:

$$E[\hat{Z}(\mathbf{x}) - Z(\mathbf{x})] = 0 \quad [9]$$

Finally, kriging is best in the sense that the variance of the residual is minimal:

$$\text{Var}[\hat{Z}(\mathbf{x}) - Z(\mathbf{x})] = E\{[\hat{Z}(\mathbf{x}) - Z(\mathbf{x})]^2\} \rightarrow \min. \quad [10]$$

It can be shown that Eq. [9] constrains the weights so that  $\sum \lambda_i = 1$ . Then the minimization in Eq. [10] with inclusion of Lagrange multiplier  $\Phi$  leads to the following system of equations.

$$\begin{pmatrix} \gamma_{11} & \gamma_{12} & \dots & \gamma_{1n} & 1 \\ \gamma_{21} & \gamma_{22} & \dots & \gamma_{2n} & 1 \\ \vdots & \vdots & \dots & \vdots & \vdots \\ \gamma_{n1} & \gamma_{n2} & \dots & \gamma_{nn} & 1 \\ 1 & 1 & \dots & 1 & 0 \end{pmatrix} \begin{pmatrix} \lambda_1 \\ \lambda_2 \\ \vdots \\ \lambda_n \\ \Phi \end{pmatrix} = \begin{pmatrix} \gamma_{01} \\ \gamma_{02} \\ \vdots \\ \gamma_{0n} \\ 1 \end{pmatrix} \quad [11]$$

where  $\gamma_{ij} = \gamma(\mathbf{x}_i - \mathbf{x}_j)$  is the value of semivariance, obtained from the semivariogram model for the vector separating points  $\mathbf{x}_i$  and  $\mathbf{x}_j$ . Weights for [8] are obtained by solving Eq. [11] (Isaaks and Srivastava, 1989; Webster and Oliver, 2007).

Kriging provides also an estimate of variance of  $\hat{Z}(\mathbf{x}_0)$ ,  $\hat{\sigma}_{KR}^2(\mathbf{x}_0)$ :

$$\hat{\sigma}_{KR}^2(\mathbf{x}_0) = (\gamma_{01} \ \gamma_{02} \ \dots \ \gamma_{0n} \ 1) (\lambda_1 \ \lambda_2 \ \dots \ \lambda_n \ \Phi)^T \quad [12]$$

where  $(\cdot)^T$  denotes transposition.

### 2.3.3 Linear model of coregionalization

When more than one regionalized variable is considered in a set  $W = \{Z_w, w=1, 2, \dots, t\}$ , spatial relationships between them can be described by cross-variograms and linear model of coregionalization (LMCR) fitted to auto and cross-variograms (Wackernagel, 2003; Webster and Oliver, 2007). Pringle and Lark (2006) used this approach to describe spatial relationships of modelled values of CO<sub>2</sub> released from soil and their error, Goovaerts (1992) presented LMCR and factorial analysis of soil data and simulated data set, and Webster and Oliver (2007) demonstrated LMCR on an example of relationships between barley yields, available P, and exchangeable potassium. Cross-variogram,  $\gamma_{uv}(\mathbf{h})$  of variables  $Z_u$  and  $Z_v$  is defined as (Webster and Oliver, 2007)

$$\gamma_{uv}(\mathbf{h}) = \frac{1}{2} E \{ [Z_u(\mathbf{x}) - Z_u(\mathbf{x} + \mathbf{h})][Z_v(\mathbf{x}) - Z_v(\mathbf{x} + \mathbf{h})] \} \quad [13]$$

When  $Z_u$  and  $Z_v$  are measured at identical locations, their cross-variogram can be estimated by method of moments:

$$\hat{\gamma}_{uv}(\mathbf{h}) = \frac{1}{2N(\mathbf{h})} \sum_{i=1}^{N(\mathbf{h})} [z_u(\mathbf{x}_i) - z_u(\mathbf{x}_i + \mathbf{h})][z_v(\mathbf{x}_i) - z_v(\mathbf{x}_i + \mathbf{h})] \quad [14]$$

where  $z_u(\mathbf{x}_i)$  and  $z_v(\mathbf{x}_i)$  are the observed values of variables  $Z_u$  and  $Z_v$  at location  $\mathbf{x}_i$  respectively. Variogram model is not fitted to the auto and cross-variograms independently, because such model of coregionalization does not guarantee positive semi-definiteness (Lark and Papritz, 2003). However, LMCR assumes that the random functions  $Z_w \in W$  with means  $\mu_w$  are linear combinations of independent random variables  $Y_j^s(\mathbf{x})$  with standard normal distribution (Pringle and Lark, 2006):

$$Z_w(\mathbf{x}) = \mu_w + \sum_{s=0}^L \sum_{j=1}^t a_{wj}^s Y_j^s(\mathbf{x}) \quad [15]$$

where  $s$  is an index, not a power,  $a_{wj}^s$  are the coefficients of the linear combination,  $L+1$  is the number of considered elementary variogram models, and  $t$  is the number of variables included in the LMCR. It is assumed that the variables  $Y_j^s(\mathbf{x})$  have a common semivariogram:

$$\frac{1}{2} E [Y_j^s(\mathbf{x}) - Y_j^s(\mathbf{x} + \mathbf{h})][Y_{j'}^{s'}(\mathbf{x}) - Y_{j'}^{s'}(\mathbf{x} + \mathbf{h})] = \delta_{jj'} \delta_{ss'} g_s(\mathbf{h}) \quad [16]$$

where  $\delta_{pq}$  is the Kronecker delta being 1 for  $p=q$  and 0 otherwise, and  $g_s(\mathbf{h})$  is the  $s$ -th elementary variogram model with unit sill. Consequently, the cross-variogram of two variables  $Z_u$  and  $Z_v$  from  $W$  can be written as follows.

$$\gamma_{uv}(\mathbf{h}) = \sum_{s=0}^L \sum_{j=1}^t a_{uj}^s a_{vj}^s g_s(\mathbf{h}) = \sum_{s=0}^L b_{uv}^s g_s(\mathbf{h}) \quad [17]$$

where  $b_{uv}^s$  represents sill of the  $s$ -th structure in the cross-variogram of  $Z_u$  and  $Z_v$  if the models  $g_s(\mathbf{h})$  are bounded (Webster and Oliver, 2007). The variogram models in a LMCR can be therefore characterized by the individual elementary models  $g_s(\mathbf{h})$  and a set of  $L+1$  positively semi-definite coregionalization matrices containing  $b_{uv}^s$ . For example when  $t=2$  and  $L+1=2$ , the models can be written as:

$$\begin{pmatrix} \gamma_{11}(\mathbf{h}) & \gamma_{12}(\mathbf{h}) \\ \gamma_{21}(\mathbf{h}) & \gamma_{22}(\mathbf{h}) \end{pmatrix} = g_0(\mathbf{h}) \begin{pmatrix} b_{11}^0 & b_{12}^0 \\ b_{21}^0 & b_{22}^0 \end{pmatrix} + g_1(\mathbf{h}) \begin{pmatrix} b_{11}^1 & b_{12}^1 \\ b_{21}^1 & b_{22}^1 \end{pmatrix} \quad [18]$$

Algorithms for fitting LMCR and methods of describing coregionalization are still subject of contemporary research as the requirement of positive semi-definiteness of LMCR is challenging (Lark and Papritz, 2003; Bishop and Lark, 2008; Emery, 2010). Same as for fitting autovariograms, simple models are recommended for fitting LMCR and usually just nugget and one or two other structures are used (Goovaerts, 1992; Carroll and Oliver, 2005; Pringle and Lark, 2006; Webster and Oliver, 2007; Bishop and Lark, 2008).

Recent developments in variogram model parameters estimation focus on maximum likelihood (ML) methods (Diggle et al., 2003; Marchant and Lark, 2007c). However, construction of experimental variogram by classical methods as described above is still respected as a tool for explanatory analysis of spatial autocorrelation and cross-correlation (Diggle et al., 2003) which was one of the objectives of this study and so classical approach was preferred.

#### 2.4 Moving Window Analysis

Geostatistical tools like cross-variograms describe correlation of the variables for the whole study area. To investigate the local spatial distribution of correlation, a moving window approach was used. Performing specific operations within a moving window drifting over a data set is a widely used technique for example for terrain analysis (Burrough and McDonnell, 2000), image processing (Richards and Jia, 1999), and for investigation of a raw data set (Isaaks and Srivastava, 1989). Grunwald et al. (2006) used moving windows to describe P in an Everglades marsh. They passed two (spatially coincident) interpolated rasters to a moving window function and calculated correlation coefficient for each cell of the interpolated rasters from cells that fell within a window of specified size centred on that cell. We used moving windows in a similar way.

### 3 Materials and Methods

#### 3.1 Study Area

Davis Pond is a fresh water marsh with area of 37.1 km<sup>2</sup>, located in the Barataria Basin, Louisiana, USA, at 29°53' N, 90°17' W (Fig. 3). Underlying material is alluvial sediment accumulated by the Mississippi River and its distributaries in geological history. The dominant soils are histosols. In 1884, a crevasse in the river levee occurred, which contributed to the marshy character of the area (Ensminger and Simon, 1993; Fortner, 2000; Gardner and White, 2010). *Panicum hemitomon* (Schult.), *Polygonum* spp. (DeLaune et al., 2008), *Sagittaria lancifolia* (L.), *Eichhornia crassipes* (Mart.), *Alternanthera philoxeroides* (Mart.), *Bidens* spp., and *Typha* spp. represent the most abundant emergent plants, *Taxodium distichum* (L.) is also present mainly in the western part (Gardner and White, 2010).

Before the diversion structure was built, precipitation, about 168 mm year<sup>-1</sup> (LNDR, 2005), was the primary water source for the marsh. The freshwater diversion became operational in 2002 (LDNR, 2005) and Davis Pond started to receive the Mississippi River water through a canal in the north. The diversion structure can divert up to about 300 m<sup>3</sup> s<sup>-1</sup> of water (Lindquist and Summer, 2007), however, the actual discharge (Fig. 2) is adjusted according to the operational plans and historical data can be requested online (LNDR, 2010; USGS, 2010). There is also a pump which pumps water accumulated after storms into the ponding area over the northern guide levee (Fig. 3). When the discharge from the diversion is low, most of the water flows through a naturally developed system of canals in the central part (Gardner and White, 2010). Basically the whole south-eastern boundary of Davis Pond is an outflow to a brackish Lake Cataouache, which is connected with larger Lake Salvador in the south. New Orleans city starts about 8 km downstream the Mississippi from the diversion, the nearest urban area is Luling, about 2 km upstream.

One of the main function of the ponding area is to slow down the water coming from the diversion before it gets further to the Barataria Basin and hence to imitate the regime of spring floods and balance the salinity level (Fortner, 2000; DeLaune et al., 2005). Few studies have been conducted in Davis Pond since 2002. DeLaune et al. (2005) reported that Davis Pond was able to remove all nitrate from the introduced river water if the diversion discharge was not pulsed or high, Gardner and White (2010) documented that denitrification activity was generally higher near the water inlet, and DeLaune et al. (2008) found that Davis Pond acted as a source of dissolved organic carbon for the adjacent Lake Cataouache and that it represented a source of ammonium-N.

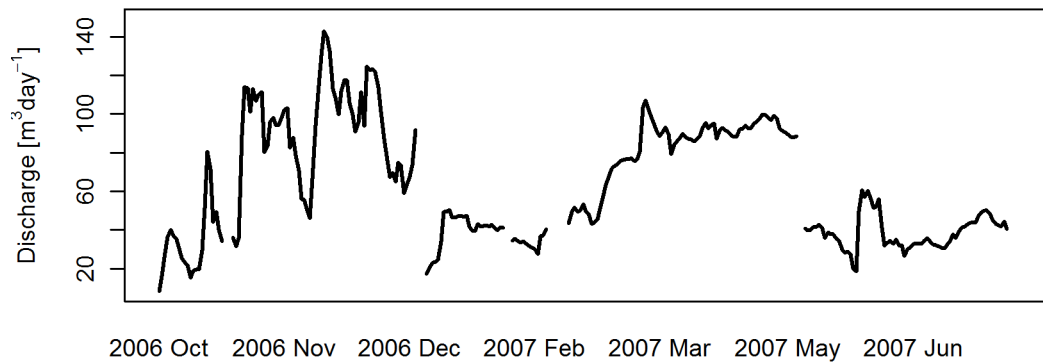


Fig. 2. Daily discharge of Davis Pond Freshwater Diversion before and during the time of soil sampling (Oct 2006 - Aug 2007) (USGS, 2010).

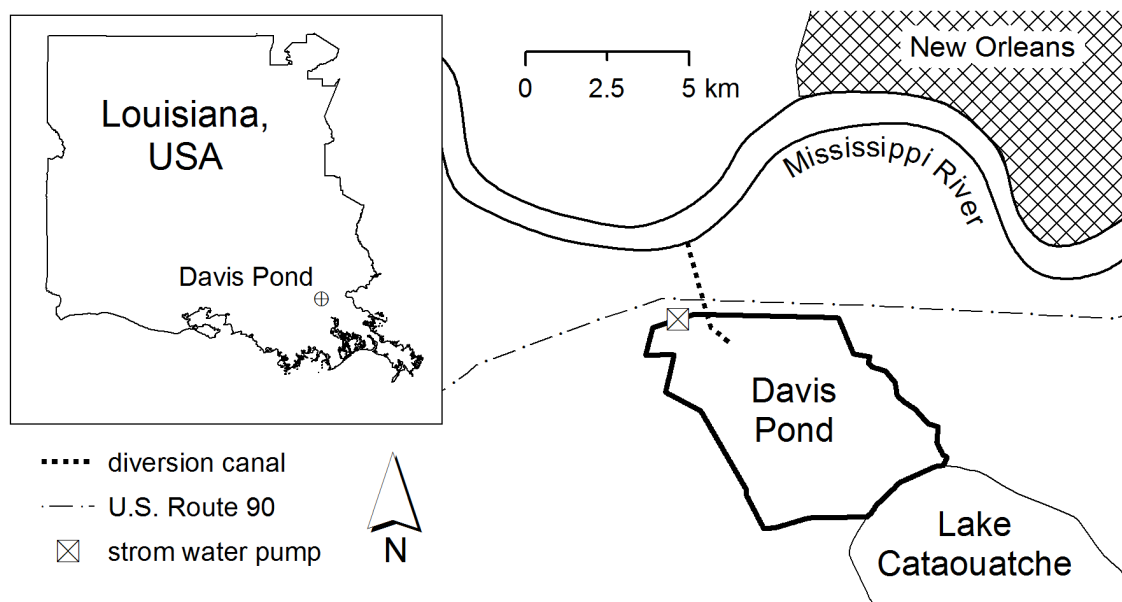


Fig. 3. Overview map of the study area, Davis Pond, Louisiana, USA.

### 3.2 Sampling and Soil Analysis

Soil samples were collected between May 13 and July 10 2007. At each location, a plexiglass tube 7 cm in diameter was used to collect a sample of the upper 20 cm of soil, which was then partitioned into 0–10 cm and 10–20 cm segments referred further as the upper (UP) and lower (LW) layer respectively. Support for each sample was therefore a 10 cm high cylinder 7 cm in diameter. Gardner and White (2010) describe details about the chemical analysis except for TP, which was determined using the absorbic acid automated colorimetric procedure (Method 365.1; USEPA, 1993). Three sampling locations were eventually excluded as outliers, which resulted in 139 sampling points for the geostatistical analysis and sampling density of  $0.0375 \text{ ha}^{-1}$ .

Sampling design was optimized for geostatistical analysis by Dr Ben Marchant from Rothamsted Research using spatial simulated annealing (SSA) (Van Groenigen et al., 1999; Van Groenigen, 2000). SSA ensures that the whole area is more or less uniformly sampled, which is desirable for kriging, but also provides broader variety of distances between points (Table 1) and thus allows to account for short range variability, which is beneficial for variography (Marchant and Lark, 2007b; Webster and Oliver, 2007). Only 11 pairs were closer than 300 m.

Seven variables were measured at each sampling point in both layers (Table 2): moisture (MOIST), bulk density (BD), pH, organic matter content (OM), content of TP, TN, and TC.

Table 1. Distribution of distances between sampling locations.

	Minimum	1st quartile	Median	Mean	3rd quartile	Maximum
Value, m	100	1905	2943	2081	4115	8588

Table 2. Variables measured at each sampling point, their units and naming convention.

Property	Units	Variable name in soil depth	
		0–10 cm	10–20 cm
Moisture	proportions	MOIST_UP	MOIST_LW
Bulk density	$\text{g cm}^{-3}$	BD_UP	BD_LW
pH	pH units	PH_UP	PH_LW
Organic matter content	proportions	OM_UP	OM_LW
Total phosphorus	$\text{mg P kg}^{-1}$ soil	TP_UP	TP_LW
Total nitrogen	$\text{g N kg}^{-1}$ soil	TN_UP	TN_LW
Total carbon	$\text{g C kg}^{-1}$ soil	TC_UP	TC_LW

### 3.3 Statistical Analysis

R software (R Development Core Team, 2010) and its packages GeoR (Ribeiro and Diggle, 2001) and Gstat (Pebesma, 2004) were used for the analysis. Steps introduced in section 2.3 were followed to produce maps. Code for calculation of codispersion coefficient, structural codispersion coefficient, moving window correlation, and other custom functions is enclosed in Appendix G together with scripts written during the analysis.

Webster and Oliver (2007) recommend 100 sampling points as a minimum for geostatistical analysis, when spatial anisotropy is not an issue, and at least 250 sampling points for multidirectional variogram estimation. Identification of outliers was done visually, only 3 points were eventually excluded based mainly on their position in scatter-grams. Histograms and normal quantile-quantile plots were drawn to investigate distribution properties, Shapiro-Wilk test of normality (De Sá, 2007) was performed. Data were investigated for presence of trend visually and by the variance ratio F-test as



suggested by Burrough and McDonnell (2000, p. 109). No trend was removed from the data, discussion on this topic can be found in Appendix A.

Experimental variograms were initially constructed for breaks 0, 200, 400, 500, 600, 1000, 1400, to 8000 m, another set of breaks was 0, 600, 1200, to 8000 m, and finally breaks 0, 300, 600, to 3300 m were considered optimal for model fitting. Spherical and exponential models were fitted and the model with the lowest weighted sum of squares between experimental and modelled semivariance was chosen. Classical method of moments (Eq. [5]) and Hawkins and Cressie robust variogram estimator (Eq. [19]) (Ribeiro and Diggle, 2001) were used.

$$\hat{\gamma}_{CH}(\mathbf{h}) = \frac{\left\{ \frac{1}{N(\mathbf{h})} \sum_{i=1}^{N(\mathbf{h})} |z(\mathbf{x}_i) - z(\mathbf{x}_i + \mathbf{h})|^2 \right\}^{\frac{1}{2}}}{0.914 + [0.988 / N(\mathbf{h})]} \quad [19]$$

Because the robust estimator did not produce visually very different experimental variograms, method of moments was used for model fitting. Number of pairs in each lag was used as weightings for weighted least squares fitting procedure.

Neither method of moments, nor robust estimator produced clear variogram of pH, but based the experimental variogram and previous studies (Fennessy and Mitsch, 2001; Bruland and Richardson, 2005; Smith et al., 2007), pH was considered spatially autocorrelated and variogram model parameters were found using the residual maximum likelihood (REML) method (Cressie, 1993; Ribeiro and Diggle, 2001; Kerry and Oliver, 2007).

Because the number of sampling points was too low to split the data set into calibration and validation sets, all points were used for variogram construction and model fitting. Cross-validation of the fitted models was performed to assess how faithfully did they express the spatial dependency. Cross-validation is done by leaving out each point  $\mathbf{x}_i$  and kriging an estimated value at its location from the remaining samples (Pebesma, 2004). One of the summative indicators that can be calculated from cross-validation results is the mean squared deviation ratio (MSDR) (Webster and Oliver, 2007):

$$MSDR = \frac{1}{n} \sum_{i=1}^n \frac{[z(\mathbf{x}_i) - \hat{Z}(\mathbf{x}_i)]^2}{\hat{\sigma}_{KR}^2(\mathbf{x}_i)} \quad [20]$$

where  $n$  is the number of points in the data set. The value of MSDR should be close to 1 (Webster and Oliver, 2007), however, Isaaks and Srivastava (1989) remind that this single value should not be regarded as a bulletproof indicator of model quality and that investigation of individual cases where the difference between measured and estimated value is high can provide useful information.

The variogram models were used for punctual ordinary kriging with global neighbourhood (Ribeiro and Diggle, 2001), i.e., all the data points were used for each estimate. Final map layouts were produced in ArcMap (ESRI, 1999–2009).

LMCR was fitted to the auto and cross-variograms of variables in the upper layer (excluding moisture) using the Gstat R package (Pebesma, 2004). Based on visual inspection of the auto and cross-variograms, just nugget (index  $s=0$ ) and exponential model with range of 1100 m (index  $s=1$ ) were included in the LMCR. This generalization of model type and unification of ranges for the LMCR is desirable because models with different ranges represent individual structures in the LMCR (Lark and Papritz, 2003; Wackernagel, 2003; Carroll and Oliver, 2005; Webster and Oliver, 2007). To obtain a valid (positively definite) LMCR, weightings for the fit were set to  $N(|\mathbf{h}|) / [\gamma(|\mathbf{h}|)^2]$ .

Codispersion coefficient  $\hat{\kappa}_{uv}(\mathbf{h})$  is calculated as  $\hat{\kappa}_{uv}(\mathbf{h}) = \hat{\gamma}_{uv}(\mathbf{h}) / \sqrt{\hat{\gamma}_{uu}(\mathbf{h}) \cdot \hat{\gamma}_{vv}(\mathbf{h})}$ , where  $\hat{\gamma}_{uv}(\mathbf{h})$ ,  $\hat{\gamma}_{uu}(\mathbf{h})$ , and  $\hat{\gamma}_{vv}(\mathbf{h})$  refer to the value of cross-variogram of variables  $Z_u$  and  $Z_v$ , autovariogram of variable  $Z_u$ , and autovariogram of variable  $Z_v$ , respectively, for certain lag vector  $\mathbf{h}$  (Pringle and Lark, 2006). Structural codispersion coefficient  $\rho_{uv}^s$  is calculated directly from the coregionalization matrices as  $\rho_{uv}^s = b_{uv}^s / \sqrt{b_{uu}^s b_{vv}^s}$ , where  $b_{ij}^s$  refers to the element at position  $(i,j)$  in the coregionalization matrix for structure  $s$ . The advantage of codispersion coefficient is that it is not affected by the LMCR fit (Lark and Papritz, 2003; Pringle and Lark, 2006). When  $\hat{\kappa}_{uv}(\mathbf{h})$  does not change with  $\mathbf{h}$ , the two variables are said to be intrinsically correlated, i.e., the correlation is the same for all spatial scales within the region (Wackernagel, 2003; Pringle and Lark, 2006; Webster and Oliver, 2007). Interpretation of  $\hat{\kappa}_{uv}(\mathbf{h})$  and  $\rho_{uv}^s$  is similar to the usual Pearson product moment correlation coefficient. Values are within interval  $[-1,+1]$  with negative values indicating association of high values of one variable with low values of the other, and positive values indicating association of high values of one variable with high values of the other variable. The closer to one (or minus one), the stronger the relationship. While  $\hat{\kappa}_{uv}(\mathbf{h})$  provides an information how does this correlation changes with different lag vectors,  $\rho_{uv}^s$  provides more general information how are the two variables related within the range of the particular structure (Pringle and Lark, 2006).

So called hulls of perfect correlation (Eq. [21], Wackernagel, 2003) represent another approach how to look at intensity of spatial correlation between two variables. Proximity of the cross-variogram to the hull of perfect correlation indicates the strength of the relationship (Webster and Oliver, 2007).

$$\text{hull}[\gamma_{uv}(\mathbf{h})] = \pm \sum_{s=0}^L \sqrt{b_{uu}^s b_{vv}^s} g^s(\mathbf{h}) \quad [21]$$

where  $s$  denotes the index of one of the  $L+1$  structures (in the case of this study,  $L=1$ ,  $s=0$  for the nugget,  $s=1$  for the exponential model with 1100 m range),  $b_{uu}^s$  and  $b_{vv}^s$  are

the sills of the  $s$ -th structure in autovariogram models of  $Z_u$  and  $Z_v$ , respectively (and are on the diagonal of the  $s$ -th coregionalization matrix), and  $g^s(\mathbf{h})$  represents the standardized form of the  $s$ -th structure.

During the moving window analysis, Pearson's product moment correlation coefficients were calculated in square windows of 6 different side sizes: 250, 500, 750, 1100, 2200, and 3300 m. These thresholds were selected with respect to the approximate common range of variograms about 1100 m. Centres of the windows were specified as a fixed grid with 100 m spacing. Only cells that fell within Davis Pond were regarded as input data points.

#### 4 Results

During the explanatory data analysis, sound deviations from normality were detected. Only pH and TP\_LW had normal distribution according to Shapiro-Wilk test of normality. However, only BD\_UP was eventually transformed by box-cox transformation with power  $-0.5$ . This transformed variable is further referred as bxBD\_UP. Transformations of other variables did not bring any substantial improvement. Univariate summary statistics with other results of explanatory data analysis are enclosed in Appendix A.

Investigation of histograms (Appendix A) and spatial location of values revealed presence of two distinct groups in the lower layer, mostly characterized by organic matter content. Highly organic samples (OM\_LW $>0.5$ , 87 points) had high moisture content (MOIST\_LW $>0.8$ ), low density (BD\_LW $<0.3$ ), and generally higher content of C and N. Remaining 52 points had OM\_LW $<0.5$ , lower moisture content, and higher density.

Scatter-grams (Appendix A) showed that there were strong non-linear relationship between density or moisture and other variables. Within the same layer, there was an obvious strong relationship between moisture and density ( $\rho \approx -1$ ). Very strong positive correlation was between TC, TN, and OM ( $\rho \approx 1$ ) and all these three variables were strongly correlated with moisture and density ( $|\rho| = 0.8$ ). Correlation of TP or pH with other variables was generally low. Between layers, relationships were weak (usually  $\rho \leq 0.5$ ), the strongest correlation ( $\rho \approx 0.7$ ) was found again between TC, TN, and OM. Pearson's (Table 3) and Spearman's rank correlation coefficients of all 14 variables can be found in Appendix A.

It was concluded that there was no spatial relationship in the lower layer and any interpolation of the variables in 10–20 cm soil depth was found meaningless. This was based on experimental variograms constructed by method of moments and Hawkins and Cressie robust estimator (Appendix B). Trend removal, directional variogram investigation, data transformation, splitting the data set into more parts, nor indicator variogram investigation (Appendix E) did not help.

Table 3. Pearson's correlation coefficients between variables in 0–10 cm soil depth in Davis Pond.†

	Moisture	BD	pH	OM	TP	TN	TC
Moisture	1.00						
BD	-0.99	1.00					
pH	-0.25	0.27	1.00				
OM	0.79	-0.78	-0.39	1.00			
TP	0.44	-0.42	0.16	0.31	1.00		
TN	0.79	-0.78	-0.39	0.97	0.38	1.00	
TC	0.78	-0.77	-0.38	0.99	0.30	0.97	1.00

†BD, bulk density; OM, organic matter content; TP, total phosphorus; TN, total nitrogen; TC, total carbon.

In the upper layer, variogram models were fitted to all variables except MOIST\_UP (Fig. 4). Appendix F describes how map of MOIST\_UP was produced. The maximal distance between points regarded for the construction of these variograms was 3300 m because variogram values calculated from points further than this distance became erratic. Appendix B contains experimental variograms also of the variables in the lower layer. Spherical variogram model fitted better for TP\_UP, but exponential model had lower sum of weighted least squares for OM\_UP, TC\_UP, TN\_UP, and bxBD\_UP (Table 4). Even in the case of TP\_UP, MSDR of the exponential model was closer to one than the MSDR of the spherical model, but spherical model fitted the nugget more realistically and was used for kriging. Parameters of the spherical model of PH\_UP were obtained using the REML method because experimental variograms were erratic for both method of moments and Hawkins and Cressie robust estimator. The assumption of normality required by the REML method (Diggle et al., 2003; Webster and Oliver, 2007) was fulfilled in the case of PH\_UP.

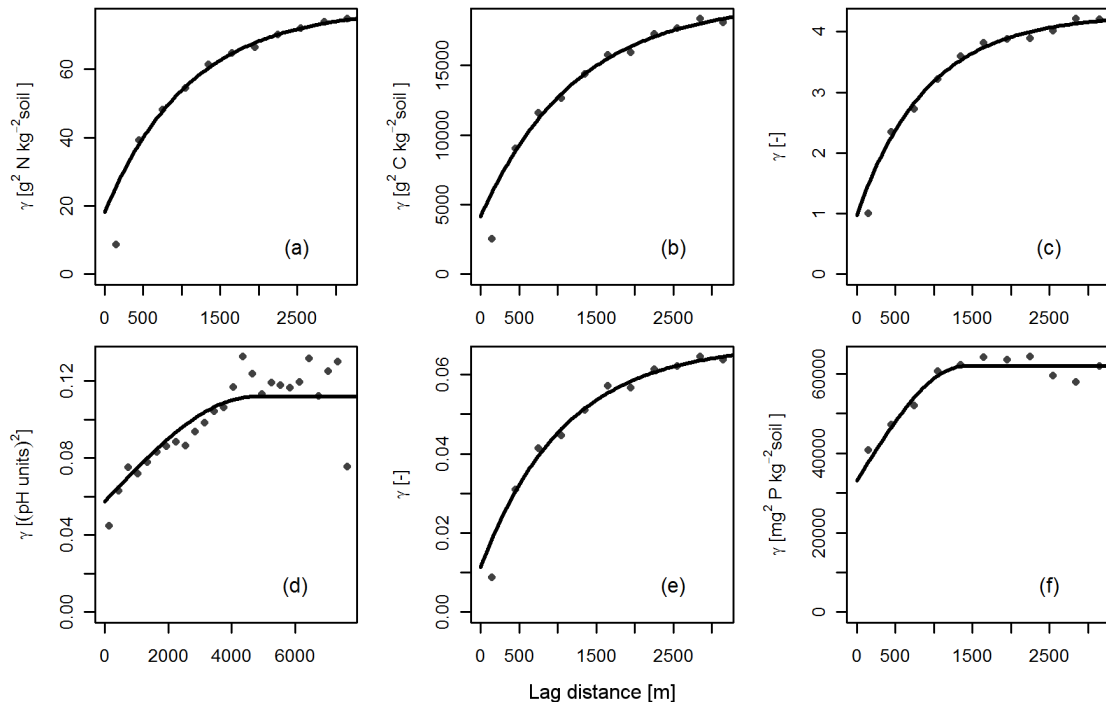


Fig. 4. Experimental autovariograms (dots) and fitted variogram models (lines) of soil properties in 0–10 cm soil depth; (a) total nitrogen, (b) total carbon, (c) bulk density transformed by box-cox transformation with power  $-0.5$ , (d) pH, (e) organic matter content, (f) total phosphorus. Model of pH was obtained by residual maximum likelihood method.

Table 4. Variogram models used for kriging of soil properties in 0–10 cm soil depth.†

Property	Model type	SSSQ‡	Nugget‡	Partial sill‡	Range	Practical range		MSDR
						m		
pH	spherical	$-1.79 \times 10^1 \S$	$5.73 \times 10^{-2}$	$5.44 \times 10^{-2}$	4694	4694	1.0057	
OM	exponential	$9.39 \times 10^{-2}$	$1.13 \times 10^{-2}$	$5.63 \times 10^{-2}$	1080	3235	1.0046	
TP	spherical	$1.60 \times 10^5$	$3.30 \times 10^4$	$2.88 \times 10^4$	1393	1393	0.9415	
TN	exponential	$7.51 \times 10^1$	$1.81 \times 10^1$	$5.98 \times 10^{-2}$	1095	3280	0.9886	
TC	exponential	$2.37 \times 10^4$	$4.15 \times 10^3$	$1.54 \times 10^4$	1237	3707	0.9995	
bxBD	exponential	$5.38 \times 10^1$	$9.69 \times 10^{-1}$	$3.31 \times 10^0$	905	2712	1.0300	

†OM, organic matter content; TP, total phosphorus; TN, total nitrogen; TC, total carbon; bxBD, bulk density transformed by box-cox transformation with power  $-0.5$ ; SSSQ, square root of weighted sum of squares of differences between experimental and modelled variogram value; MSDR, mean square deviation ratio obtained by cross-validation.

‡ Units are  $(\text{pH Units})^2$ ,  $\text{mg}^2 \text{P kg}^{-2} \text{ soil}$ ,  $\text{g}^2 \text{N kg}^{-2} \text{ soil}$ , and  $\text{g}^2 \text{C kg}^{-2} \text{ soil}$  for pH, TP, TN, TC, respectively, otherwise the quantities are dimensionless.

§ maximized loglikelihood obtained by residual maximum likelihood method, dimensionless.

Maps of BD\_UP, PH\_UP, TC\_UP, and TP\_UP (Fig. 5) with the estimated standard deviations disclosed that spatial distribution of TC\_UP and BD\_UP was similar. Both TP\_UP and PH\_UP exhibited different spatial pattern. The uniformly high standard

deviation of PH\_UP and TP\_UP was a consequence of high nugget effect. OM\_UP and TN\_UP exhibited the same pattern as TC\_UP. All maps are enclosed in Appendix H.

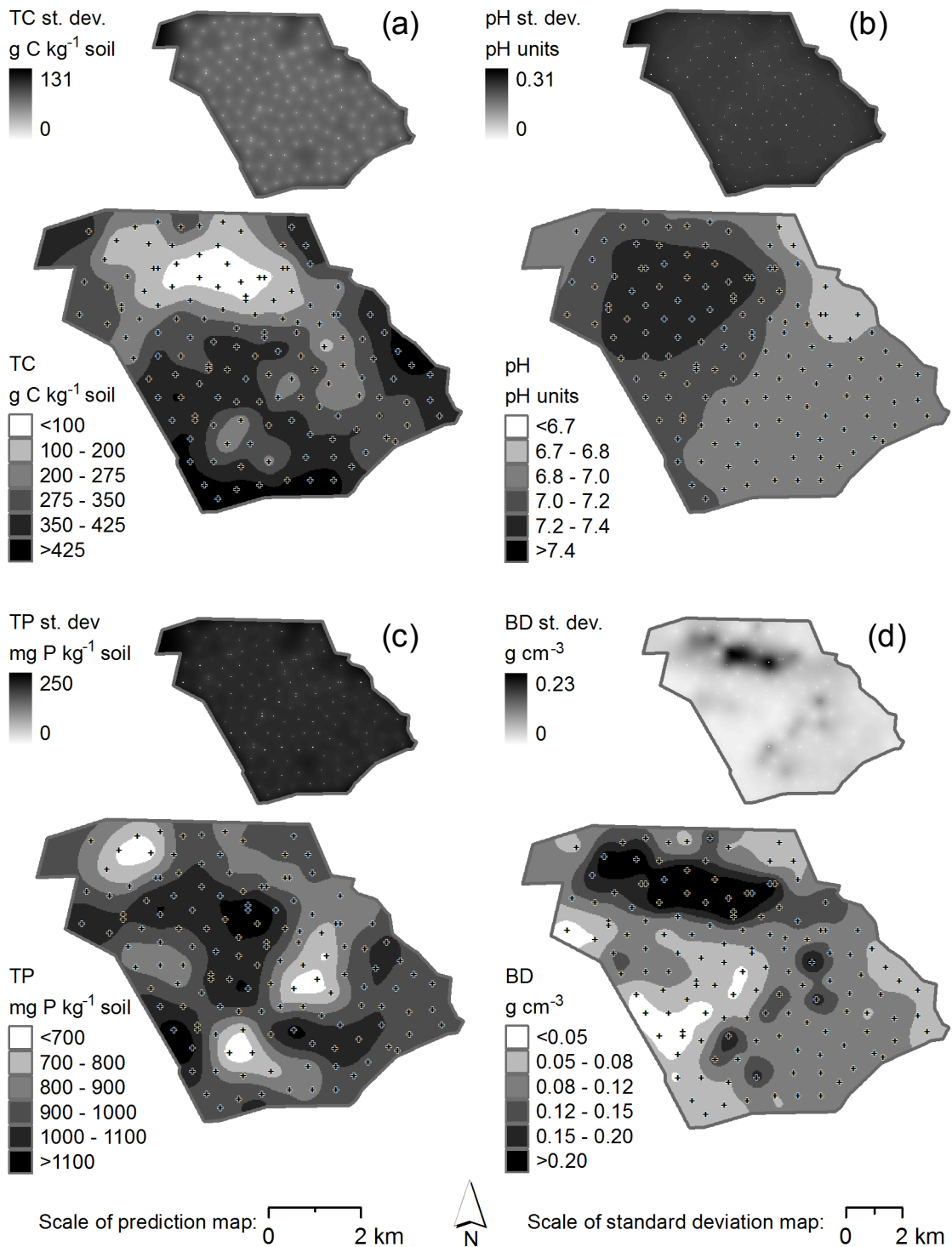


Fig. 5. Maps of (a) total carbon (TC), (b) pH, (c) total phosphorus (TP), and (d) bulk density (BD) in 0–10 cm soil depth and associated estimated standard deviations. Gray line is Davis Pond boundary, black crosses are sampling locations.

Mean range of exponential variograms of OM\_UP, TN\_UP, and TC\_UP (Table 4) was 1137 m, hence LMCR with nugget and exponential model with 1100 m range was fitted to the autovariograms (Fig. 7) and cross-variograms (Fig. 6) of the variables in the upper layer (Table 5). MOIST\_UP was not included.

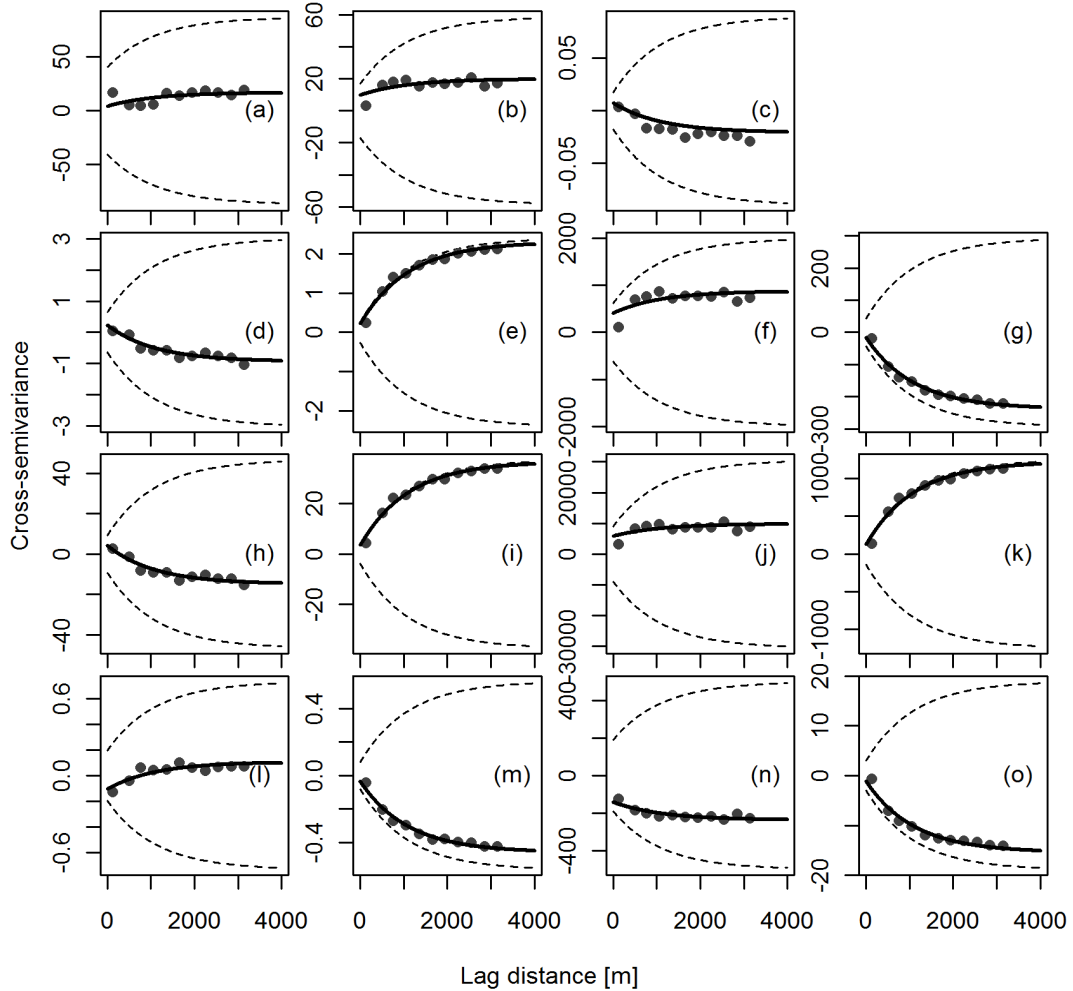


Fig. 6. Experimental cross-variograms (dots) of pH, bulk density transformed by box-cox transformation with power  $-0.5$  (bxBD), organic matter content (OM), total phosphorus (TP), total nitrogen (TN), and total carbon (TC) in 0–10 cm soil depth and fitted linear model of coregionalization with exponential model of 1100 m range (solid line). Proximity of the exponential model to the hull of perfect correlation (dashed lines) indicates strength of spatial relationship between the involved soil properties: (a) pH and TP, (b) OM and TP, (c) pH and OM, (d) pH and TN, (e) OM and TN, (f) TP and TN, (g) TC and bxBD, (h) pH and TC, (i) OM and TC, (j) TP and TC, (k) TN and TC, (l) pH and bxBD, (m) OM and bxBD, (n) TP and bxBD, (o) TN and bxBD.

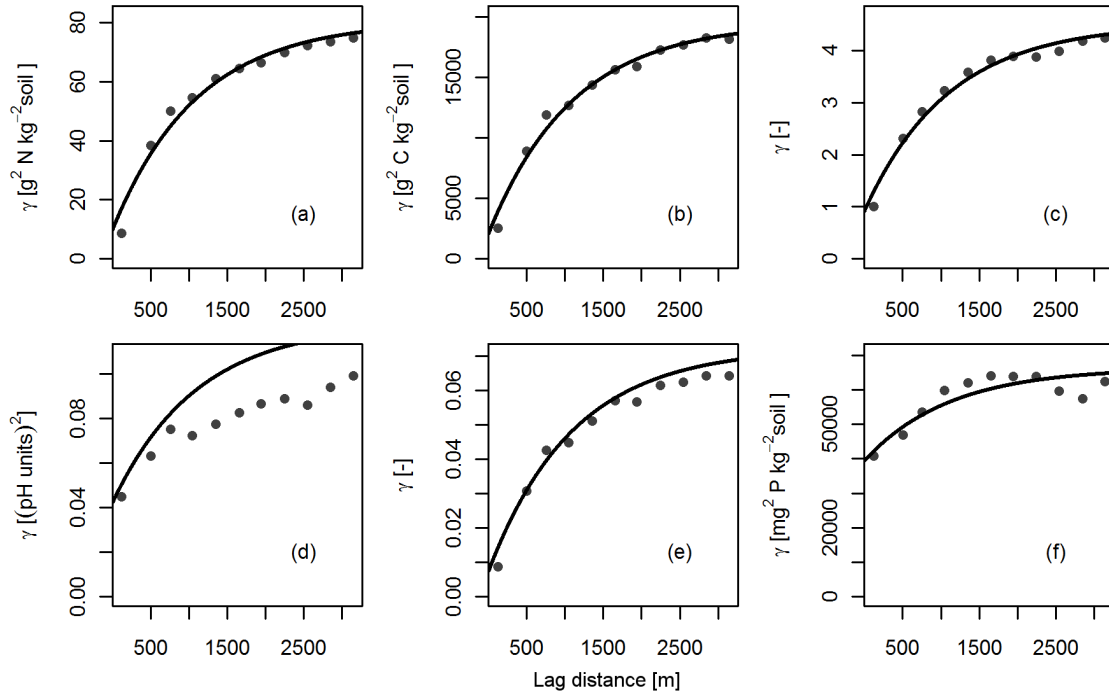


Fig. 7. Experimental autovariograms (dots) of soil properties in 0–10 cm soil depth and fitted linear model of coregionalization with exponential model of 1100 m range (line); (a) pH, (b) organic matter content, (c) total phosphorus, (d) total nitrogen, (e) total carbon, (f) bulk density transformed by box-cox transformation with power  $-0.5$ .

Codispersion coefficients calculated for a series of lag distances (Fig. 8) suggested that OM\_UP, TN\_UP, and TC\_UP were intrinsically correlated, which corresponded to the close proximity of the cross-variograms of these three variables to hulls of perfect correlation (Fig. 6) and  $\rho_{uv}^1$  of almost 1 (Table 6). Codispersion coefficients between TP\_UP and OM\_UP, TN\_UP, or TC\_UP were approximately 0.5 within the first 1000 m and then decreased below 0.4. Weak spatial relationship of TP\_UP to other variables was documented also by  $\rho_{uv}^1 < 0.5$  and  $\rho_{uv}^0 > 0.7$ . This was in accord with cross-variograms being close to pure nugget when TP\_UP was involved, and actually also the autovariogram model of TP\_UP had nugget to sill ratio almost 0.75.

The LMCR and its proximity to hulls of perfect correlation suggested moderate negative spatial correlation of PH\_UP with OM\_UP, TN\_UP, or TC\_UP ( $\rho_{uv}^1 \approx -0.5$ ) and relatively strong spatial correlation between PH\_UP and TP\_UP ( $\rho_{uv}^1 > 0.7$ ). However, experimental cross-variograms with PH\_UP, as well as the values of  $\hat{\kappa}_{uv}(\mathbf{h})$ , indicated much weaker, if any, spatial relationship of PH to the other variables.



Table 5. Parameters of linear model of coregionalization of soil properties in 0–10 cm soil depth. Model type is exponential with fixed range of 1100 m. †

Properties	Nugget	Partial sill
pH, (pH units) <sup>2</sup>	4.21×10 <sup>-2</sup>	8.05×10 <sup>-2</sup>
OM	7.30×10 <sup>-3</sup>	6.49×10 <sup>-2</sup>
TP, mg <sup>2</sup> P kg <sup>-2</sup> soil	394×10 <sup>2</sup>	269×10 <sup>2</sup>
TN, g <sup>2</sup> N kg <sup>-2</sup> soil	9.75×10 <sup>0</sup>	7.08×10 <sup>1</sup>
TC, g <sup>2</sup> C kg <sup>-2</sup> soil	2.05×10 <sup>3</sup>	1.75×10 <sup>4</sup>
bxBD	9.17×10 <sup>-1</sup>	3.60×10 <sup>0</sup>
pH and OM	7.30×10 <sup>-3</sup>	-2.83×10 <sup>-2</sup>
pH and TP	4.23×10 <sup>0</sup>	1.27×10 <sup>1</sup>
pH and TN	2.30×10 <sup>-1</sup>	-1.17×10 <sup>0</sup>
pH and TC	4.12×10 <sup>0</sup>	-1.92×10 <sup>1</sup>
pH and bxBD	-1.05×10 <sup>-1</sup>	2.10×10 <sup>-1</sup>
OM and TP	9.78×10 <sup>0</sup>	1.00×10 <sup>1</sup>
OM and TN	2.23×10 <sup>-1</sup>	2.08×10 <sup>0</sup>
OM and TC	3.51×10 <sup>0</sup>	3.31×10 <sup>1</sup>
OM and bxBD	-3.51×10 <sup>-2</sup>	-4.26×10 <sup>-1</sup>
TP and TN	4.10×10 <sup>2</sup>	4.65×10 <sup>2</sup>
TP and TC	5.80×10 <sup>3</sup>	3.98×10 <sup>3</sup>
TP and bxBD	-1.42×10 <sup>2</sup>	-9.57×10 <sup>1</sup>
TN and TC	1.25×10 <sup>2</sup>	1.10×10 <sup>3</sup>
TN and bxBD	-1.14×10 <sup>0</sup>	-1.43×10 <sup>1</sup>
TC and bxBD	-1.64×10 <sup>1</sup>	-2.23×10 <sup>2</sup>

†OM, organic matter content; TP, total phosphorus; TN, total nitrogen; TC, total carbon; bxBD, bulk density transformed by box-cox transformation with power -0.5

Table 6. Structural codispersion coefficients of each structure and variable in the linear model of coregionalization.

Properties	$\rho_{uv}^0$	$\rho_{uv}^1$
pH and OM	0.42	-0.39
pH and TP	0.10	0.27
pH and TN	0.36	-0.49
pH and TC	0.44	-0.51
pH and bxBD	-0.54	0.39
OM and TP	0.58	0.24
OM and TN	0.84	0.97
OM and TC	0.91	0.98
OM and bxBD	-0.43	-0.88
TP and TN	0.66	0.34
TP and TC	0.65	0.18
TP and bxBD	-0.75	-0.31
TN and TC	0.89	0.99
TN and bxBD	-0.38	-0.90
TC and bxBD	-0.38	-0.89

†OM, organic matter content; TP, total phosphorus; TN, total nitrogen; TC, total carbon; bxBD, bulk density transformed by box-cox transformation with power -0.5;  $\rho_{uv}^0$  and  $\rho_{uv}^1$  are structural codispersion coefficients for nugget and exponential model with 1100 m range respectively.

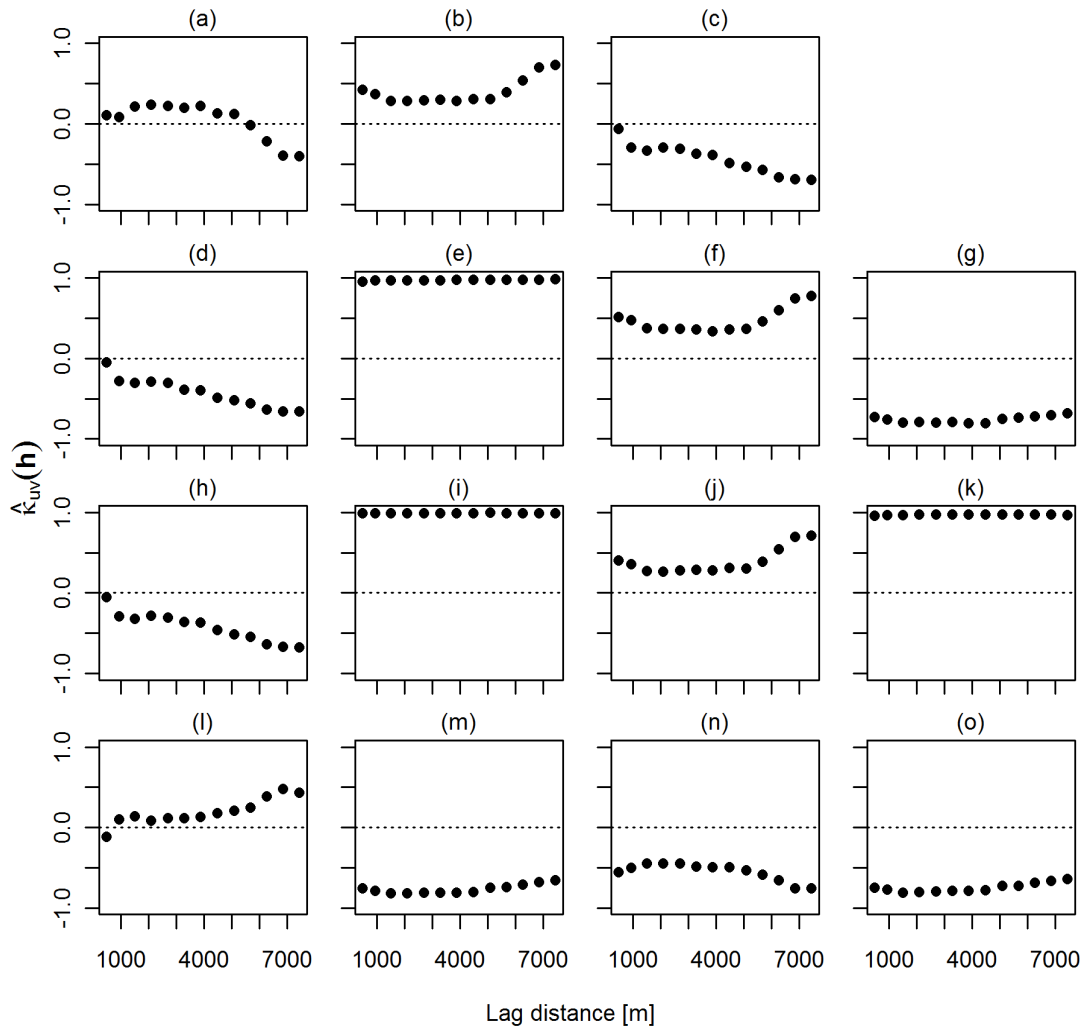


Fig. 8. Codispersion coefficients (dots) of pH, bulk density transformed by box-cox transformation with power  $-0.5$  (bxBD), organic matter content (OM), total phosphorus (TP), total nitrogen (TN), and total carbon (TC) in 0–10 cm soil depth for lag distances from 300 to 8000 m by 600 m. The dashed line is constant zero; (a) pH and TP, (b) OM and TP, (c) pH and OM, (d) pH and TN, (e) OM and TN, (f) TP and TN, (g) TC and bxBD, (h) pH and TC, (i) OM and TC, (j) TP and TC, (k) TN and TC, (l) pH and bxBD, (m) OM and bxBD, (n) TP and bxBD, (o) TN and bxBD.

Moving window correlation surfaces (Appendix C) depict spatial distribution of correlation between variables, correlation surface between TC\_UP and PH\_UP and TP\_UP is shown as an example (Fig. 9). There was a general tendency that correlation surface became smoother with increasing window size. This was caused by increasing overlap of adjacent windows. At larger scale (window size  $>750$  m), OM\_UP, TN\_UP, and TC\_UP were positively correlated. There were small patches of negative correlation in southern part of the region at smaller scale (window size  $\leq 750$  m), most pronounced near the southern boundary and when TN\_UP was one of the variables involved. Correlation coefficient surfaces for TP\_UP with the three discussed variables exhibited irregular patches of positive and negative correlation at smaller scale. With large window sizes, there was a big area of negative correlation in the northern part of the

region and near the south-eastern boundary, otherwise the correlation coefficient was positive. Correlation of TP\_UP with any other variable in smaller windows was highly patchy and patches of both strong positive and strong negative correlation were present. With increasing window size, it became more apparent that correlation (with TP\_UP) in the northern part was predominantly negative, while patches of positive correlation were more abundant in south-western part of Davis Pond. A ‘doughnut-shape’ feature in the northern part of the region was more or less distinct in all correlation surfaces, except between OM\_UP, TN\_UP, and TC\_UP. This feature was most apparent in correlation surfaces between PH\_UP and OM\_UP, TN\_UP, or TC\_UP (Fig. 9a). Correlation surface of BD\_UP with OM\_UP, TN\_UP, or TC\_UP was generally strongly negative. The correlation surface of BD\_UP and PH\_UP exhibited pattern similar to correlation surfaces of PH\_UP with any other variable, but with the opposite sign, thus predominantly negative correlation in the south and positive in the northern part. The pattern of correlation between BD\_UP and TP\_UP was very similar to the pattern of correlation between TP\_UP and OM\_UP, TN\_UP, or TC\_UP.

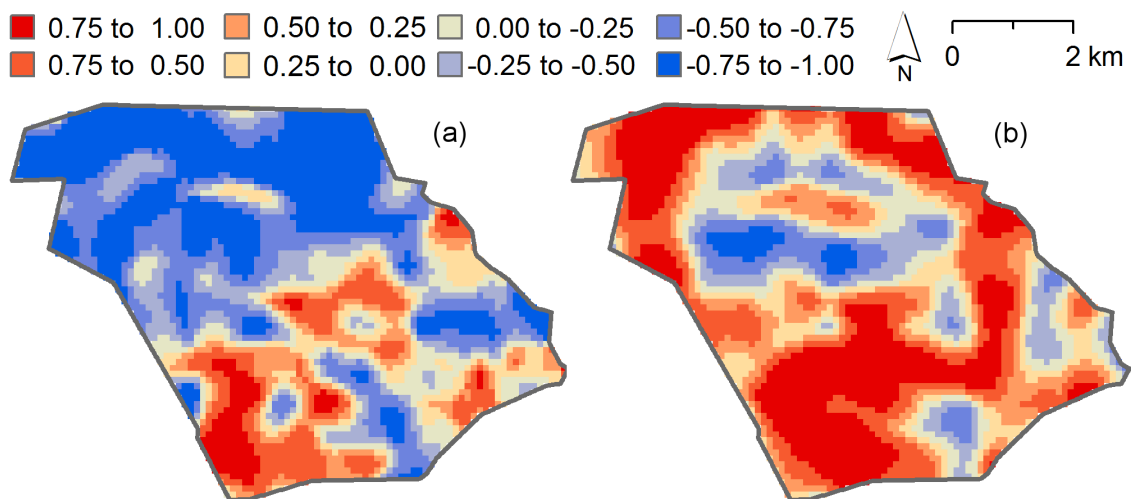


Fig. 9. Moving window correlation surfaces of (a) total carbon and pH, and (b) total carbon and total phosphorus in 0–10 cm soil depth.

## 5 Discussion

When the crevasse in the river levee occurred in 1884, a large amount of predominantly mineral material was spread over Davis Pond and settled in patches (J.R. White, personal communication, 2010). This can explain the bimodal distribution of some variables as well as absence of a spatial relationship in the lower layer. Some samples were most probably taken from areas of these highly mineral patches, while others were collected at locations that did not receive the sudden mineral material load.

All our analyses indicated very close relationships between OM\_UP, TC\_UP, and TN\_UP. These close relationships are not that surprising because C and N in marshes are present mostly in organic forms and represent considerable portion of organic matter (Mitsch and Gosselink, 2000; DeBusk et al., 2001). For simplicity, only TC\_UP is discussed further as a representative of these three variables.

Spherical model of TP\_UP with approximately 1400 m range suggested that the processes affecting TP\_UP act on finer spatial scale than processes that determine distribution of TC\_UP with practical range of the exponential model about 3700 m. The high nugget in case of TP\_UP indicated that the processes causing the high TP\_UP variability operate at distances shorter than the minimum sampling interval (100 m). This does not agree with what was found in Everglades, where TP had usually longer range than TC or TN (Grunwald and Reddy, 2008). However, no long-range spatial autocorrelation structure was found in the variogram of TP\_UP in Davis Pond. Maps of kriged values showed that TP\_UP tended to form patches of low and high values about 1400 m meters in diameter, which was coherent with the range of the spherical variogram (Webster and Oliver, 2007). Few small patches (diameter about 500 m) of very high values were present and they probably contributed to the high nugget to sill ratio of the TP\_UP variogram. High nugget resulted in high kriging variance even in close proximity of the sampling points (standard deviation about 210 mg P kg<sup>-1</sup> soil).

Spherical model of PH\_UP had the longest range (more than 4500 m) and the highest nugget to sill ratio, which indicates weak spatial autocorrelation and resulted in a kriged surface with low gradients and kriging standard deviation of about 0.25 pH units even in close proximity of the sampling points. Considering the narrow range of predicted PH\_UP (6.1 to 7.7 pH units), any conclusions about the spatial behaviour of PH\_UP are associated with high uncertainty.

The variogram of bxBD\_UP suggested that bulk density had similar spatial properties as TC\_UP, even the spatial patterns of kriged maps of bxBD\_UP and TC\_UP are obviously similar. The atypical pattern of kriging variance surface of bxBD\_UP (thus also MOIST\_UP) is a consequence of extreme skewness of the original distribution of BD\_UP and the box-cox back transformation of kriging variance.

Cross-variograms and LMCR suggested that TP\_UP was only loosely related to any of the other variables considered in this study and this was reflected in  $\hat{\kappa}_{uv}(\mathbf{h})$  and  $\rho_{uv}^s$ . Dynamics of P is likely to be determined by interactions with inorganic material more strongly than C or N (Mitsch and Gosselink, 2000). However, saying that TP\_UP is driven by abiotic processes would be an oversimplification. For example Rivero et al. (2007) found that about 2/3 of TP were in organic form in Water Conservation Area 2A, Everglades.

Pringle and Lark (2006) warn that close proximity of cross-variogram to the hull of perfect correlation may not truthfully reflect the relationship between variables and can be caused by poor fit of the LMCR. The variograms of OM\_UP, TC\_UP, and TN\_UP were almost coincident with the hulls of perfect correlation, however, the natural explanation of relationships between these three variables, strong simple correlation ( $\rho \approx 1$ ), and the shape of autovariograms make the LMCR fit reasonable.

The LMCR did not fit the autovariograms and cross-variograms with PH\_UP or TP\_UP that closely because the range of the model (1100 m) was set according to OM\_UP, TC\_UP, and TN\_UP. However, also the codispersion coefficients, which do not depend on the LMCR fit, confirmed weak spatial relationship of PH\_UP to other variables. The relationships appeared to be even weaker (Table 6) in the case of TP\_UP. Codispersion coefficients suggested that TP\_UP was more strongly correlated to TC\_UP and bxBD\_UP at shorter range. However, different choice of LMCR model and, more importantly, more sampling points separated by distances shorter than 300 m would be necessary to confirm this.

Interpretation of the moving window correlation surfaces should be done with caution. Correlation coefficient generally fails to indicate presence of other than linear relationship (De Sá, 2007). It should be remembered that  $\rho_w$  was calculated from the kriging estimates and that kriging as an interpolation technique smooths extremes towards the sample mean (Webster and Oliver, 2007). Due to spatial autocorrelation of each variable, neighbouring cells had similar values, consequently scatter-gram of two variables within a window produced often a peculiar cloud. It is the case when spatial autocorrelation complicates utilisation of otherwise commonly used statistics (Cressie, 1993). Furthermore, kriging variance was not utilized to express any level of confidence about  $\rho_w$ . Smoothing of the correlation surface with increasing window size is explained in section 4. Although  $\rho_w$  can help to interpret properties of two raster surfaces, it cannot be recommended as a rigorous tool for exploration of the local spatial relationships between variables. Nevertheless, two major trends were interesting.

Negative  $\rho_w$  of PH\_UP and TC\_UP occurred in the northern part with generally higher PH\_UP. In the southern part, with predicted PH\_UP values mostly below 7, areas of positive correlation were present. Association of rather acidic conditions with organic matter could be explained by higher concentrations of humic substances coming from the microbial degradation of dead plant tissues (Reddy and DeLaune, 2008).

On the other hand, maps and correlation surfaces showed that areas of high organic matter content were associated with high moisture content which implies reduced conditions and consequently higher pH.

Another striking property of most correlation surfaces was the presence of the 'doughnut-shape' feature in the north, where was an area of continuously low values of TC\_UP. Perhaps the constellation of this cold spot of TC resulted in this distinct feature. The relationship between TC\_UP and TP\_UP in the northern part may be more affected by the river water because the water inlet is in the north. As already mentioned, high estimated standard deviation of PH\_UP implies high level of uncertainty associated with conclusions about PH\_UP and the same is true for TP\_UP.

The similar pattern of correlation surface between any variable versus TC\_UP, OM\_UP, or TN\_UP and correlation surface of that variable versus bxBD\_UP can be expected because bulk density was strongly negatively correlated with TC\_UP, as documented also by the correlation surface of TC\_UP and bxBD\_UP.

Absence of spatial autocorrelation in the lower layer does not allow for many insights and makes interpolation in this layer by any method unreasonable. However, spatial continuity in the upper layer suggests that the freshwater intrusion plays an important role in interactions of the studied variables. Although there is no direct evidence that this spatial continuity has been developed because of the water inlet, we assume that the river water carrying nutrients and sediments also mobilises material at the surface of the marsh and redistributes it. Transport and redistribution are likely to be the primary forces that are amplified by freshwater intrusion. Higher mobility and influx of sediment and nutrients alter the rates of more complicated processes related to microbial activity and vegetation communities. Although these processes are crucial for marsh accretion, it is impossible to judge the influence of freshwater intrusion on these complex interactions based on our results. Links to biogeochemistry or vegetation are also missing in other recent studies that assess the impact of freshwater intrusion on marsh accretion (DeLaune et al., 2003; Boustany, 2010).

The accretion rate of Louisiana marshes is driven predominantly by organic matter accumulation (DeLaune et al., 2003) which is again determined by the level of primary production and rate of OM decomposition. Information about vegetation should be therefore recorded and analysed together with soil properties in future research. Corstanje et al. (2006) also suggested that inclusion of an up-to-date vegetation map would be beneficial for further research in Everglades.

Comparison of results from Davis Pond with other marshes is not straightforward for two reasons. One is the uniqueness of hydrologic conditions in each marsh (Mitsch and Gosselink, 2000), the second is of methodological nature. Davis Pond has been receiving river water since 2002, which strongly altered the hydrologic regime. Geostatistical studies investigating freshwater marsh under similar conditions have not been published yet. Although studies of the same soil properties exist, mainly from the

Everglades, the hydrologic regime and the objectives of protection or restoration plans differ. Furthermore, researches often use different data transformations to fit variograms and, more importantly, different sampling densities. Also the size of the area of interest varies widely. Sampling density in Davis Pond ( $0.0375 \text{ ha}^{-1}$ ) was closer to the level of studies from Everglades (sampling density about  $0.002 \text{ ha}^{-1}$ ) than to the studies of individual fields with sampling densities several orders higher than  $1 \text{ ha}^{-1}$  (Grunwald and Reddy, 2008). Different sampling density, minimum distance between sampling points and in practice also the size of the study area affect the scale of autocorrelation structures that can be revealed. Taking Everglades as an example, spatial continuity of soil properties was studied in individual conservation areas at scale of several kilometres (Bruland et al., 2006; Corstanje et al., 2006; Grunwald et al., 2006; Rivero et al., 2007; Grunwald and Reddy, 2008), but the variograms changed considerably at regional scale of tens of kilometres (Corstanje et al., 2008). This makes it difficult to generalize soil properties from individual marshes and compare independent studies.

Variogram parameter estimation in this study was based on classical geostatistics and the method of moments. Studies from Everglades generally adopted the same approach (Bruland et al., 2006; Corstanje et al., 2006; Grunwald et al., 2006; Rivero et al., 2007; Corstanje et al., 2008; Grunwald and Reddy, 2008). The classical approach brings in the need to make several arbitrary decisions. Perhaps the most critical are the choice of breaks for the experimental variogram, the choice of estimator type (method of moments or robust estimators), and the choice of weightings for the fitting procedure. Rather pragmatic attitude is generally recommended in the literature, when the decisions are made based on visual impression and trial (Clark, 1979; Webster and Oliver, 2007) or (cross-)validation (Lark, 2000). ML methods reduce the need for arbitrary decisions (Diggle et al., 2003; Chai et al., 2008). In the original form, ML methods rely on the assumption of normal distribution of residuals from the structural component (Cressie, 1993), but robust ML method of variogram parameter estimation has been proposed (Marchant and Lark, 2007c) and even LMCR parameters have been estimated by ML method (Marchant and Lark, 2007a). These, however, have not yet been implemented in generally available software. Our experience was that the procedure that implements REML in GeoR (Ribeiro and Diggle, 2001) was extremely sensitive to the initial settings of the range parameter and usually did not alter the initial range and converged to the same maximized likelihood value as for different initial settings. The numerical complexity of ML methods represents major challenge for practical application, but the theoretical background of ML methods (Cressie, 1993; Diggle et al., 2003) provides a vital alternative to the classical approach and we recommend them as a way forward.

It is worth to mention several observations in case that sampling in Davis Pond should be repeated to assess changes in soil properties and possibly develop a framework for monitoring of similar systems. Optimized sampling design for geostatistical analysis ensures relatively uniform coverage of the region, which is beneficial for kriging, but also provides sufficient variety in lag instances for variography (Lark, 2002; Marchant and Lark, 2007b; Webster and Oliver, 2007). The optimization is in principle based on



minimization of kriging variance and the variance arising from the variogram uncertainty (Burrough and McDonnell, 2000; Marchant and Lark, 2007b). The constellation of sampling points for this study was designed using SSA with the variogram models of TP from Everglades, because no variogram from Davis Pond was available (R. Corstanje, personal communication, 2010). Final sampling design contained 10 point pairs separated by 100 m. Paradoxically, variograms of TC\_UP, OM\_UP, TN\_UP, and bulk density were successfully depicted, but TP\_UP had high nugget. PH\_UP is even more challenging variable as it had both high nugget and long range. We suggest using similar approach for ongoing sampling campaigns, but taking one additional sample 50 m from one of the points in the pairs separated by 100 m (Fig. 10). This form of nested sampling is not the most efficient from the kriging perspective, but we expect it would substantially help to describe the short range variability and to lower the nugget of TP\_UP and PH\_UP variograms. Another option is to perform new SSA based on variograms presented in this paper. The high nugget of TP\_UP variogram may be partly caused by different behaviour of organic and inorganic forms of P (Grunwald et al., 2006). Rather than investing resources into gathering even more samples, we assume that differentiation of TP into organic and inorganic fraction would help to understand P dynamics in Davis Pond.

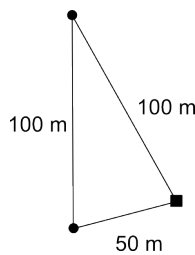


Fig. 10. Concept of recommended extension of sampling design for future sampling in Davis Pond. Black circles represent the original points, black square is the newly added sampling point.

Material presented in this paper can be used to formulate hypotheses about soil properties in Davis Pond. The distinct cold spot on maps of TC\_UP, OM\_UP, and TN\_UP brings doubts whether stationarity is a reasonable assumption. Testing stationarity requires sample size much larger than are realistic requirements for Davis Pond (Corstanje et al., 2008). However, it is the northern part that should be sampled with higher density if stratified sampling is concerned.

## 6 Conclusions

The results presented in this study set a first benchmark for soil dynamics monitoring in Davis Pond. OM, TC, and TN in 0–10 cm soil depth exhibited similar spatial pattern with distinct area of low values in the northern part of Davis Pond and were highly correlated at all spatial scales. These three variables were also highly spatially correlated with BD. Very strong linear relationship was found between moisture and BD, map of BD was produced by kriging and the linear relationship was used to map moisture. We explain these relationships by the role of vegetation in marsh ecosystems.

Accumulation of dead plant tissues as soil organic matter, in which C and N represent abundant elements, leads to low bulk density and consequently high moisture. Distribution of TP was driven by processes that act at finer spatial scale (practical range 1400 m) than in the case of OM, TN, TC (practical range 3300 m), and BD (practical range 2700 m) in 0–10 cm soil depth. TP was highly variable even at distances shorter than the minimum sampling interval (100 m) and correlation with any of the other variables was low at all spatial scales. We expect that differentiation of TP into organic and inorganic fraction and taking 10 more samples in the near range would help to explain the short range variability and to understand the dynamics of P in Davis Pond. High nugget to sill ratio in the case of TP and pH in 0–10 cm soil depth resulted in high uncertainty associated with interpolated values. Spatial correlation of pH with any of the other variables was low and the role of pH remains unclear. However, variogram of pH suggested that, although weakly, pH was autocorrelated within Davis Pond (range of 4500 m). No spatial relationships were found in 10–20 cm soil depth. Therefore, interpolation in the lower layer was not performed.

## **7 Acknowledgements**

The authors would like to thank Dr John R. White and his team from the Department of Oceanography and Coastal Sciences, Louisiana State University, who kindly provided the data set and support throughout this study.

## References

- Allison, M.A., and E.A. Meselhe. 2010. The use of large water and sediment diversions in the lower Mississippi River (Louisiana) for coastal restoration. *J. Hydrol.* 387:346–360.
- Barras, J.A. 2006. Land area change in coastal Louisiana after the 2005 hurricanes: A series of three maps [Online] Available at <http://pubs.usgs.gov/of/2006/1274/> (verified 27 Aug. 2010).
- Bishop, T.F.A., and R.M. Lark. 2008. A comparison of parametric and non-parametric methods for modelling a coregionalization. *Geoderma* 148:13–24.
- Boustany, R.G. 2010. Estimating the benefits of freshwater introduction into coastal wetland ecosystems in Louisiana: Nutrient and sediment analyses. *Ecological Restoration* 28:160–174.
- Bruland, G.L., and C.J. Richardson. 2005. Spatial variability of soil properties in created, restored, and paired natural wetlands. *Soil Sci. Soc. Am. J.* 69:273–284.
- Bruland, G.L., S. Grunwald, T. Z. Osborne, K. R. Reddy, and S. Newman. 2006. Spatial distribution of soil properties in Water Conserv. Area 3 of the Everglades. *Soil Sci. Soc. Am. J.* 70:1662–1676.
- Burrough, P.A., and R. McDonnell. 2000. Principles of geographical information systems. Oxford University Press, New York.
- Carroll, Z.L., and M.A. Oliver. 2005. Exploring the spatial relations between soil physical properties and apparent electrical conductivity. *Geoderma* 128(3–4 SPEC. ISS.):354–374.
- Chai, X., C. Shen, X. Yuan, and Y. Huang. 2008. Spatial prediction of soil organic matter in the presence of different external trends with REML-EBLUP. *Geoderma* 148:159–166.
- Clark, I. 1979. Practical Geostatistics. Geostokos Limited, Alloa, UK.
- Conley, D.J., H.W. Paerl, R.W. Howarth, D.F. Boesch, S.P. Seitzinger, K.E. Havens, C. Lancelot, and G.E. Likens. 2009. Ecology - controlling eutrophication: Nitrogen and phosphorus. *Science* 323:1014–1015.
- Corstanje, R., S. Grunwald, and R.M. Lark. 2008. Inferences from fluctuations in the local variogram about the assumption of stationarity in the variance. *Geoderma* 143:123–132.
- Corstanje, R., S. Grunwald, K.R. Reddy, T.Z. Osborne, and S. Newman. 2006. Assessment of the spatial distribution of soil properties in a northern Everglades marsh. *J. Environ. Qual.* 35:938–949.
- Cressie, N.A.C. 1993. Statistics for spatial data, revised edition. John Wiley & Sons, New York.

- Day, J.W., J.E. Cable, J.H. Cowan, R. DeLaune, K. DeMutsert, B. Fry, H. Mashriqui, D. Justic, P. Kemp, R.R. Lane, J. Rick, L.P. Rozas, G. Snedden, E. Swnsone, R.R. Twilley, and B. Wissel. 2009. The impacts of pulsed reintroduction of river water on a Mississippi delta coastal basin, *J. Coastal Res.* SI(54)225–243.
- DeBusk, W.F., J.R. White, and K.R. Reedy. 2001. Carbon and nitrogen dynamics in wetland soils. p. 27–48. *In* M.J. Shaffer et al. (ed.) *Modeling carbon and nitrogen dynamics for soil management*. CRC Press, Boca Raton, FL.
- DeLaune, R.D., C.B. Johnson, R.P. Gambrell, and A. Jugsujinda. 2008. Export of dissolved organic carbon from a ponded freshwater marsh receiving diverted Mississippi River water. *TheScientificWorldJournal* 8:1210–1216.
- DeLaune, R.D., A. Jugsujinda, G.W. Peterson, and W.H. Patrick, Jr. 2003. Impact of Mississippi River freshwater reintroduction on enhancing marsh accretionary processes in a Louisiana estuary. *Estuarine, Coastal and Shelf Sci.* 58:653–662.
- DeLaune, R.D., A. Jugsujinda, J.L. West, C.B. Johnson, and M. Kongchum. 2005. A screening of the capacity of Louisiana freshwater wetlands to process nitrate in diverted Mississippi River water. *Ecological Engineering* 25:315–321.
- De Sá, J.P.M. 2007. *Applied statistics using SPSS, STATISTICA, MATLAB and R*. Springer-Verlag, Heidelberg, Germany.
- Diggle, P.R., P.J. Ribeiro, Jr., and O.F. Christensen. 2003. An introduction to model based geostatistics. p. 43–86. *In* J. Moller (ed.) *Spatial Statistics and Computational Methods*. Lecture notes in statistics. 137. Springer-Verlag, New York.
- Dodds, W.K. 2006. Nutrients and the "dead zone": The link between nutrient ratios and dissolved oxygen in the northern Gulf of Mexico. *Frontiers in Ecology and the Environ.* 4:211–217.
- Emery, X. 2010. Iterative methods of fitting linear model of coregionalization. *Comput. Geosci.* 36:1150–1160.
- Engle, V.D., J.K. Summers, and J.M. Macauley. 1999. Dissolved oxygen conditions in northern Gulf of Mexico estuaries. *Environ. Monitoring and Assessment* 57:1–20.
- Ensminger, A. and C. Simon. 1993. Vegetative delineation report, Davis Pond Freshwater Diversion Project (BA-1) [Online]. Available at <http://dnr.louisiana.gov/crm/D%20R%20S%20Reports/Contracted%20Study2/BA-01%20VDR.pdf> (verified 25 July 2010).
- ESRI. 1999–2009. ArcGIS Desktop Geographical Information system, version 9.3.1. ESRI, Redlans, CA.
- Evers, D.E., J.G. Gosselink, C.E. Sasser, and J.M. Hill. 1992. Wetland loss dynamics in southwestern Barataria basin, Louisiana (USA), 1945–1985. *Wetlands Ecology and Management* 2:103–118.
- Fennessy, M.S., and W.J. Mitsch. 2001. Effects of hydrology on spatial patterns of soil development in created riparian wetlands. *Wetlands Ecology and Management* 9:103–120.

- Fortner, B. 2000. Mississippi diversion. *Civil Engineering* 70:46–51.
- French, J.R., T. Spencer, A.L. Murray, and N.S. Arnold. 1995. Geostatistical analysis of sediment deposition in two small tidal wetlands, Norfolk, UK. *J. Coastal Res.* 11:308–321.
- Gardner, L.M., and J.R. White. 2010. Denitrification enzyme activity as an indicator of nitrate movement through a diversion wetland. *Soil Sci. Soc. Am. J.* 74:1037–1047.
- Goovaerts, P. 1992. Factorial kriging analysis: A useful tool for exploring the structure of multivariate spatial soil information. *J. Soil Sci.* 43:597–619.
- Goovaerts, P. 1999. *Geostatistics for natural resources evaluation*. Oxford University Press, New York.
- Grunwald, S., R. Corstanje, B.E. Weinrich, and K.R. Reddy. 2006. Spatial patterns of labile forms of phosphorus in a subtropical wetland. *J. Environ. Qual.* 35:378–389.
- Grunwald, S., and K.R. Reddy. 2008. Spatial behavior of phosphorus and nitrogen in a subtropical wetland. *Soil Sci. Soc. Am. J.* 72:1174–1183.
- Gutknecht, J.L. M., R.M. Goodman, and T.C. Balsler. 2006. Linking soil process and microbial ecology in freshwater wetland ecosystems. *Plant Soil* 289:17–34.
- Hatton, R.S., R.D. Delaune, and W.H. Patrick Jr. 1983. Sedimentation, accretion, and subsidence in marshes of Barataria basin, Louisiana. *Limnol. Oceanogr.* 28:494–502.
- Isaaks, E.H., and R.M. Srivastava. 1989. *An introduction to applied geostatistics*. Oxford University Press, New York.
- Kayranli, B., M. Scholz, A. Mustafa, and Å Hedmark. 2010. Carbon storage and fluxes within freshwater wetlands: A critical review. *Wetlands* 30:111–124.
- Kerry, R., and M.A. Oliver. 2007. Comparing sampling needs for variograms of soil properties computed by the method of moments and residual maximum likelihood. *Geoderma* 140:383–396.
- Lark, R.M. 2000. A comparison of some robust estimators of the variogram for use in soil survey. *Eur. J. Soil Sci.* 51:137–157.
- Lark, R.M. 2002. Optimized spatial sampling of soil for estimation of the variogram by maximum likelihood. *Geoderma* 105:49–80.
- Lark, R.M., and A. Papritz. 2003. Fitting a linear model of coregionalization for soil properties using simulated annealing. *Geoderma* 115:245–260.
- Lark, R.M., and R. Webster. 2006. Geostatistical mapping of geomorphic variables in the presence of trend. *Earth Surf. Processes Landforms* 31:862–874.
- Lindquist, D.C., and R.M. Summer. 2007. *Coastal Restoration Annual Project Reviews: December 2007*. Louisiana Dep. of Nat. Resources, Baton Rouge, LA.
- LNDR. 2005. *Davis Pond freshwater diversion project*. Louisiana Dep. of Nat. Resources, Baton Rouge, LA.

- LDNR. 2009. Louisiana coastal facts [Online] Available at <http://dnr.louisiana.gov/crm/webfactsheet09-14-2009.pdf> (verified 14 Mar. 2010).
- LNDR. 2010. BA-01 Davis Pond Freshwater Diversion [Online]. Available at <http://dnr.louisiana.gov/crm/coastres/project.asp?id=BA-01> (verified 18 June 2010).
- Marchant, B.P., and R.M. Lark. 2007a. Estimation of linear models of coregionalization by residual maximum likelihood. *Eur. J. Soil Sci.* 58:1506–1513.
- Marchant, B.P., and R.M. Lark. 2007b. Optimized sample schemes for geostatistical surveys. *Mathematical Geol.* 39:113–134.
- Marchant, B.P., and R.M. Lark. 2007c. Robust estimation of the variogram by residual maximum likelihood. *Geoderma* 140:62–72.
- Mitsch, W.J., and J.R. Gosselink. 2000. *Wetlands*. 3rd ed. John Wiley & Sons, New York.
- Pebesma, E.J. 2004. Multivariable geostatistics in S: the gstat package. *Comput. Geosci.* 30:683–691.
- Pringle, M.J., and R.M. Lark. 2006. Spatial analysis of model error, illustrated by soil carbon dioxide emissions. *Vadose Zone J.* 5:168–183.
- R Development Core Team. 2010. *R: A language and environment for statistical computing version 2.11.1*. R Foundation for Statistical Comput., Vienna, Austria.
- Rabalais, N.N., R.E. Turner, W.J. Wiseman, Jr., and Q. Dortch. 1998. Consequences of the 1993 Mississippi River flood in the Gulf of Mexico. *River Res. and Applications* 14:161–177.
- Reddy, K.R., and R.D. DeLaune. 2008. *Biogeochemistry of wetlands: Sci. and applications*. CRC Press, Boca Raton, FL.
- Reed, D.J. 1989. Patterns of sediment deposition in subsiding coastal salt marshes, Terrebonne bay, Louisiana: The role of winter storms. *Estuaries* 12:222–227.
- Ribeiro, P.J., Jr., and P.J. Diggle. 2001. GeoR: A package for geostatistical analysis. *R-NEWS* 1(2):15–18.
- Richards, J.A., and X. Jia. 1999. *Remote sensing digital image analysis: An introduction*. 3rd ed. Springer-Verlag, Berlin, Germany.
- Rivero, R.G., S. Grunwald, T.Z. Osborne, K.R. Reddy, and S. Newman. 2007. Characterization of the spatial distribution of soil properties in water Conserv. Area 2A, Everglades, Florida. *Soil Sci.* 172:149–166.
- Smith, M.J., E.S.G. Schreiber, M. Kohout, K. Ough, R. Lennie, D. Turnbull, C. Jin, and T. Clancy. 2007. Wetlands as landscape units: Spatial patterns in salinity and water chemistry. *Wetlands Ecology and Management* 15:95–103.
- Taylor, J.C., G.A. Wood, R. Earl, and R.J. Godwin. 2003. Soil factors and their influence on within-field crop variability, part II: Spatial analysis and determination of management zones. *Biosystems Engineering* 84:441–453.

- Turner, R.E., and D.R. Cahoon (ed.) 1987. Causes of wetland loss in the coastal central Gulf of Mexico. Vol. I: Executive Summary. Miner. Management Serv., New Orleans, LA.
- Turner, R.E., and N.N. Rabalais. 1994. Coastal eutrophication near the Mississippi river delta. *Nature* 368:619–621.
- Turner, R.E., N.N. Rabalais, R.B. Alexander, G. McIsaac, and R.W. Howarth. 2007. Characterization of nutrient, organic carbon, and sediment loads and concentrations from the Mississippi River into the northern Gulf of Mexico. *Estuaries and Coasts* 30:773–790.
- USEPA. 1993. Methods for determination of inorganic substances in environmental samples. Environmental Monitoring Systems Lab, Cincinnati, OH, USA.
- USGS. 2003. 100+ years of land change for coastal Louisiana [Online]. USGS National Wetland Res. Center, Lafayette, LA. Available at <http://www.nwrc.usgs.gov/upload/landloss11X17.pdf>, (verified 14 Apr. 2010).
- USGS. 2010. USGS Real-time water data for USGS 295501090190400 Davis Pond Freshwater Diversion near Boutte, LA [Online]. Available at [http://waterdata.usgs.gov/nwis/dv?cb\\_00055=on&cb\\_63160=on&cb\\_00060=on&format=gif\\_default&begin\\_date=2006-11-19&end\\_date=2007-09-19&site\\_no=295501090190400&referred\\_module=sw](http://waterdata.usgs.gov/nwis/dv?cb_00055=on&cb_63160=on&cb_00060=on&format=gif_default&begin_date=2006-11-19&end_date=2007-09-19&site_no=295501090190400&referred_module=sw) (verified 23 June 2010).
- Van Groenigen, J.W. 2000. The influence of variogram parameters on optimal sampling schemes for mapping by kriging. *Geoderma* 97:223–236.
- Van Groenigen, J.W., W. Siderius, and A. Stein. 1999. Constrained optimisation of soil sampling for minimisation of the kriging variance. *Geoderma* 87:239–259.
- Wackernagel, H. 2003. *Multivariate geostatistics*. Springer-Verlag, Berlin, Germany.
- Webster, R., and M.A. Oliver. 2007. *Geostatistics for Environmental Scientists*. John Wiley & Sons, Chichester, UK.

## Appendix A Explanatory Data Analysis

Table A.1 shows summary statistics for all the soil properties included in this study, thus moisture (MOIST), bulk density (BD), pH (PH), organic matter content (OM), content of total phosphorus (TP), content of total nitrogen (TN), and content of total carbon (TC), from 0–10 cm (UP) and 10–20 cm (LW) soil depth, bxBD is BD transformed by box-cox transform with power  $-0.5$ . All results presented are without the three sampling points that were excluded as outliers, hence number of observations is 139. Data distribution properties and deviations from normal distribution were investigated visually by histograms (Fig. A.1) and quantile-quantile plots (Fig. A.2) and by Shapiro-Wilk test of normality (Table A.2). Only pH in both layers and TP in the lower layer followed normal distribution, the P value for TP\_UP was 0.009. Relationships between soil properties not regarding the spatial domain are expressed by Pearson's product moment correlation coefficients and Spearman's rank correlation coefficients (Table A.3) and visually on scatter-grams (Fig. A.3) which can be found also on the enclosed CD. Spearman's rank correlation coefficient should perform better as a measure of correlation when the relationship is non-linear (De Sá, 2007). However, both types of correlation coefficient returned similar values (Table A.3).

Table A.1. Summary statistics of soil properties obtained from 139 samples. †

Property	Layer	Units	Min	Q1	Median	Mean	Q3	Max.	Sd	Skw
MOIST	UP	proportion	0.58	0.89	0.92	0.90	0.94	0.98	0.08	-2.07
BD	UP	g cm <sup>-3</sup>	0.03	0.06	0.08	0.12	0.12	0.55	0.10	2.32
PH	UP	PH units	6.07	6.83	7.09	7.04	7.24	7.72	0.31	-0.41
OM	UP	proportion	0.08	0.39	0.65	0.59	0.80	0.93	0.25	-0.49
TP	UP	mg P kg <sup>-1</sup> soil	359.60	842.00	961.80	942.50	1073.00	1521.00	235.47	-0.37
TN	UP	g N kg <sup>-1</sup> soil	2.52	12.28	21.64	19.48	26.66	34.32	8.71	-0.44
TC	UP	g C kg <sup>-1</sup> soil	26.38	184.90	319.50	292.10	407.40	499.20	134.85	-0.43
bxBD	UP	N/A	-10.02	-6.04	-5.03	-4.88	-3.77	-0.69	1.96	-0.01
MOIST	LW	proportion	0.36	0.79	0.91	0.84	0.93	0.98	0.15	-1.72
BD	LW	g cm <sup>-3</sup>	0.02	0.07	0.09	0.20	0.23	0.98	0.24	2.09
PH	LW	PH units	5.90	6.67	6.97	6.92	7.19	8.13	0.36	-0.01
OM	LW	proportion	0.09	0.32	0.72	0.60	0.87	0.93	0.30	-0.50
TP	LW	mg P kg <sup>-1</sup> soil	331.80	577.60	715.90	713.50	832.50	1163.00	191.38	0.13
TN	LW	g N kg <sup>-1</sup> soil	1.34	9.69	23.76	19.62	28.19	34.94	10.27	-0.50
TC	LW	g C kg <sup>-1</sup> soil	17.77	148.10	358.40	298.20	441.50	495.90	160.89	-0.48

†MOIST, moisture; BD, bulk density; OM, organic matter content; TP, total phosphorus; TN, total nitrogen; TC, total carbon; bxBD, bulk density transformed by box-cox transformation with power  $-0.5$ ; UP, 0–10 cm soil depth; LW, 10–20 cm soil depth; Min, minimum; Q1, first quartile; Q3, third quartile; Max, maximum; Sd, standard deviation; Skw, skewness.



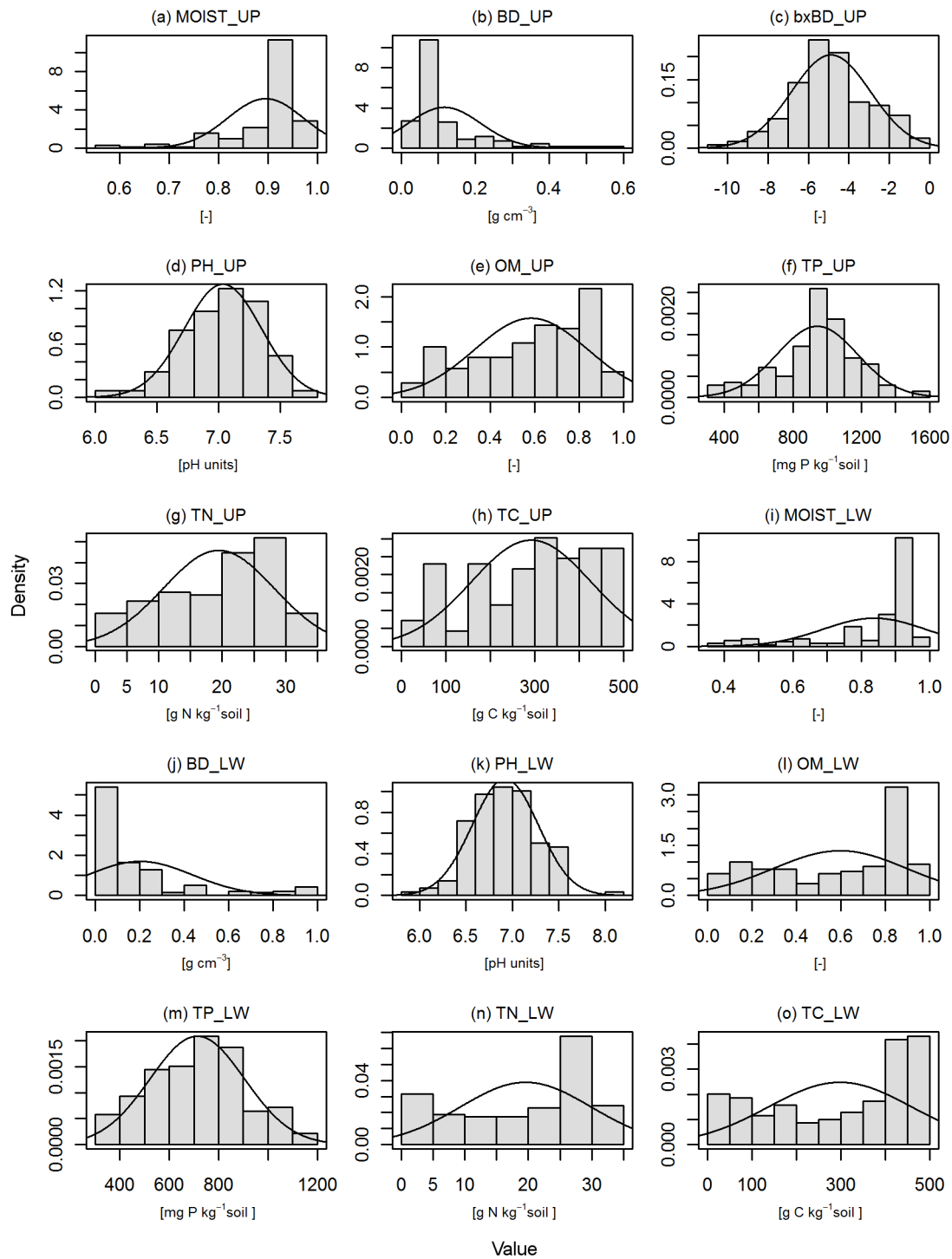


Fig. A.1. Histograms of moisture (MOIST), bulk density (BD), bulk density transformed by box-cox transformation with power  $-0.5$  (bxBD), pH (PH), organic matter content (OM), total phosphorus (TP), total nitrogen (TN), and total carbon (TC) in 0–10 cm ( $\_UP$ , a to h) and 10–20 cm ( $\_LW$ , i to o) soil depth with probability density function of normal distribution with mean and standard deviation of the sample superimposed.

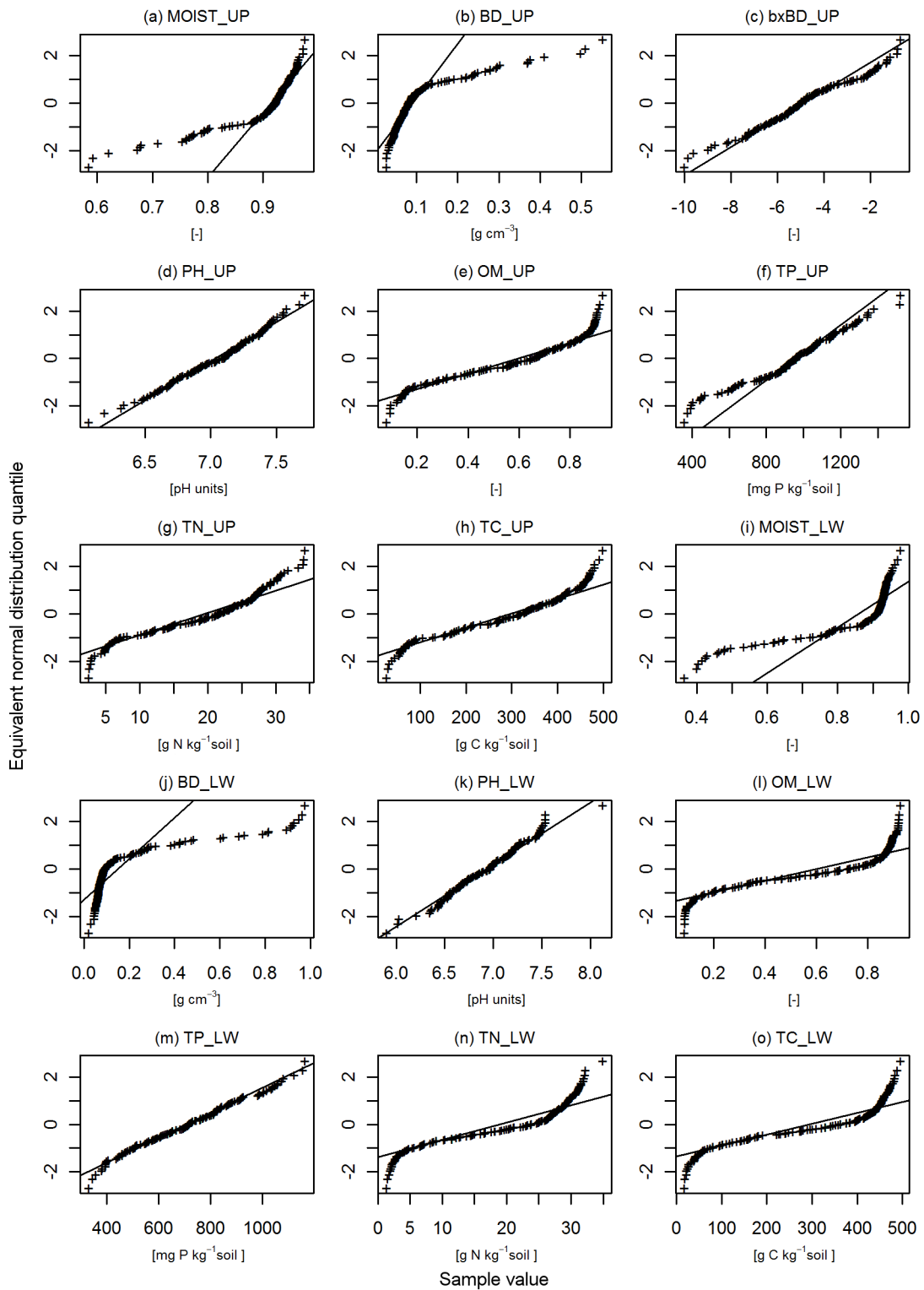


Fig. A.2. Normal distribution quantile-quantile plots of soil moisture (MOIST), bulk density (BD), bulk density transformed by box-cox transformation with power  $-0.5$  (bxBD), pH (PH), organic matter content (OM), total phosphorus (TP), total nitrogen (TN), and total carbon (TC) in 0–10 cm ( $_{UP}$ , a to h) and 10–20 cm ( $_{LW}$ , i to o) soil depth.

Table A.2. Results of Shapiro-Wilk normality test.†

Property	Soil depth			
	0–10 cm		10–20 cm	
	Shapiro W statistics	P value	Shapiro W statistics	P value
Moisture	0.744	0.000	0.718	0.000
Bulk density	0.703	0.000	0.649	0.000
pH	0.986	0.155‡	0.988	0.241‡
Organic matter content	0.920	0.000	0.850	0.000
Total phosphorus	0.974	0.009	0.986	0.183‡
Total nitrogen	0.938	0.000	0.881	0.000
Total carbon	0.937	0.000	0.863	0.000

† Sample size was 139.

‡ P value > 0.05

Table A.3. Correlation coefficients between soil properties. Lower triangle contains Pearson's product moment correlation coefficients, upper triangle contains Spearman's rank correlation coefficients.†

	MT <sub>U</sub>	BD <sub>U</sub>	PH <sub>U</sub>	OM <sub>U</sub>	TP <sub>U</sub>	TN <sub>U</sub>	TC <sub>U</sub>	MT <sub>L</sub>	BD <sub>L</sub>	PH <sub>L</sub>	OM <sub>L</sub>	TP <sub>L</sub>	TN <sub>L</sub>	TC <sub>L</sub>
MT <sub>U</sub>	1	-0.98	-0.12	0.76	0.46	0.75	0.75	0.57	-0.56	0.15	0.46	0.29	0.47	0.48
BD <sub>U</sub>	-0.99	1	0.14	-0.78	-0.45	-0.76	-0.77	-0.58	0.59	-0.11	-0.49	-0.28	-0.49	-0.50
PH <sub>U</sub>	-0.25	0.27	1	-0.36	0.18	-0.36	-0.35	-0.23	0.25	0.53	-0.38	0.06	-0.36	-0.37
OM <sub>U</sub>	0.79	-0.78	-0.39	1	0.26	0.96	0.99	0.59	-0.57	-0.16	0.68	0.20	0.67	0.69
TP <sub>U</sub>	0.44	-0.42	0.16	0.31	1	0.34	0.26	0.34	-0.33	0.22	0.23	0.58	0.29	0.26
TN <sub>U</sub>	0.79	-0.78	-0.39	0.97	0.38	1	0.97	0.60	-0.58	-0.15	0.67	0.26	0.72	0.71
TC <sub>U</sub>	0.78	-0.77	-0.38	0.99	0.30	0.97	1	0.57	-0.55	-0.15	0.65	0.19	0.66	0.69
MT <sub>L</sub>	0.43	-0.43	-0.34	0.50	0.35	0.52	0.48	1	-0.96	-0.10	0.82	0.64	0.81	0.83
BD <sub>L</sub>	-0.42	0.43	0.33	-0.47	-0.34	-0.49	-0.45	-0.99	1	0.12	-0.80	-0.59	-0.79	-0.81
PH <sub>L</sub>	0.01	0.02	0.47	-0.20	0.21	-0.19	-0.19	-0.25	0.23	1	-0.32	0.02	-0.29	-0.30
OM <sub>L</sub>	0.50	-0.50	-0.41	0.69	0.25	0.69	0.67	0.84	-0.78	-0.37	1	0.46	0.92	0.97
TP <sub>L</sub>	0.27	-0.26	0.08	0.19	0.59	0.24	0.17	0.62	-0.58	0.04	0.49	1	0.54	0.48
TN <sub>L</sub>	0.50	-0.50	-0.40	0.68	0.29	0.69	0.66	0.84	-0.79	-0.35	0.98	0.54	1	0.95
TC <sub>L</sub>	0.50	-0.50	-0.41	0.70	0.25	0.70	0.68	0.83	-0.78	-0.36	1.00	0.49	0.99	1

† MT, moisture; BD, bulk density; PH, pH; OM, organic matter content; TP, total phosphorus; TN, total nitrogen; TC, total carbon; index U and L refers to 0–10 cm and 10–20 cm soil depth respectively.

When spatial trend (external drift) affects the investigated variable, assumption of stationarity is not valid. One method used to obey with trend is to fit a polynomial surface to the data, subtract it from the original values, fit a variogram model and kriging the residuals, and finally add the trend surface to the kriging estimates (Isaaks and Srivastava, 1989; Webster and Oliver, 2007). This method is equivalent to universal kriging if all the data points are used in the kriging procedure (Lark and Webster, 2006; Webster and Oliver, 2007). Isaaks and Srivastava (1989) point out that fitting a

polynomial surface directly to the data may not produce sensible trend surface coherent with nature of the trend. The problem is mainly that the estimated trend surface parameters have associated some error with them as well, and that the estimates of variogram of the residuals is underestimated, particularly for increasing lag distances (Lark and Webster, 2006). This makes it impossible to obtain unbiased estimates of the kriging variance and residual maximum likelihood method (REML) is suggested as a way forward. Lark and Webster (2006) demonstrated that kriging estimates obtained using variogram model fitted to experimental variogram of residuals from trend surface is similar to that obtained using the model found by REML, however, the estimated variance was much higher for the REML method as the variogram of residuals from the trend was largely underestimated.

Burrough and McDonnell (2000) point out that coefficient of determination increases with the order of the fitted polynomial surface, but generally only low orders are sensible. The choice of the order of the polynomial is based on the practitioner's understanding of the process that induced the trend (Isaaks and Srivastava, 1989; Cressie, 1993) and judgement of the effect of trend removal on the experimental variogram (Lark and Webster, 2006). Alternative option to trend surface removal is to estimate the variogram only as a directional variogram in a trend-free direction. Directional variograms were visually investigated also in this study, but they had to be interpreted with caution because of the insufficient sample size. Mainly the direction of potential tides and location of the inflow canal would make trend removal reasonable. Trend was detected in all variables in our data set, except TP, using the variance ratio F-test as suggested by Burrough and McDonnell (2000, p.109), but the highest coefficient of determination was 0.37 for second order polynomial surface fitted to OM\_UP (Table A.4), hence trends were generally weak. Trends were eventually not removed from the data, because the detection of trend and its properties were affected by few extreme values and because trend removal did not contribute much to clarity of variograms.

*Table A.4. Coefficients of determination of polynomial trend surfaces fitted to the original data.*

Property	Coefficient of determination for the trend surface in a soil depth			
	0–10 cm		10–20 cm	
	1st order trend	2nd order trend	1st order trend	2nd order trend
Moisture	0.10	0.16	0.17	0.19
Bulk density	0.10	0.17	0.14	0.17
pH	0.18	0.22	0.24	0.28
Organic matter content	0.27	0.37	0.30	0.32
Total phosphorus	0.01	0.03	0.02	0.05
Total nitrogen	0.30	0.35	0.30	0.32
Total carbon	0.28	0.36	0.30	0.31

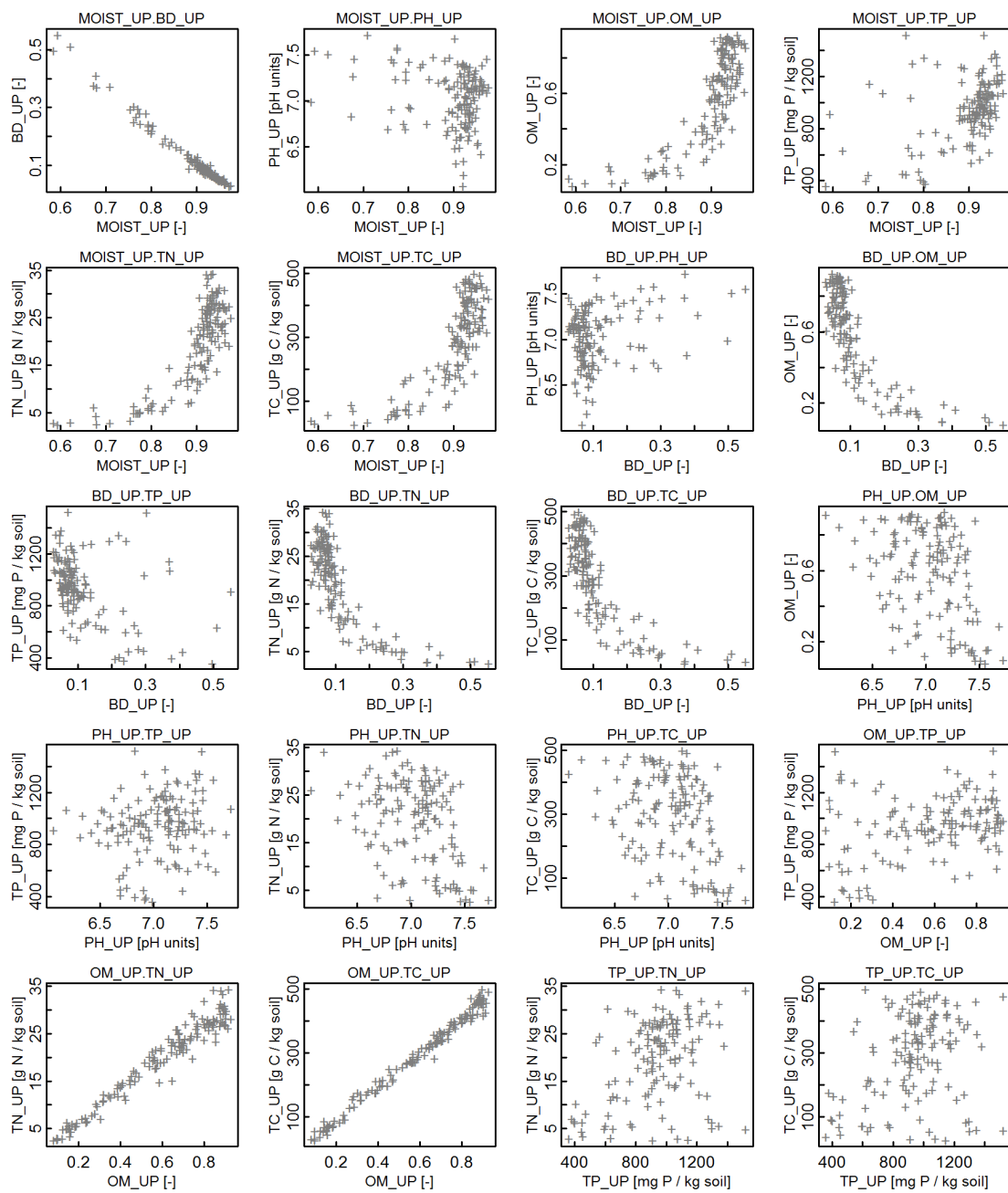


Fig. A.3 (1 of 4). Scatter-grams of soil moisture (MOIST), bulk density (BD), pH (PH), organic matter content (OM), total phosphorus (TP), total nitrogen (TN), and total carbon (TC) in 0–10 cm (*\_UP*) and 10–20 cm (*\_LW*) soil depth. The figure continues on the next page.

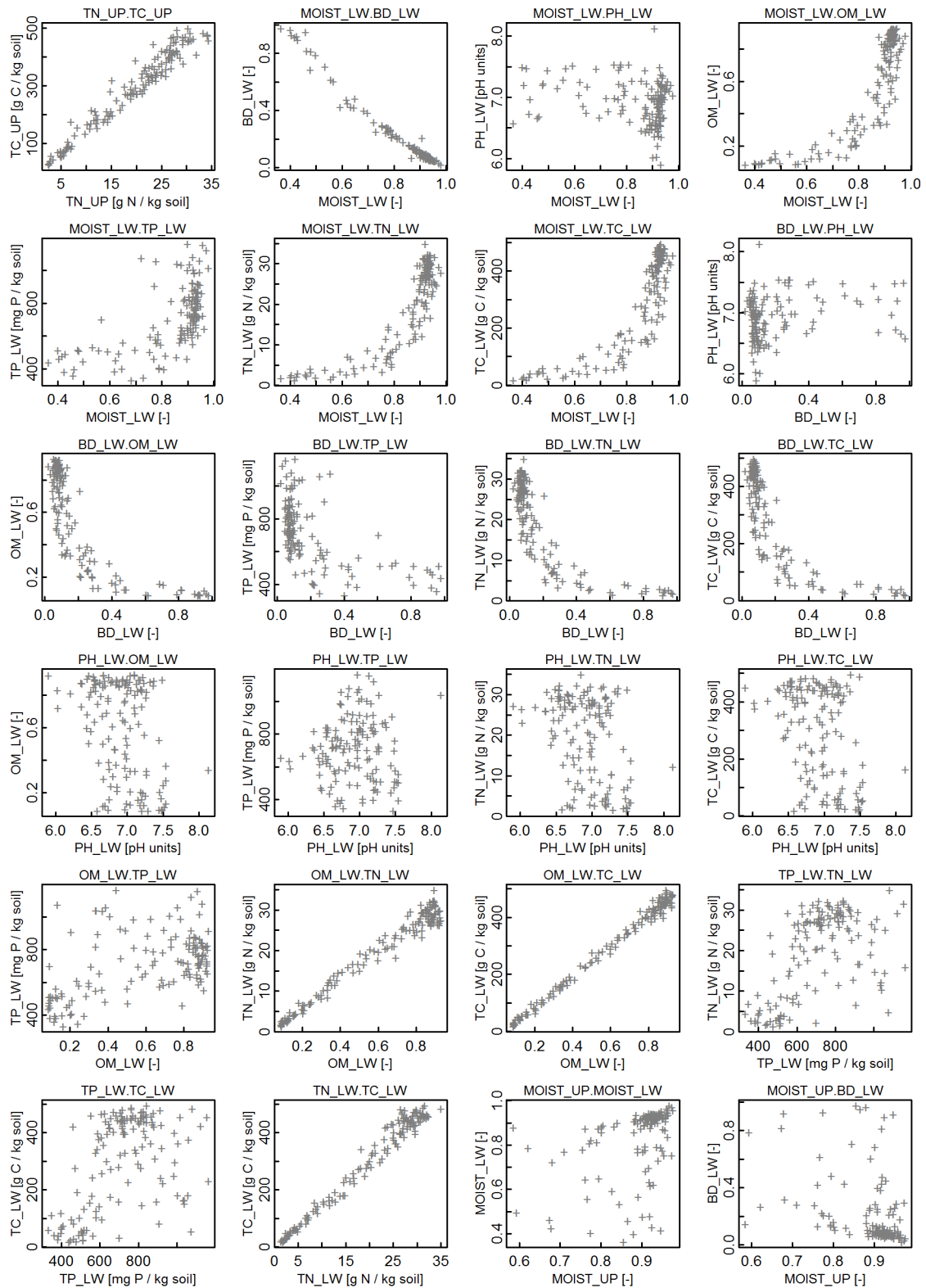


Fig. A.3 continued (2 of 4). Scatter-grams of soil moisture (MOIST), bulk density (BD), pH (PH), organic matter content (OM), total phosphorus (TP), total nitrogen (TN), and total carbon (TC) in 0–10 cm (\_UP) and 10–20 cm (\_LW) soil depth. The figure continues on the next page.

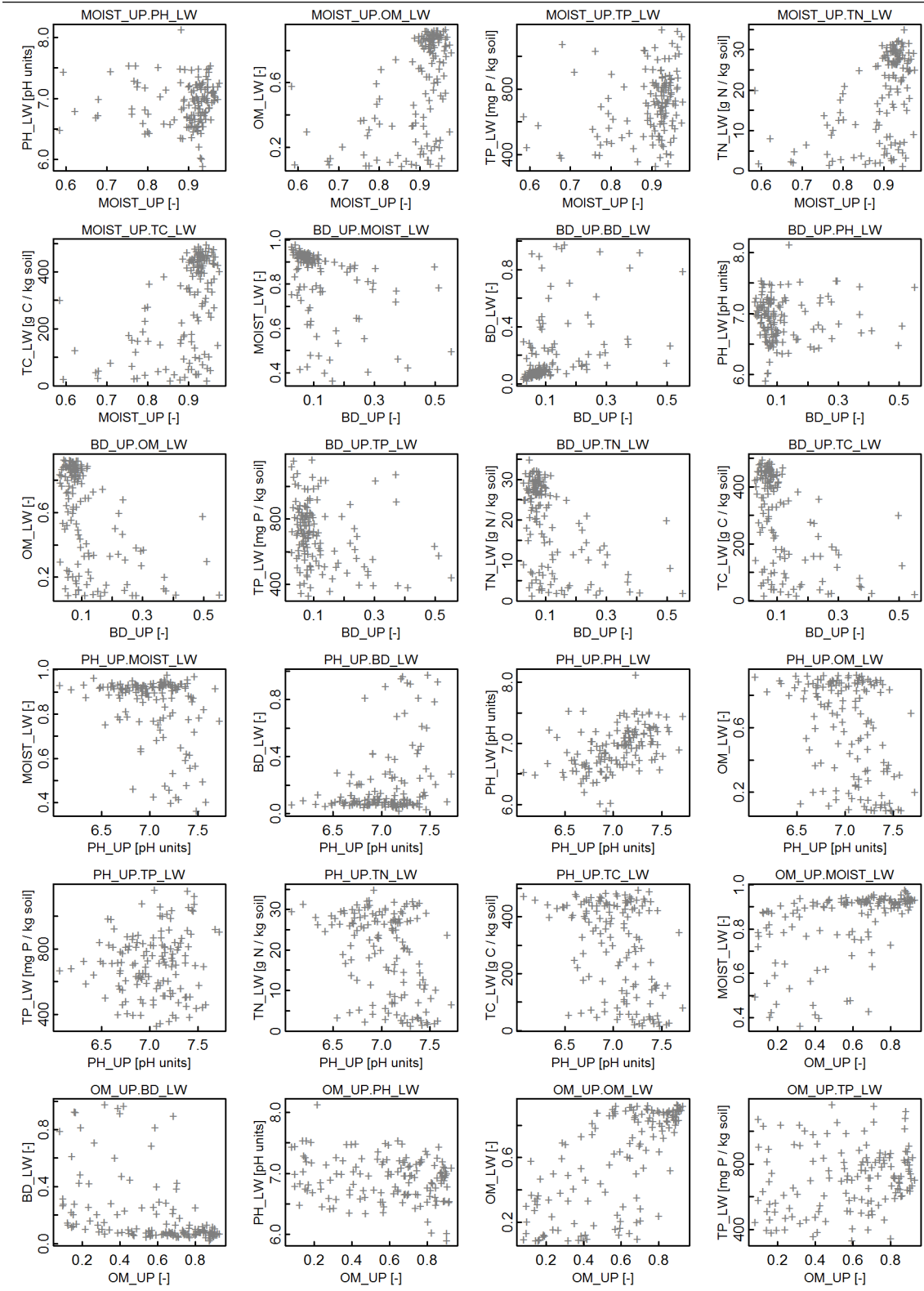


Fig. A.3 continued (3 of 4). Scatter-grams of soil moisture (MOIST), bulk density (BD), pH (PH), organic matter content (OM), total phosphorus (TP), total nitrogen (TN), and total carbon (TC) in 0–10 cm (*\_UP*) and 10–20 cm (*\_LW*) soil depth. The figure continues on the next page.

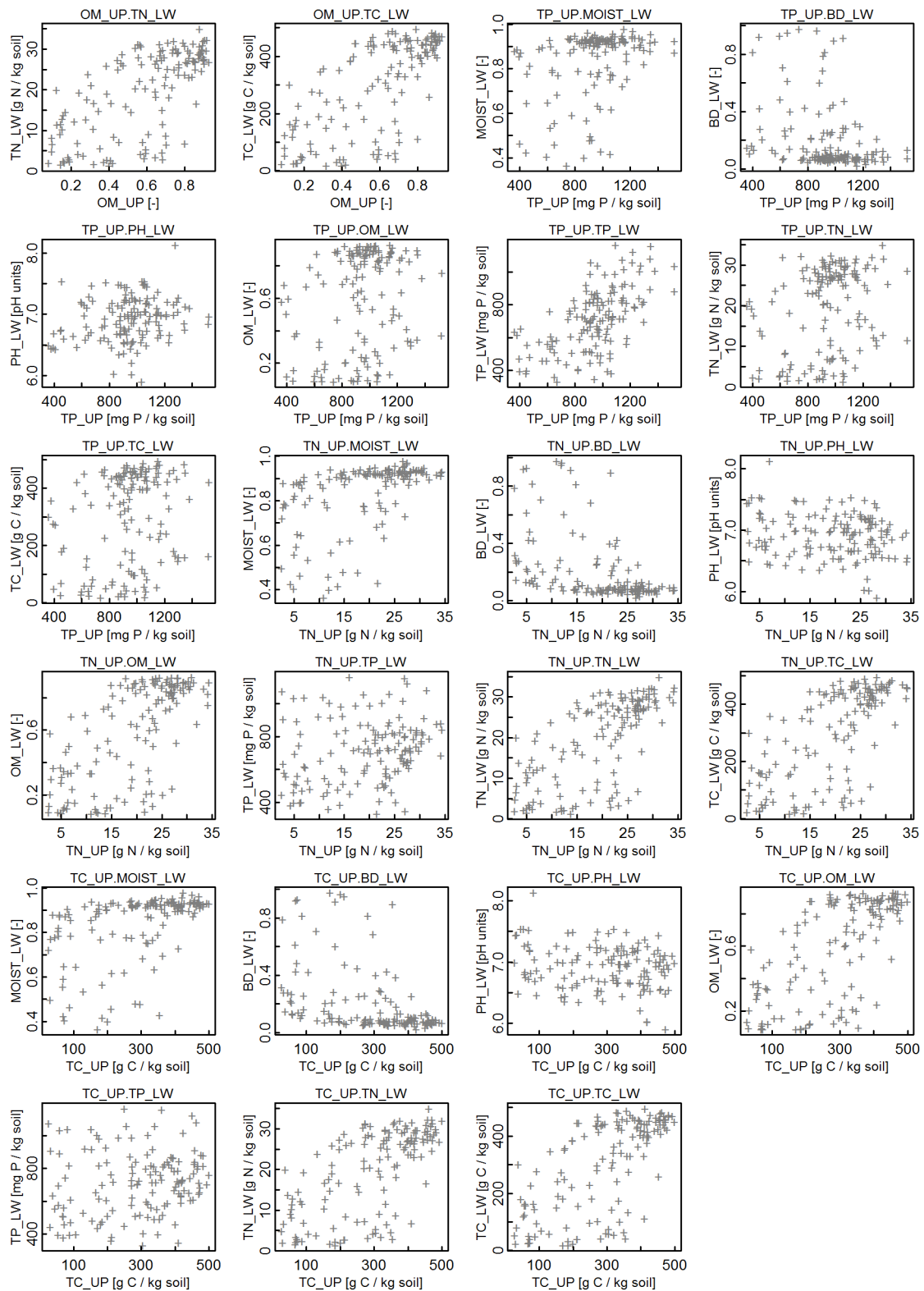


Fig. A.3 continued (4 of 4). Scatter-grams of soil moisture (MOIST), bulk density (BD), pH (PH), organic matter content (OM), total phosphorus (TP), total nitrogen (TN), and total carbon (TC) in 0–10 cm (*\_UP*) and 10–20 cm (*\_LW*) soil depth.



## Appendix B Variograms of the Original Variables

Experimental variograms of soil properties in 0–10 cm (Fig. B.1) and 10–20 cm (Fig. B.2) soil depth provide insights into spatial relationships between sampling locations.

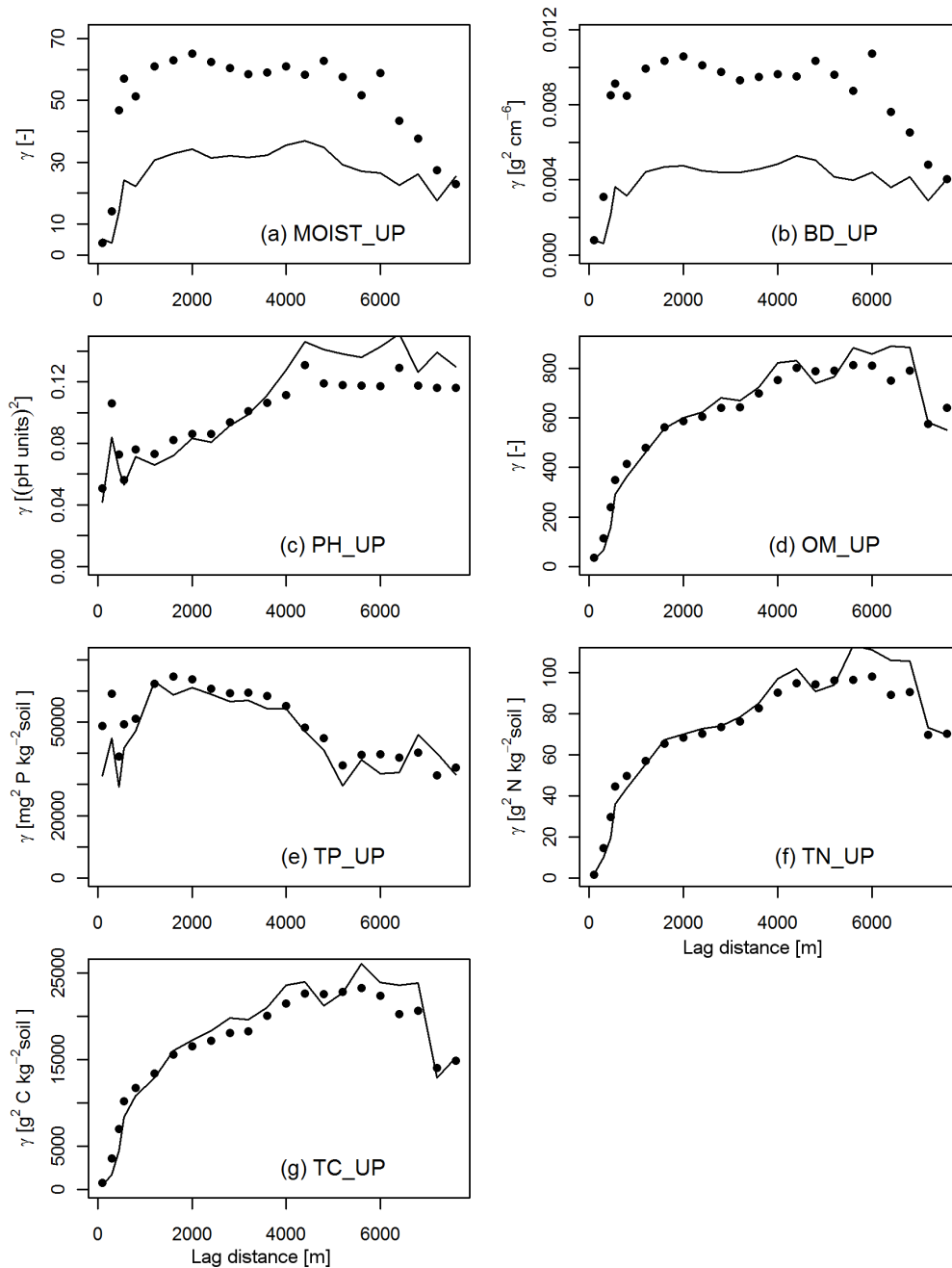


Fig. B.1. Experimental variograms of (a) soil moisture, (b) bulk density, (c) pH, (d) organic matter content, (e) total phosphorus, (f) total nitrogen, and (g) total carbon in 0–10 cm soil depth constructed by method of moments (dots) and Hawkins and Cressie estimator (line). Breaks were 0, 200, 400, 500, 600, 1000 to 8000 by 400 m.

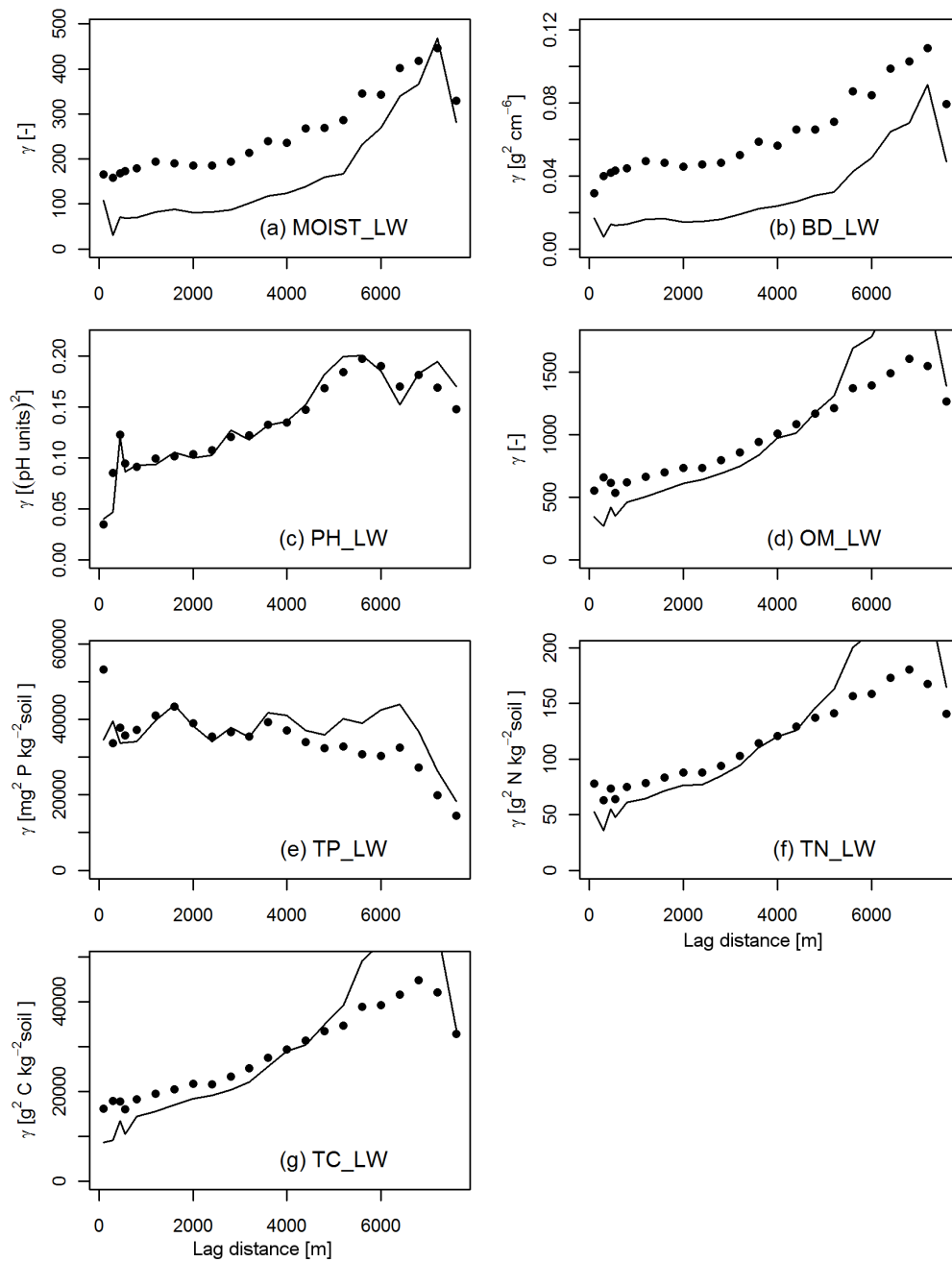


Fig. B.2. Experimental variograms of (a) soil moisture, (b) bulk density, (c) pH, (d) organic matter content, (e) total phosphorus, (f) total nitrogen, and (g) total carbon in 10–20 cm soil depth constructed by method of moments (dots) and Hawkins and Cressie estimator (line). Breaks were 0, 200, 400, 500, 600, 1000 to 8000 by 400 m.

Experimental variables were also constructed for mass per volume units of P, N, and C (Fig. B.3). Units were converted using the measurements of bulk density.

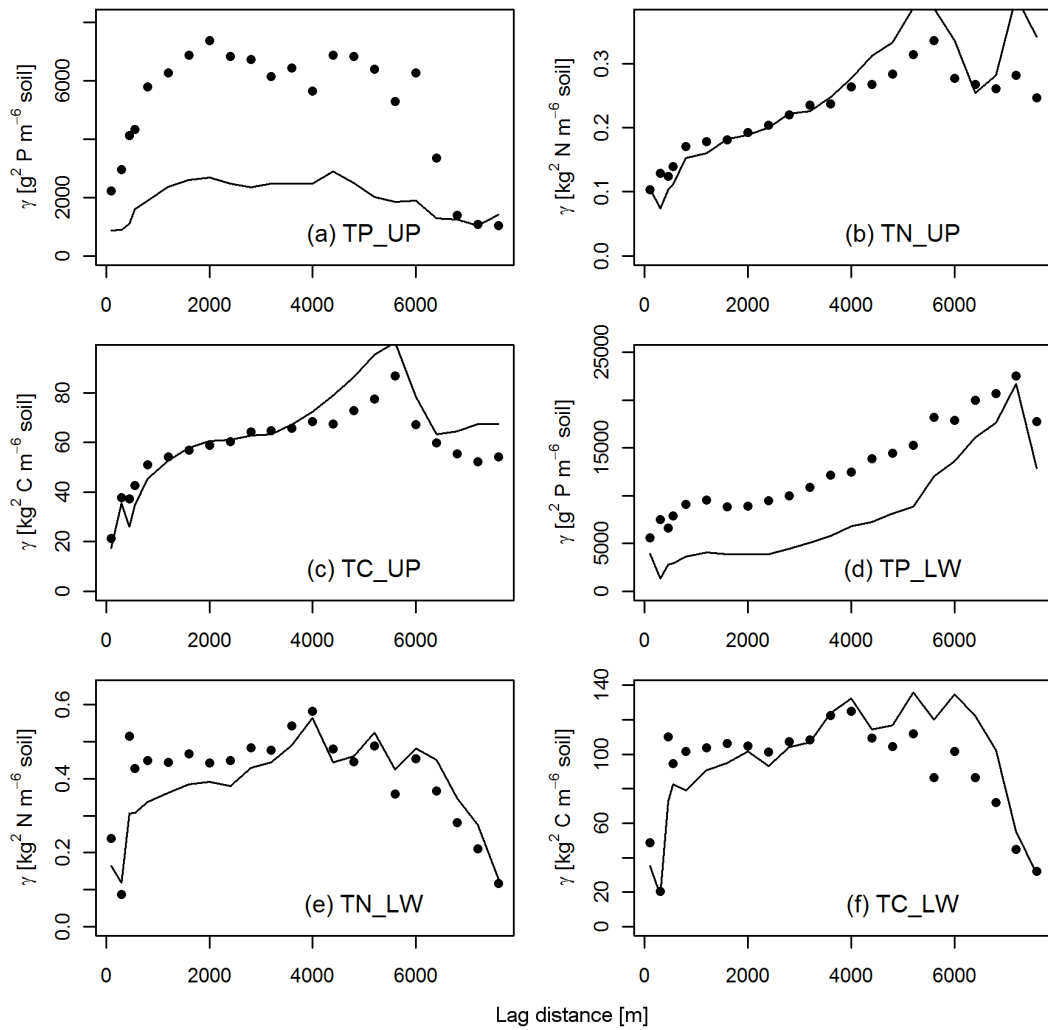


Fig. B.3. Experimental variograms of total phosphorus (TP), total nitrogen (TN), and total carbon (TC) in 0–10 cm (UP, a to c) and 10–20 cm (LW, d to f) soil depth constructed by method of moments (dots) and Hawkins and Cressie estimator (line) using mass per volume units. Breaks were 0, 200, 400, 500, 600, 1000 to 8000 by 400 m.

## Appendix C Correlation Surfaces

Pearson's product moment correlation coefficients were calculated in windows of sizes 250, 500, 750, 1100, 2200, and 3300 m on a grid with 100 m spacing (Fig. C.1, Fig. C.2). These surfaces provide information about spatial distribution of areas where predicted values of two soil properties were positively or negatively correlated. Input data were the kriged estimates of each variable on a grid with 25 m spacing. Resulting rasters can be found on the enclosed CD.

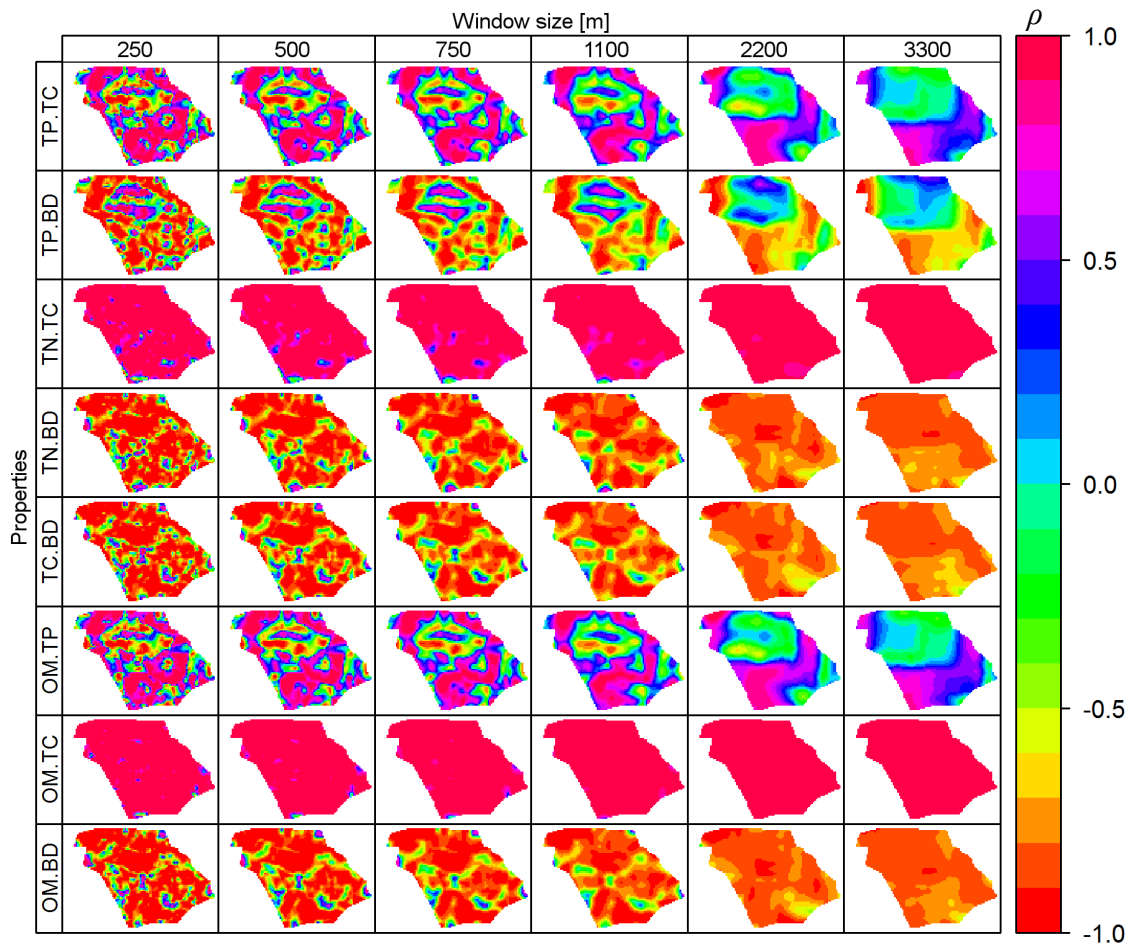


Fig. C.1. Correlation surfaces between organic matter content (OM), bulk density (BD), total carbon (TC), total phosphorus (TP), and total nitrogen (TN) in 0–10 cm soil depth (variables involved in each surface are separated by dot).

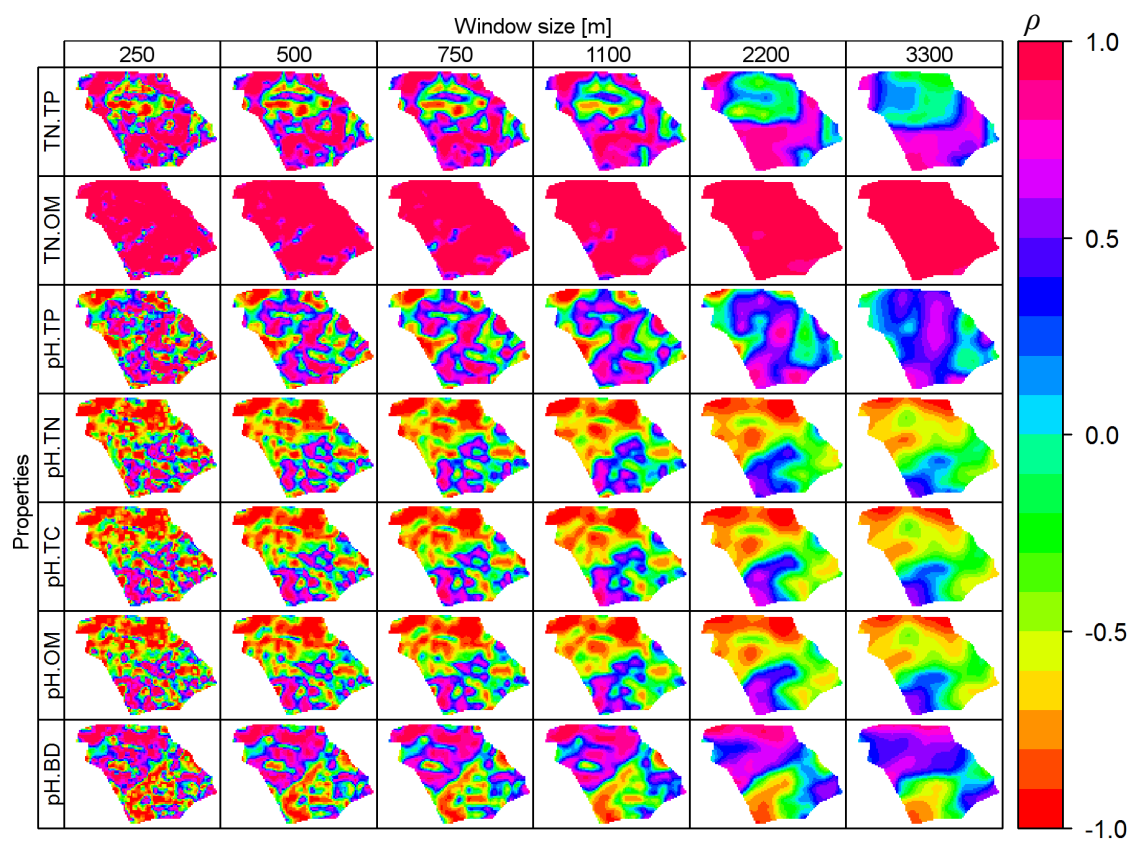


Fig. C.2. Correlation surfaces between organic matter content (OM), bulk density (BD), total carbon (TC), total phosphorus (TP), total nitrogen (TN), and pH in 0–10 cm soil depth (variables involved in each surface are separated by dot).

## Appendix D Derivation of Regional Stocks

Function of wetlands as sinks and/or sources of carbon has become relevant also with increasing concern about global climate change. This appendix explains how the overall amount of total carbon stored in Davis Pond was calculated. Stocks of total nitrogen and phosphorus were estimated in a similar way.

Instead of using ordinary punctual kriging, we can use ordinary block kriging with block size  $25 \text{ m} \times 25 \text{ m}$  (Fig. D.1). For each block  $B_i$  in the pond region  $R$ , we obtain estimated concentration of total carbon,  $\hat{Z}_{TC}(B_i)$ , in  $\text{g C kg}^{-1}$  soil, and its block kriging variance  $\hat{\sigma}_{TC}^2(B_i)$  in  $\text{g}^2 \text{C kg}^{-2}$  soil. Further, we need to block krige soil density,  $\hat{Z}_{DENS}(B_i)$ , in  $\text{g cm}^{-3}$  with its variance  $\hat{\sigma}_{DENS}^2(B_i)$  in  $\text{g}^2 \text{cm}^{-6}$ . We get the content of total carbon in a unit of volume of soil ( $\text{kg m}^{-3}$ ) within each block  $B_i$  and its variance (under assumption of no correlation, see Burrough and McDonnell, 2000, p. 248) as follows.

$$\begin{aligned}\hat{Z}_{TC, VOL}(B_i) &= \hat{Z}_{TC}(B_i) \cdot \hat{Z}_{DENS}(B_i) \\ \hat{\sigma}_{TC, VOL}^2(B_i) &= \hat{Z}_{DENS}^2 \cdot \hat{\sigma}_{TC}^2 + \hat{Z}_{TC}^2 \cdot \hat{\sigma}_{DENS}^2\end{aligned}$$

To get the estimate of overall amount of total carbon in one block, we need to account for the volume of the block, thus:

$$\begin{aligned}\hat{Z}_{T, TC, VOL}(B_i) &= \hat{Z}_{TC, VOL}(B_i) \cdot 0.1 \cdot 25^2 = \hat{Z}_{TC, VOL}(B_i) \cdot 62.5 \\ \hat{\sigma}_{T, TC, VOL}^2(B_i) &= \hat{\sigma}_{TC, VOL}^2(B_i) \cdot (62.5)^2\end{aligned}$$

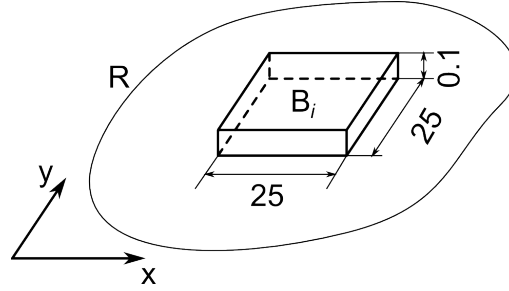


Fig. D.1. Block dimensions and schematic orientation (units are metres).

Finally, the overall estimate of total carbon storage in the whole region  $R$ ,  $\hat{\Omega}_{TC}$ , (in kg) is the sum of the amount of carbon stored in individual blocks and its variance should be derived from covariance model:

$$\begin{aligned}\hat{\Omega}_{TC} &= \sum_{i|B_i \in R} \hat{Z}_{T, TC, VOL}(B_i) \\ \hat{\sigma}_{TC, \Omega}^2 &= \sum_i \sum_j cov(\hat{Z}_{T, TC, VOL}(B_i), \hat{Z}_{T, TC, VOL}(B_j))\end{aligned}$$

Regional stocks (Table D.1) were estimated using the described procedure. ArcGIS Geostatistical Analyst (ESRI, 1999–2009) was used for kriging with global neighbourhood, each block was represented by  $4 \times 4$  regular point grid to obtain the block estimate (Isaaks and Srivastava, 1989). Variance of the regional estimates was not derived as the covariance model was unknown. In the lower layer, the total stock was calculated from the original sampling points by converting variables to mass per volume units, taking sample mean and multiplying it by the area of Davis Pond ( $37071250 \text{ m}^2$ ) and by 0.1 to account for 10 cm layer thickness. Same calculation was used also in the upper layer. Maps of elements content per volume in 0–10 cm soil depth are included in Appendix H. When block kriging is used, it is possible to map the distribution of elements, while the sample mean provides only one value for the whole region. Webster and Oliver (2007, p. 168), describe interesting influence of the nugget effect on block kriging variance estimation, Isaaks and Srivastava (1989, chapter 13), present useful practicalities of block kriging.

Table D.1. Estimated elements stocks in Davis Pond.†

Element	Stock in soil depth					
	0–10 cm				10–20 cm	
	Using block kriging		Using sample mean		Using sample mean	
	t	t ha <sup>-1</sup>	t	t ha <sup>-1</sup>	t	t ha <sup>-1</sup>
C	97029	26.17	88986 (2494)	24.00 (0.67)	115357 (3246)	31.12 (0.88)
N	6470	1.75	5976 (150)	1.61 (0.04)	7725 (215)	2.08 (0.06)
P	337	0.09	372 (25)	0.10 (0.01)	440 (33)	0.12 (0.01)

† C, carbon; N, nitrogen; P, phosphorus, numbers in parentheses are standard error, sample size was 139.

## **Appendix E Indicator Variograms of Variables in the Lower Layer**

Indicator kriging is a technique for kriging categorical variables or classified continuous variables. For continuous variables, values are classified as 1 or 0 according a specified threshold. Indicator experimental variograms can be then constructed as usually. Details and applications can be found for example in Webster and Oliver (2007, chapter 11). We investigated indicator variograms of the variables in 10–20 cm soil depth to see if any spatial relationship can be revealed (Fig. E.1). The R code written for this purpose is enclosed in Appendix G.

The only variogram that would be sensible to model was the organic matter content with threshold of 0.8. The model fitted to this indicator variogram was exponential with sill 0.1295, range 1381 m, and nugget 0.1244. The minimized weighted sum of squares was 0.4091. Other variograms did not indicate any spatial autocorrelation. There was also little evidence (based mainly on investigation of histogram) that the value of 0.8 would be of particular importance for organic matter content and indicator kriging was not performed.



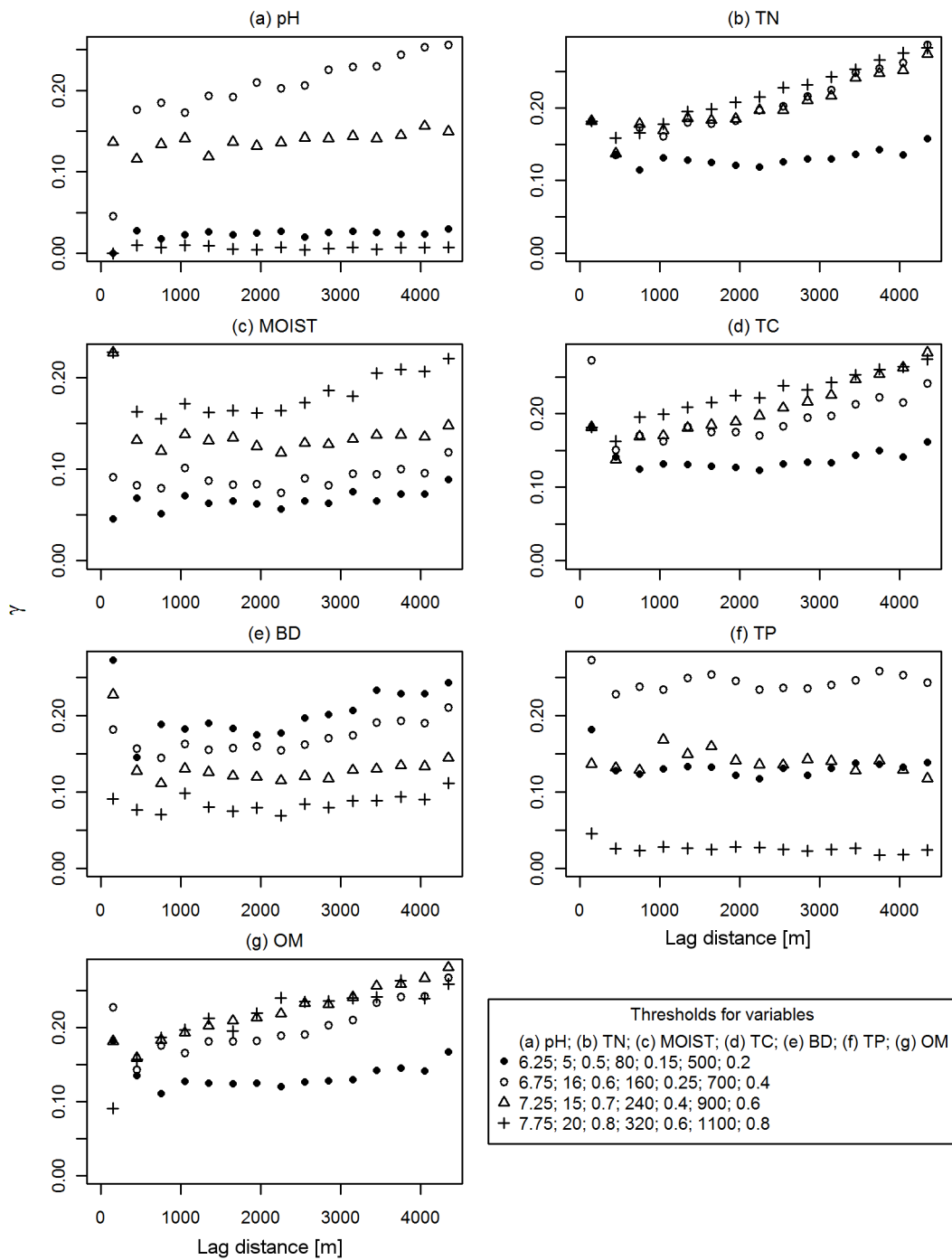


Fig. E.1. Experimental indicator variograms for the variables in 10–20 cm soil depth. (a) pH, (b) moisture, (c) bulk density, (d) organic matter content, (e) total phosphorus, (f) total nitrogen, (g) total carbon. Breaks were a sequence from 0 to 4500 by 300.

## Appendix F Mapping Moisture According to Density

There was a close linear relationship between moisture (MT) and bulk density (BD) in 0–10 cm soil depth (Fig. F.1, Table F.1), which was utilised for mapping MT. Variogram model was not fitted to experimental variogram of MT because it was not that clear as the variogram of BD. Map of BD was produced by ordinary kriging and the close linear relationship between the two variables was used to map MT. The regression model was a general line  $MT = \beta_0 + \beta_1 \cdot BD + \epsilon$ , where  $\beta_0$  and  $\beta_1$  are regression parameters and  $\epsilon$  is the residual error term. The regression formula with estimated parameters (Table F.1) was used to obtain the estimated value of MT for each cell. To accept this linear model, we had to ignore the spatial correlation between measurements of BD (Heuvelink, G.B.M. 1998. Error propagation in environmental modelling with GIS. Taylor & Francis, London, UK). Skewness of the distributions was neglected because the relationship was very strong.

Table F.1. Results of linear regression between moisture and bulk density in 0–10 cm soil depth.  $R^2 = 0.98$ ,  $F$ -statistic: 7882 on 1 and 137 degrees of freedom. †

Parameter	Estimate	Standard error	t value
$\beta_0$	0.99†	0.0013	740
$\beta_1$	-0.78†	0.0088	-89
$\epsilon$	0.0	0.0101	N/A

† Computed  $P$  values were  $< 1 \times 10^{-15}$ .

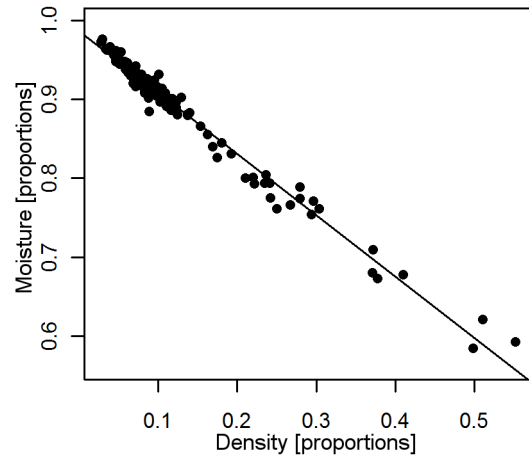


Fig. F.1. Regression line of Moisture = 0.99 - 0.78 Density,  $R^2 = 0.98$ .

The linear regression was based on the original measurements, with assumption that the independent variable was measured with negligible error. However, kriged BD values had associated error with them. Standard error of the predicted MT in each cell was calculated according to general rules for error propagation (Burrough and McDonnell, 2000). Correlation coefficient between parameters  $\beta_0$  and  $\beta_1$  was  $\rho_{0,1} = -0.7661$ , otherwise elements on the right side of the regression equation were considered uncorrelated. This led to the following error propagation equation:

$$\delta(MT)^2 = \delta(\hat{\beta}_0)^2 + BD^2 \cdot \delta(\hat{\beta}_1)^2 + \hat{\beta}_1^2 \cdot \delta(BD)^2 + \delta(\hat{\epsilon})^2 + BD \cdot \delta(\hat{\beta}_0) \cdot \delta(\hat{\beta}_1) \cdot \rho_{0,1}$$

where  $\delta(\cdot)$  denotes standard error,  $\hat{\cdot}$  expresses estimate, and  $\delta(BD)^2$  is the kriging variance of BD.

## Appendix G R Code

Most of the analysis was performed in R statistical software, version 2.11.1. (R Core Development Team, 2010), packages GeoR (Ribeiro and Diggle, 2001) and Gstat (Pebesma, 2004) were highly utilized. The convention for variable names in the R code is that UP indicates 0–10 cm soil depth, LW indicates 10–20 cm soil depth. Soil properties were moisture (MOIST), bulk density (DENS), bulk density transformed by box-cox transformation with power  $-0.5$  (bxDENS), pH (PH), organic matter content (ORGAN), total phosphorus (TP), total nitrogen (TN), and total carbon (TC).

Four scripts (Table G.1) are presented in this appendix. When code lines had to be truncated to fit in the page, symbol “..” at the end of a line and at the beginning of the subsequent line indicates that the two lines are the same line of code. All four scripts can be found on the enclosed CD without the lines truncated.

*Table G.1. R scripts used during the analysis.*

Script name	Page	Description
main.r	57	Contains variography, kriging, fitting of the linear model of correlogram, and moving window analysis. Represents the core script for the whole analysis.
rfunctions.r	68	Contains custom functions used in main.r script including function for moving window analysis.
regional_stocks.r	80	Derivation of regional stocks of carbon, nitrogen and phosphorus from sample means.
indicator.variograms.r	81	Indicator variograms of soil properties in 10–20 cm soil depth.

**# main.r #**

```
#main script for the analysis
```

```
#set directories
```

```
setwd("E:/cranfield/00_thesis/data")
```

```
outpath<-"E:/cranfield/00_thesis/data/outputs/variograms/"
```

```
prefix<-" " #prefix for outputs
```

```
suffix<-" " #suffix for outputs
```

```
#load packages and functions
```

```
source("./rfunctions.r")
```

```
require(foreign)
```

```
require(geoR)
```

```
require(gstat)
```

```
require(lattice)
```

```
require(maptools)
```

```
require(spatstat)
```

```
#load the data
```

```
dta.orig<-read.dbf("son.dbf")
```

```
  dta.orig<-dta.orig[dta.orig$OUT!=1,] #exclude points labeled as outliers ("OUT"==1)
```

```
  dta.orig<-dta.orig[,1:(length(dta.orig[1,])-1)] #remove the OUT column
```

```
dta.all<-dta.orig[,c("PID", "XCOORD", "YCOORD", "SID", "PH_UP", "ORGAN_UP", "TP_UP", "TN_UP", "TC_UP", "", "DENS_U..  
..P")]
```

```
gdt.all<-as.geodata(dta.all, coords.col=2:3, data.col=5:length(names(dta.all)), na.action='ifany')
```

```
#####
```

```
#####
```

```
##### VARIOGRAPHY #####
```

```
#####
```

```
#####
```

```
xv<-list() #list to store cross-validations
```

```
##### ORGAN_UP ##### proportions #####
```

```
g<-as.geodata(dta.all, coords.col=2:3, data.col="ORGAN_UP")
```

```
summary(g); plot(g); print("skewness"); f_skewness(g$data)
```

```
vg.dir<-variog4(g); plot(vg.dir);
```

```
vg.mom<-variog(g); points(vg.mom$u, vg.mom$v)
```

```
vg.rob<-variog(g, estimator="modulus"); points(vg.rob$u, vg.rob$v, pch="+")
```

```
maxd<-3500; br<-seq(0,maxd,300)
```

```
vg.mom<-variog(g, trend="cte", breaks=br, max.dist=maxd)
```

```
points(vg.mom$u, vg.mom$v, pch=16)
```

```

#so the final variogram for fitting is:
vg<-variog(g, trend="cte", breaks=br, max.dist=maxd)
#models
pars.sig<-seq(0.04,0.055, 0.005); pars.phi<-seq(500,2500,500); pars.nug<-c(0,seq(0.01,0.04, 0.01))
rslt.sph<-fitting(vg, "spherical", maxd=maxd, pars.sig=pars.sig, pars.phi=pars.phi, pars.nug=pars.nug)
model.sph<-variofit(vg, ini=c(0.048, 2500), cov.model="spherical", nug=0.033, weights="npairs", max.dist=maxd)
lines(model.sph, lwd=2)
pars.phi<-pars.phi/3
rslt.exp<-fitting(vg, "exponential", maxd=maxd, pars.sig=pars.sig, pars.phi=pars.phi, pars.nug=pars.nug)
model.exp<-variofit(vg, ini=c(0.067, 1080), cov.model="exponential", nug=0.028, weights="npairs", max.dist=maxd)
lines(model.exp, lwd=2)
#by reml
reml<-f_likfit(g, model="unspecified", pars.sig=c(0.05,0.01,0.01), pars.phi=c(2000,500,500), trend="cte", lines=TRUE, cl..
.r="red", method="REML")
lines(reml.sph$model$s0.04p2500, col="red", lwd=2)
#so finally:
vg.ORGAN_UP<-vg
model.ORGAN_UP.sph<-model.sph
model.ORGAN_UP.exp<-model.exp
model.ORGAN_UP.reml<-reml$model$s0.04p500
#cross-validation
msdrvar<-"ORGAN_UP"; xv[[msdrvar]]<-xvalid(g, model=model.ORGAN_UP.exp, trend="cte")
windows(); layout(matrix(1:10, 2,5, byrow=T)); plot(xv[[msdrvar]])
mean(((xv[[msdrvar]]$data-xv[[msdrvar]]$predicted)^2)/xv[[msdrvar]]$krige.var)

##### TC_UP ##### [g/kg] #####
g<-as.geodata(dta.all, coords.col=2:3, data.col="TC_UP")
summary(g); plot(g); print("skewness"); f_skewness(g$data)
vg.dir<-variog4(g); plot(vg.dir)
vg.mom<-variog(g); points(vg.mom$u, vg.mom$v)
vg.rob<-variog(g, estimator="modulus"); points(vg.rob$u, vg.rob$v, pch="+")
maxd<-3500; br<-seq(0,maxd,300)
vg.mom<-variog(g, trend="cte", breaks=br, max.dist=maxd)
points(vg.mom$u, vg.mom$v, pch=16, col="red")
vg<-variog(g, trend="cte", breaks=br, max.dist=maxd)
#models
pars.sig<-seq(10000,18000,1000); pars.phi<-seq(500,2500,500); pars.nug<-seq(5000,10000,1000)
rslt.sph<-fitting(vg, "spherical", maxd=maxd, pars.sig=pars.sig, pars.phi=pars.phi, pars.nug=pars.nug)
model.sph<-variofit(vg, ini=c(11250, 2900), cov.model="spherical", nug=6834, weights="npairs", max.dist=maxd)
lines(model.sph, lwd=2)
pars.phi<-pars.phi/3
rslt.exp<-fitting(vg, "exponential", maxd=maxd, pars.sig=pars.sig, pars.phi=pars.phi, pars.nug=pars.nug)
model.exp<-variofit(vg, ini=c(15400, 1240), cov.model="exponential", nug=4150, weights="npairs", max.dist=maxd)

```

```

lines(model.exp, lwd=2)
#so finally:
vg.TC_UP<-vg
model.TC_UP.exp<-model.exp
model.TC_UP.sph<-model.sph
#cross-validation
msdrvar<-"TC_UP"; xv[[msdrvar]]<-xvalid(g, model=model.TC_UP.exp, trend="cte")
windows(); layout(matrix(1:10, 2,5, byrow=T)); plot(xv[[msdrvar]])
mean(((xv[[msdrvar]]$data-xv[[msdrvar]]$predicted)^2)/xv[[msdrvar]]$krige.var)

##### TN_UP ##### [g/kg] #####
g<-as.geodata(dta.all, coords.col=2:3, data.col="TN_UP")
##g<-as.geodata.except(dta.all, data.col="TN_UP", val=c(7051, 7052, 7074, 7107)) #exclude some points if you want
summary(g); plot(g); print("skewness"); f_skewness(g$data)
vg.dir<-variog4(g); plot(vg.dir)
vg.mom<-variog(g); points(vg.mom$v, vg.mom$v, pch=16)
vg.rob<-variog(g, estimator="modulus"); points(vg.rob$v, vg.rob$v, pch="+")
maxd<-3500; br<-seq(0,maxd,300)
vg.mom<-variog(g, trend="cte", breaks=br, max.dist=maxd)
points(vg.mom$v, vg.mom$v, pch=16, col="red")
vg<-variog(g, trend="cte", breaks=br, max.dist=maxd)
#models
pars.sig<-seq(40,60,10); pars.phi<-seq(500,3000,500); pars.nug<-seq(25,35,5)
rslt.sph<-fitting(vg, "spherical", maxd=maxd, pars.sig=pars.sig, pars.phi=pars.phi, pars.nug=pars.nug)
model.sph<-variofit(vg, ini=c(43, 2830), cov.model="spherical", nug=31, weights="npairs", max.dist=maxd)
lines(model.sph, lwd=2)
pars.phi<-pars.phi/3
rslt.exp<-fitting(vg, "exponential", maxd=maxd, pars.sig=pars.sig, pars.phi=pars.phi, pars.nug=pars.nug)
model.exp<-variofit(vg, ini=c(60, 1094), cov.model="exponential", nug=18, weights="npairs", max.dist=maxd)
lines(model.exp, lwd=2)
#so finally:
vg.TN_UP<-vg
model.TN_UP.sph<-model.sph
model.TN_UP.exp<-model.exp
#cross-validation
msdrvar<-"TN_UP"; xv[[msdrvar]]<-xvalid(g, model=model.TN_UP.exp, trend="cte")
windows(); layout(matrix(1:10, 2,5, byrow=T)); plot(xv[[msdrvar]])
mean(((xv[[msdrvar]]$data-xv[[msdrvar]]$predicted)^2)/xv[[msdrvar]]$krige.var)

##### TP_UP ##### [mg/kg] #####
#g<-as.geodata.except(dta.all, coords.col=2:3, data.col="TP_UP", col="PID", val=c(7051,7052,7056,7074,7141,7080)) #exclu..
..de some points if you want
g<-as.geodata(dta.all, coords.col=2:3, data.col="TP_UP")

```

09

```

summary(g); plot(g); print("skewness"); f_skewness(g$data)
vg.dir<-variog4(g); plot(vg.dir)
vg.mom<-variog(g); points(vg.mom$u, vg.mom$v)
vg.rob<-variog(g, estimator="modulus"); points(vg.rob$u, vg.rob$v, pch="+")
maxd<-3500; br<-seq(0,maxd,300)
vg.mom<-variog(g, trend="cte", breaks=br, max.dist=maxd)
points(vg.mom$u, vg.mom$v, pch=16, col="red")
vg<-variog(g, trend="cte", breaks=br, max.dist=maxd)
#models
pars.sig<-seq(10000,25000,5000); pars.phi<-seq(500,3000,500); pars.nug<-seq(30000,45000,5000)
rslt.sph<-fitting(vg, "spherical", maxd=maxd, pars.sig=pars.sig, pars.phi=pars.phi, pars.nug=pars.nug)
model.sph<-variofit(vg, ini=c(28840, 1359), cov.model="spherical", nug=33038, weights="npairs", max.dist=maxd)
lines(model.sph, lwd=2)
pars.phi<-pars.phi/3
rslt.exp<-fitting(vg, "exponential", maxd=maxd, pars.sig=pars.sig, pars.phi=pars.phi, pars.nug=pars.nug)
model.exp<-variofit(vg, ini=c(49567, 365), cov.model="exponential", nug=12474, weights="npairs", max.dist=maxd)
lines(model.exp, lwd=2)
#so finally:
vg.TP_UP<-vg
model.TP_UP.sph<-model.sph
model.TP_UP.exp<-model.exp
#cross-validation
msdrvar<-"TP_UP"; xv[[msdrvar]]<-xvalid(g, model=model.TP_UP.exp, trend="cte")
windows(); layout(matrix(1:10, 2,5, byrow=T)); plot(xv[[msdrvar]])
mean(((xv[[msdrvar]]$data-xv[[msdrvar]]$predicted)^2)/xv[[msdrvar]]$krige.var)

##### PH_UP ##### [ pH = -log(c(H+)) ] #####
g<-as.geodata(dta.all, coords.col=2:3, data.col="PH_UP")
summary(g); plot(g); print("skewness"); f_skewness(g$data)
vg.dir<-variog4(g); plot(vg.dir)
vg.mom<-variog(g); points(vg.mom$u, vg.mom$v)
vg.rob<-variog(g, estimator="modulus", breaks=seq(0,8000,300)); points(vg.rob$u, vg.rob$v, pch="+")
maxd<-8000; br<-seq(0, maxd, 300)
vg.mom<-variog(g, trend="cte", breaks=br, max.dist=maxd)
points(vg.mom$u, vg.mom$v, pch=16, col="red")
vg<-variog(g, trend="cte", breaks=br, max.dist=maxd)
#models
pars.sig<-seq(0.005,0.04,0.005); pars.phi<-seq(4000,6500,500); pars.nug<-seq(0.05,0.07,0.005)
rslt.sph<-fitting(vg, "spherical", maxd=maxd, pars.sig=pars.sig, pars.phi=pars.phi, pars.nug=pars.nug)
model.sph<-variofit(vg, ini=c(0.068, 6390), cov.model="spherical", nug=0.0557, weights="npairs", max.dist=maxd)
model.sph<-variofit(vg, ini=c(0.03, 1500), cov.model="spherical", nug=0.04, weights="npairs", max.dist=maxd)
model.sph<-variofit(vg, ini=c(0.1, 0), cov.model="power", nug=0, weights="npairs", max.dist=maxd)
lines(model.sph, lwd=2)

```

```

pars.phi<-pars.phi/3
rslt.exp<-fitting(vg, "exponential", maxd=maxd, pars.sig=pars.sig, pars.phi=pars.phi, pars.nug=pars.nug)
model.exp<-variofit(vg, ini=c(0.06, 1000), cov.model="exponential", nug=0.03, weights="npairs", max.dist=maxd)
lines(model.exp, lwd=2)
#by reml
reml.sph<-likfit(g, ini.cov.pars=c(0.09,5250), cov.model = "spherical", lik.method = "REML")
reml.exp<-likfit(g, ini.cov.pars=c(0.09,3000), cov.model = "exponential", lik.method = "REML")
lines(reml.sph, col="red", lwd=2)
lines(reml.exp, col="blue", lwd=2)
#so finally:
vg.PH_UP<-vg
model.PH_UP.exp<-model.exp
model.PH_UP.sph<-model.sph
model.PH_UP.reml.sph<-reml.sph
model.PH_UP.reml.exp<-reml.exp
#cross-validation
msdrvar<-"PH_UP"; xv[[msdrvar]]<-xvalid(g, model=model.PH_UP.reml.sph, trend="cte")
windows(); layout(matrix(1:10, 2,5, byrow=T)); plot(xv[[msdrvar]])
mean(((xv[[msdrvar]]$data-xv[[msdrvar]]$predicted)^2)/xv[[msdrvar]]$krige.var)

```

```

19 ##### DENS_UP ##### g/cm^3 #####
g<-as.geodata(dta.all, coords.col=2:3, data.col="DENS_UP")
summary(g); plot(g); print("skewness"); f_skewness(g$data); print("variance"); var(g$data)
vg.dir<-variog4(g, lambda=-0.5); plot(vg.dir) #note that transformation is applied (lambda=-0.5)
vg.mom<-variog(g, lambda=-0.5); points(vg.mom$u, vg.mom$v)
vg.rob<-variog(g, estimator="modulus", breaks=seq(0,8000,300), lambda=-0.5); points(vg.rob$u, vg.rob$v, pch="+")
maxd<-3500; br<-seq(0, maxd, 300)
vg.mom<-variog(g, trend="cte", breaks=br, max.dist=maxd, lambda=-0.5)
points(vg.mom$u, vg.mom$v, pch=16, col="red")
vg<-variog(g, trend="cte", breaks=br, max.dist=maxd, lambda=-0.5)
plot(vg)
pars.sig<-seq(2.5,3.5,0.5); pars.phi<-seq(500,2500,500); pars.nug<-seq(0.5,1.5,0.5)
rslt.sph<-fitting(vg, "spherical", maxd=maxd, pars.sig=pars.sig, pars.phi=pars.phi, pars.nug=pars.nug)
model.sph<-variofit(vg, ini=c(2.4, 2380), cov.model="spherical", nug=1.69, weights="npairs", max.dist=maxd)
lines(model.sph, lwd=2)
pars.phi<-pars.phi/3
rslt.exp<-fitting(vg, "exponential", maxd=maxd, pars.sig=pars.sig, pars.phi=pars.phi, pars.nug=pars.nug)
model.exp<-variofit(vg, ini=c(0.69, 817), cov.model="exponential", nug=0.18, weights="npairs", max.dist=maxd)
#so finally:
vg.bxDENS_UP<-vg
model.bxDENS_UP.exp<-model.exp
model.bxDENS_UP.sph<-model.sph
dta.all$bxDENS_UP<-bcx(dta.all$DENS_UP, lam=-0.5)

```



```

#cross-validation ('lambda' slot must be set manually to 1)
msdrvar<-"bxDENs_UP"
tmp<-model.bxDENs_UP.exp
tmp$lambda<-1
xv[[msdrvar]]<-xvalid(coords=g$coords, data=bcx(g$data, lam=-0.5), model=tmp, trend="cte")
windows(); layout(matrix(1:10, 2,5, byrow=T)); plot(xv[[msdrvar]])
mean(((xv[[msdrvar]]$data-xv[[msdrvar]]$predicted)^2)/xv[[msdrvar]]$krige.var)
median(((xv[[msdrvar]]$data-xv[[msdrvar]]$predicted)^2)/xv[[msdrvar]]$krige.var)

##### MOIST_UP ##### proportions #####
#EVENTUALLY, MAP OF MOIST_UP WAS DERIVED FROM MAP OF DENs_UP (Kra1, 2010)
g<-as.geodata(dta.all, coords.col=2:3, data.col="MOIST_UP")
g$data<-log(g$data/(1-g$data)) #logit transformation
summary(g); plot(g); print("skewness"); f_skewness(g$data); print("variance"); var(g$data)
vg.dir<-variog4(g); plot(vg.dir)
vg.mom<-variog(g); points(vg.mom$u, vg.mom$v)
vg.rob<-variog(g, estimator="modulus", breaks=seq(0,8000,300)); points(vg.rob$u, vg.rob$v, pch="+")
maxd<-4500; br<-seq(0, maxd, 300)
vg.mom<-variog(g, trend="cte", breaks=br, max.dist=maxd)
points(vg.mom$u, vg.mom$v, pch=16, col="red")
vg<-variog(g, trend="cte", breaks=br, max.dist=maxd)
plot(vg)
abline(a=var(g$data), b=0)
pars.sig<-seq(0.1,0.4,0.1); pars.phi<-seq(1000,2500,500); pars.nug<-seq(0.2,0.3,0.1)
rslt.sph<-fitting(vg, "spherical", maxd=maxd, pars.sig=pars.sig, pars.phi=pars.phi, pars.nug=pars.nug)
model.sph<-variofit(vg, ini=c(0.27, 1969), cov.model="spherical", nug=0.21, weights="npairs", max.dist=maxd)
lines(model.sph, lwd=2)
pars.phi<-pars.phi/3
rslt.exp<-fitting(vg, "exponential", maxd=maxd, pars.sig=pars.sig, pars.phi=pars.phi, pars.nug=pars.nug)
model.exp<-variofit(vg, ini=c(0.40, 605), cov.model="exponential", nug=0.08, weights="npairs", max.dist=maxd)
lines(model.exp, lwd=2)
#so finally:
vg.ltmOIST_UP<-vg
model.ltmOIST_UP.exp<-model.exp
model.ltmOIST_UP.sph<-model.sph
dta.all$ltmOIST_UP<-log(dta.all$MOIST_UP/(1-dta.all$MOIST_UP))
#cross-validation
msdrvar<-"ltmOIST_UP"
xv[[msdrvar]]<-xvalid(g, model=model.ltmOIST_UP.sph, trend="cte")
windows(); layout(matrix(1:10, 2,5, byrow=T)); plot(xv[[msdrvar]])
mean(((xv[[msdrvar]]$data-xv[[msdrvar]]$predicted)^2)/xv[[msdrvar]]$krige.var)
median(((xv[[msdrvar]]$data-xv[[msdrvar]]$predicted)^2)/xv[[msdrvar]]$krige.var)
reml.sph<-likfit(g, ini.cov.pars=c(0.5,1970), cov.model="spherical", lik.method="REML")

```

```

lines(reml.sph, col="blue")

##### DENS_LW ##### g/cm^3 #####
g<-as.geodata(dta.orig, coords.col=2:3, data.col="DENS_LW")
summary(g); plot(g); print("skewness"); f_skewness(g$data); print("variance"); var(g$data)
hist(log(g$data-0.0)); hist(bcx(g$data, lam=-0.5))
#g$data<-f_normal_score(g$data)[[1]]
vg.dir<-variog4(g); plot(vg.dir)
vg.mom<-variog(g); points(vg.mom$u, vg.mom$v)
vg.rob<-variog(g, estimator="modulus", breaks=seq(0,8000,300)); points(vg.rob$u, vg.rob$v, pch="+")
maxd<-4500; br<-seq(0, maxd, 300)
vg.mom<-variog(g, trend="cte", breaks=br, max.dist=maxd)
points(vg.mom$u, vg.mom$v, pch=16, col="red")
vg<-variog(g, trend="cte", breaks=br, max.dist=maxd)
#Any transformation did not reveal any clear variogram

##### MOIST_LW ##### g/cm^3 #####
g<-as.geodata(dta.orig, coords.col=2:3, data.col="MOIST_LW")
summary(g); plot(g); print("skewness"); f_skewness(g$data); print("variance"); var(g$data)
hist(bcx(g$data, lam=3))
hist(log(g$data/(1-g$data)))
#g$data<-f_normal_score(g$data)[[1]]
vg.dir<-variog4(g); plot(vg.dir)
vg.mom<-variog(g); points(vg.mom$u, vg.mom$v)
vg.rob<-variog(g, estimator="modulus", breaks=seq(0,8000,300)); points(vg.rob$u, vg.rob$v, pch="+")
maxd<-4500; br<-seq(0, maxd, 300)
vg.mom<-variog(g, trend="cte", breaks=br, max.dist=maxd)
points(vg.mom$u, vg.mom$v, pch=16, col="red")
vg<-variog(g, trend="cte", breaks=br, max.dist=maxd)
#Any transformation did not reveal any clear variogram

#####
#####
##### KRIGING #####
#####
#####

krg<-list() #list to store all the kriged maps
#list of models used for kriging
mdl<-list(model.PH_UP.reml.sph,model.ORGAN_UP.exp,model.TP_UP.sph,model.TN_UP.exp,model.TC_UP.exp, model.bxDENS_UP.exp) . .
. .
names(mdl)<-c("PH_UP","ORGAN_UP","TP_UP","TN_UP","TC_UP", "bxDENS_UP")
#region and raster grid definition

```

```

res<-25
region<-list(x=seq(756500,766600,res), y=seq(3305400,3312400,res), xbounds=list(min=756500, max=766600), ybounds=list(mi..
..n=3305400,max=3312400), res=res)
ras<-expand.grid(x=seq(region$xbounds$min,region$xbounds$max, region$res), y=seq(region$ybounds$min,region$ybounds$max, ..
..region$res))

for(i in names(mdls)){#kriging itself
  if(i=="bxDENS_UP"){
    g<-as.geodata(dta.all, coords.col=2:3, data.col="DENS_UP")
    krg[[i]]<-krige.conv(g, locations=ras, krige=krige.control(type="ok", obj.mod=mdls[[i]], lambda=-0.5))
  }else{
    g<-as.geodata(dta.all, coords.col=2:3, data.col=i)
    krg[[i]]<-krige.conv(g, locations=ras, krige=krige.control(type="ok", obj.mod=mdls[[i]]))
  }
}

#regression of MOIST_UP~DENS_UP
reg<-lm(dta.all$MOIST_UP~dta.all$DENS_UP)
plot(dta.all$MOIST_UP~dta.all$DENS_UP, asp=1, xlab="DENS_UP", ylab="MOIST_UP", pch=16)
abline(a=reg$coefficients[1],b=reg$coefficients[2])
reg.pred<-reg$coefficients[1]+reg$coefficients[2]*krg[["bxDENS_UP"]]$pred
db_0<-summary(reg)[[4]][1,2]; db_1<-summary(reg)[[4]][2,2] #SE of beta_i
b_0<-reg$coefficients[1]; b_1<-reg$coefficients[2] #beta_i
#error propagation
reg.var<-db_0^2 + (krg[["bxDENS_UP"]]$pred^2)*(db_1^2) + (b_1^2)*(krg[["bxDENS_UP"]]$krige.var) + summary(reg)$sigma^2 +..
.. krg[["bxDENS_UP"]]$pred*db_0*db_1*(-0.76610515905554088522677602668409235775470733642578) #the long number is correla..
..tion coefficient between b_0 and b_1, derived from covatiance matrix of b~N(beta, inv(X'X)*sigma^2)
krg[["bxMOIST_UP"]]<-list(predict=reg.pred, krige.var=reg.var)

#crate a mask to mask out pixels that are not in Davis Pond
shp<-readShapePoly("bnd.shp")
shp.win<-as(as(shp, "SpatialPolygons"), "owin") #convert shapefile to owin
ras.mask<-inside.owin(x=ras$x,y=ras$y,w=shp.win) #vector, TRUE when cell is within Davis Pond, FALSE otherwise.
for(i in names(krg)){ #mask out the cells out of Davis Pond
  krg[[i]]$predict[!ras.mask]<--9999
  krg[[i]]$krige.var[!ras.mask]<-10000000000
}

#write all the kriging predictions and variances to ascii grids
for(v in c("PH_UP", "ORGAN_UP", "TP_UP", "TN_UP", "TC_UP", "bxDENS_UP", "bxMOIST_UP")){
  map.pred<-matrix(krg[[v]]$pred,ncol=length(region$x), nrow=length(region$y), byrow=TRUE)
  map.var<-matrix(krg[[v]]$krige.var,ncol=length(region$x), nrow=length(region$y), byrow=TRUE)
  map.sd<-matrix(sqrt(krg[[v]]$krige.var),ncol=length(region$x), nrow=length(region$y), byrow=TRUE)
}

```

```

mx2asciigrid(map.pred, outpath%p%prefix%p%v%p%"_pred"%p%suffix%p%".txt", 25, xll=756500, yll=3305400)
mx2asciigrid(map.var, outpath%p%prefix%p%v%p%"_var"%p%suffix%p%".txt", 25, xll=756500, yll=3305400, nodata=1000000000..
..)
mx2asciigrid(map.sd, outpath%p%prefix%p%v%p%"_sd"%p%suffix%p%".txt", 25, xll=756500, yll=3305400, nodata=sqrt(10000000..
..000))
}

#####
#####
##### LINEAR MODEL OF COREGIONALIZATION #####
#####
#####

d<-dta.all
vars<-c("PH_UP", "ORGAN_UP", "TP_UP", "TN_UP", "TC_UP", "bxDENS_UP")
#build the gstat object
if(exists("gs")){rm(gs)}
gs<-gstat(id=vars[1], formula=as.formula(paste(vars[1], "~1")), locations=~XCOORD+YCOORD, data=d[,c("XCOORD", "YCOORD", vars[1]..
..)], degree=0)
for(i in vars[-1]){
65   gs<-gstat(gs, id=i, formula=as.formula(paste(i, "~1")), locations=~XCOORD+YCOORD, data=d[,c("XCOORD", "YCOORD", i)], degree=0)..
..
}
#variograms
vgrams<-variogram(gs, boundaries=seq(0,3500,300))
#fit LMCR
lmc<-fit.lmc(vgrams, gs, model=vgm(100,"Exp",1100,1), fit.ranges=FALSE, fit.lmc=TRUE, correct.diagonal=1.0, fit.sills=TR..
..UE, fit.method=2)
for(i in names(lmc$model)){ #insert the models into the gstat object
  vname<-unlist(strsplit(i, "\\."))
  gs<-gstat(gs, id=vname, model=lmc$model[[i]])
}
plot(vgrams, model=gs$model)

#coregionalization matrices and hulls of perfect correlation
lmc<-f_lmc_mx(gs, structures=c("Nug", "Exp"), hulls=TRUE, hulls.x=1:4000)

#plotting hulls
windows()
vgr<-vgrams
lyt<-matrix(0, nrow(lmc$nmx)-1, ncol(lmc$nmx)-1)
lyt[lower.tri(lyt, diag=TRUE)]<-1:length(lmc$nmx[lower.tri(lmc$nmx)])
x<-1:4000

```

```

layout(lyt)
for(v in lmcrc$nmx[lower.tri(lmcrc$nmx)]){
  h<-lmcrc$hull[[v]]
  par(mar=c(2,2,2,1))
  plot(x,h, ylim=c(-max(h), max(h)), type="l", main=v, xlab="", ylab="")
  lines(x,-h)
  points(vgr[vgr$id==v,]$dist, vgr[vgr$id==v,]$gamma)
  mdl<-gs$model[[v]]
  lines(x, mdl[1,2] + mdl[mdl[,1]=="Exp",2]*Exp(x, range=mdl[mdl[,1]=="Exp",3] , sill=1), lwd=2)
} #end plotting hulls

#codispersion coefficients
codisp<-ccc(variogram(gs, tol.hor=180, boundaries=seq(0,8000,600)))
#structural codispersion coefficients
ccc_mx<-ccc_structural(lmcrc)

#####
#####          #####
##### MOVING WINDOW #####
#####          #####
#####

#constitute the matrix of predicted values
mw.variables<-c("PH_UP", "TN_UP", "ORGAN_UP", "TP_UP", "TC_UP", "bxDENS_UP") #variables to include in the moving window ..
..analysis
mw.data<-matrix(NA,nrow=length(krg[[1]]$predict), ncol=length(mw.variables), dimnames=list(NULL, mw.variables))
for(i in dimnames(mw.data)[[2]]){ mw.data[,i]<-krg[[i]]$predict }
mw.data[!ras.mask,]<-NA #mask out the cells out of the Davis Pond

#set the properties of the grid of moving window centres
mw.grdsp<-100 #grid spacing
mw.region<-list(x=seq(min(region$x),max(region$x), mw.grdsp), y=seq(min(region$y),max(region$y),mw.grdsp))
mw.grd<-expand.grid(x=mw.region$x, y=mw.region$y)
mw.wws<-c(250,500,750,1100,2200,3300) #a vecotr of window widths to use
mw.rslt<-list() #for storing the results of moving window

#run the moving window analysis
for(w in mw.wws){
  mw.rslt[[paste("win", w, sep="")]<-movin(gridx=mw.grd$x, gridy=mw.grd$y, ww=w, wh=w, datx=ras$x, daty=ras$y, dat=as.d..
  ..ata.frame(mw.data), corr=TRUE)
  print(w) #just to keep the user informed
}

```

```

#mask the grid cells (centres of moving windows) that are out of Davis Pond
#mask values in all columns except("gridx","gridy","nofpts","nofpts.compl")
mw.mask<-inside.owin(x=mw.grd$x,y=mw.grd$y,w=shp.win)
for(i in names(mw.rslt)){
  mw.rslt[[i]][,-(1:4)][!mw.mask,]<--9999
}

#write the moving window results into files
for(i in names(mw.rslt)){
  tmp<-mw.rslt[[i]]
  write.csv(tmp, outpath%p%i%p"_vec.csv")
  for(j in names(tmp)[grep("rho", names(tmp))]){
    map.rast<-matrix(tmp[,j],ncol=length(mw.region$x), nrow=length(mw.region$y), byrow=TRUE)
    mx2asciigrd(map.rast, outpath%p%prefix%p%i%p%"_"%p%(paste(strsplit(j, "\\.")[[1]], collapse="2"))%p%"_rast"%p%suffi..
    ..x%p%.txt", 100, xll=min(mw.region$x), yll=min(mw.region$y))
  }
}

```

## # rfunctions.r #

#custom functions used during the project:

```
#bcx, f_xvalid, movin, mx2asciigrid, ccc_structural, ccc, Sph, Exp, f_lmcr_mx, f_likfit, f_dowd, hist.data.frame, f_tren..  
..d, f_normal_score, f_normal_score_back, "%p%", as.geodata.except, fitting, hist.pdf.normal, f_skewness_desa, f_skewnes..  
..s, f_pca
```

```
bcx<-function(x, lam=1){#Box-Cox transformation with parameter lambda  
  if(lam==0){return(log(x))} else { return( (x^lam - 1) / lam ) }  
}
```

```
f_xvalid<-function(x,y,z, model){  
#variogram model cross-validation  
#e.g.: x=dta$X, y=dta$Y, z=dta$TN_UP, model=vgm(832,"Sph",2000,236)  
#NO INPUT CHECKING IS PERFORMED!  
  n<-length(x); predictions<-numeric(n); variances<-numeric(n)  
  for(i in 1:n){#leave one out  
    left_out<-data.frame(x=x[i], y=y[i]) #coordinates of the left-out point  
    d_tmp<-data.frame(x=x[-i],y=y[-i],z=z[-i])  
    gs_tmp<-gstat(id="z", formula=z~1, locations=~x+y, data=d_tmp)  
    gs_tmp<-gstat(gs_tmp, id="z", model=model)  
    p<-predict(gs_tmp, left_out)  
    predictions[i]<-p[1,3];  
    variances[i]<-p[1,4]  
  }  
  return(data.frame(Z.orig=z, Z.pred=predictions, Z.var=variances))  
}
```

89

```
movin<-function(gridx=c(0), gridy=c(0), ww=1, wh=1, datx, daty, dat, corr=TRUE){  
#Moving window statistics  
#gridx, gridy: vector of x (and y) coordinates of points of the grid (centres of the windows)  
#ww,wh: window width and window height define a window as (x,y)+-(ww/2,wh/2)  
#datx, daty: vector of x (and y) coordinates of the data points  
#dat: vector, data.frame, or matrix of data values with columns as vectors of data values (it is convenient to use a dat..  
..a frame with named columns to make the output easy to understand)  
#corr: if TRUE, correlation coefficients of variables in each window are included in the output  
#  
#Returns a data frame where each row represents one window with columns:  
# gridx, gridy (same as input), mean_name1, .., mean_nameM, var_name1, var_nameM for all the M variables (columns) in da..  
..t input, nofpts reports number of points in the window, nofpts.comp1 is number of rows that have non-NA values in the ..  
..window  
# if corr==TRUE, then also columns rho_name1.name2 etc. of correlation coefficients of corresponding variables in each w..
```

```

..indow are included
#NOTE that NA values are removed from calculation of means and variances, sample variance is calculated (1/(N-1)), the u..
..se parameter for cor() function is "na.or.complete" (see ?cor details for description)
#
#201006281130

nvar<-ncol(dat) #number of variables
nms<-names(dat) #names of variables
if(is.null(nms)){nms<-1:nvar}
w<-ww/2; h<-wh/2 #half of the window size
dat<-as.matrix(dat)
if(length(gridx)!=length(gridy)){ print("gridx and gridy must have the same length"); return();}
if(corr && length(dat[,1])<2){ print("dat must have more than one column to enable correlation coefficients computation..
.."); return()}
if(length(datx)!=length(daty) || length(datx)!=length(dat[,1]) || length(dat[,1])!=length(daty)){print("datx,daty,dat[.
..,i] must have the same length"); return();}

#declare outputs
means<-data.frame(gridx,gridy)
vars<-data.frame(gridx,gridy)
np<-numeric() #number of data points in each window
np.compl<-numeric() #number of complete measurements in each window
cr<-list() #correlation matrices for each window

for(i in 1:length(gridx)){
  winx<-which((datx>=gridx[i]-w & datx<=gridx[i]+w) & (daty>=gridy[i]-h & daty<=gridy[i]+h)) #indexes of rows of dat t..
  ..hat are within the current (i-th) window
  np[i]<-length(winx)
  if(np[i]>0){ #if there is a data point in the window then proceed
    curwin<-dat[winx,, drop=F] #extract the points in current window to a separate variable
    np.compl[i]<-0; for(r in 1:np[i]){ if(all(!is.na(curwin[r,])))}{np.compl[i]<-np.compl[i]+1} } #count the number of ..
    ..complete measurements in the current window
    for(k in 1:nvar){
      means[i,k+2]<-mean(curwin[,k], na.rm=TRUE)
      vars[i,k+2]<-var(curwin[,k], na.rm=TRUE)
    }
    if(corr){#note that cor returns NA for one point or when sd=0
      cr[[i]]<-cor(curwin, use="na.or.complete")
    }
  }
}
}

#finishing outputs (names etc.)

```



```

out<-data.frame(gridx, gridy, np, np.compl)
outnames<-c("gridx", "gridy", "nofpts", "nofpts.compl")
for(i in 3:length(names(means))){
  out[,length(names(out))+1]<-means[,i]
  outnames<-c(outnames, paste("mean_", nms[i-2], sep=""))
}
for(i in 3:length(names(vars))){
  out[,length(names(out))+1]<-vars[,i]
  outnames<-c(outnames, paste("var_", nms[i-2], sep=""))
}
if(corr){
  rho.nms<-c()
  for(k in 2:nvar){rho.nms<-c(rho.nms, paste(nms[k-1], nms[k:nvar], sep="."))}
  rho<-matrix(NA,nrow=length(gridx), ncol=length(rho.nms))
  j<-1; for(i in cr){ rho[j,]<-i[lower.tri(i)]; j<-j+1 }
  rho<-as.data.frame(rho)
  names(rho)<-paste("rho_", rho.nms, sep="")
}
names(out)<-outnames
if(corr){return(data.frame(out,rho))} else {return(out)}
}

mx2asciigrid<-function(mx, filename="map.txt", resolution, xll, yll, nodata=-9999, offset=TRUE){
#Writes matrix 'mx' to a file 'filename' as an ascii grid prepared to import to ArcGIS by ASCII to Raster tool.
#'resolution' is the cell size, 'xll' and 'yll' are the coordinates of lower left cell of the matrix 'mx',
#'nodata' is the value that should be used to indicate nodata (note that the actual value for no data in 'mx' is not alt..
..ered and this must be handled by the user)
#if 'offset' is TRUE then the origin is shifted half the cell size so that values are associated with cell centres in th..
..e resulting ascii grid file
#201006112000
hdr<-data.frame(c("ncols","nrows","xllcorner","yllcorner","cellsize","NODATA_value"), c(ncol(mx), nrow(mx), xll, yll, ..
..resolution, nodata))
if(offset){hdr[3,2]<-(xll-resolution/2); hdr[4,2]<-(yll-resolution/2)}
write.table(hdr, filename, col.names=FALSE, row.names=FALSE, sep=" ", quote=FALSE)
for(k in nrow(mx):1){
  write.table(t(mx[k,]), filename, col.names=FALSE, row.names=FALSE, sep=" ", append=TRUE)
}
}

ccc_structural<-function(lmcr){
#Calculate structural correlation coefficients for linear model of coregionalization.
#lmcr: output of function f_lmcr_mx() containing the $b: coregionalization matrices for individual structures, $nmx: mat..
..rix of names of variables to facilitate queries

```

#Returns a named matrix of structural correlation coefficients for each combination of variables and structures.  
 #NOTE that variable names containing more than one period in the lmcr will cause problems.

#201006112000

```

structures<-names(lmcr$b) #names of the structures present in lmcr
u.v<-lmcr$nmx[lower.tri(lmcr$nmx)] #names of the combinations of variables
out<-matrix(NA, length(u.v), length(structures), dimnames=list(u.v, structures))
for (struct in structures){#for each structure present in the lmcr$b
  bi<-lmcr$b[[struct]] #coregionalization matrix of particular structure in the struct loop
  cc<-numeric()
  for (i in 1:length(u.v)){ #for each combination of variables
    u<-strsplit(u.v[i], "\\."[[1]]
    v<-u[length(u)]
    u<-u[1]
    inx.uv<-which(lmcr$nmx==u.v[i], arr.ind=TRUE)[1,] #indices of the particular combination in the i loop
    inx.u<-as.numeric(inx.uv[2])
    inx.v<-as.numeric(inx.uv[1])
    cc[i]<-bi[inx.u,inx.v]/sqrt(bi[inx.u,inx.u]*bi[inx.v,inx.v])
  }
  out[,struct]<-cc
}
return(out)
}

```

71

```

ccc<-function(vgrm){
#Calculate codispersion coefficient.
#vgrm: experimental variogram obtained from gstat::variogram function, must contain at least two variables and their com..
..bination (cross-variogram)
#Returns a data frame (similar to that which returns function gstat::variogram)
# values of codispersion coefficient (column 'gamma') are calculated at specific lag distances (column 'dist') for the p..
..articular variable (column 'id')
# at each lag h, the codispersion coefficient is calculated according to equation 8 in Pringle and Lark (2006), i.e. ccc..
..=gamma_uv(h)/sqrt(gamma_u(h)*gamma_v(h)), where gamma stands for the value of experimental variogram.
#NOTE that variable names in the vgrm containing more than one period will cause problems.
#201006112000
out.d<-numeric(); out.c<-numeric(); out.v<-character()
u.v<-levels(as.factor(vgrm$id))
for(i in 1:length(u.v)){
  u<-strsplit(u.v[i], "\\."[[1]]
  zetor<-6 #limit for zero tolerance (used for evaluating two distances as the same if the difference is at a further ..
  ..than zetor-th decimal place)
  vgrm$dist<-trunc(vgrm$dist*10^(zetor))/(10^zetor)
  if(length(u)>1){
    v<-u[length(u)]

```

```

    u<-u[1]
    vg.uv<-vgrm[vgrm$id==u.v[i],]
    vg.u<-vgrm[vgrm$id==u,]
    vg.v<-vgrm[vgrm$id==v,]
    h<-vg.uv[vg.uv$id==u.v[i],]$dist #lag distances
    cc<-numeric() #codispersion coefficient
    for(j in 1:length(h)){
      cc[j]<-vg.uv[vg.uv$dist==h[j],]$gamma/sqrt(vg.u[vg.u$dist==h[j],]$gamma*vg.v[vg.v$dist==h[j],]$gamma)
    }
    out.d<-c(out.d, h); out.c<-c(out.c, cc); out.v<-c(out.v, rep(u.v[i], length(h)))
  }
}
return(data.frame(dist=out.d, gamma=out.c, id=out.v))
}

```

```

Sph<-function(x, range, sill){
#Spherical variogram model function (Webster and Oliver, 2007, p. 88)
#201006111000
k<-length(x); y<-numeric(k)
for(i in 1:k){ if(x[i]<=0){y[i]<-NaN}else{ if(x[i]>range){y[i]<-sill} else {y[i]<-sill*((3*x[i])/(2*range) - 0.5*((x[i..
..]/range)^3))}}}}
return(y)
}

```

```

Exp<-function(x, range, sill){
#Exponential variogram model function (Webster and Oliver, 2007, p. 88)
#201006111000
k<-length(x); y<-numeric(k)
for(i in 1:k){ y[i]<-sill*(1-exp(-x[i]/range)) }
return(y)
}

```

```

f_lmcr_mx<-function(gs, structures=c("Nug", "Exp"), hulls=FALSE, hulls.x=NULL){
#Extract coregionalization matrices from the object gs (gstat::gstat).
#gs: gstat object with fitted linear model of coregionalization by gstat::fit.lmc
#structures: a character vector specifying which structures are present in the LMCR, currently just models like Nug+Exp+..
..Sph are supported, not Nug+Exp+Exp
#hulls: if TRUE, then also a list of hulls of perfect correlation is returned
#hulls.x: numeric vector to specify at which lag distances to calculate the hull of perfect correlation (e.g., 1:4000)
#Returns a list with items:
# b: a list of coregionalization matrices for individual structures in the linear model of coregionalization of object g..
..S
# nm: a matrix of names that correspond to each element in the items of b

```

```

# hull: a list of vectors defining the hull of perfect correlation (can be used for plotting the hulls)
#201006112000
v.v<-names(gs$model)
b<-list() #list for coregionalization matrices for individual structures
ord<-length(names(gs$data)) #order of the coregionalization matrix
nmx<-matrix(NA, ord, ord) #"matrix of names of the variables to facilitate further queries
structures<-structures
for(s in structures){
  b[[s]]<-matrix(rep(NA,ord^2), nrow=ord)
  elm<-numeric()
  for(v in v.v){
    elm[v]<-gs$model[[v]][gs$model[[v]]==s,][,2]
  }
  #fill in the lower triangle and diagonal
  k<-1
  for(j in 1:ord){ for(i in j:ord){
    nmx[i,j]<-v.v[k]
    b[[s]][i,j]<-gs$model[[v.v[k]]][gs$model[[v]]==s,][,2] ; k<-k+1
  } }
  #fill in the upper triangle symmetrically to lower triangle
  for(j in 2:ord){ for(i in 1:j){
    b[[s]][i,j]<-b[[s]][j,i]
    nmx[i,j]<-nmx[j,i]
  } }
}

#calculate hulls of perfect correlation if requested
if(hulls){
  if(is.null(hulls.x)){print("Parameter hulls.x must be specified when hulls=TRUE. Using default settings: hulls.x=1:4..
  ..000"); hulls.x<-1:4000} else {x<-hulls.x}
  combinations<-nmx[lower.tri(nmx)]
  allhulls<-list()
  for(comb in combinations){
    v<-strsplit(comb, "\\.")[[1]]
    hll<-numeric(length(x))
    for(s in names(b)){
      if(s=="Nug") {
        b_uu<-b$Nug[which(nmx==v[1], arr.ind=TRUE)]
        b_vv<-b$Nug[which(nmx==v[2], arr.ind=TRUE)]
        hll<-hll+sqrt(b_uu*b_vv)
      }
      if(s=="Sph") {
        b_uu<-b$Sph[which(nmx==v[1], arr.ind=TRUE)]

```

```

    b_vv<-b$Sph[which(nmx==v[2], arr.ind=TRUE)]
    hll<-hll+sqrt(b_uu*b_vv)*Sph(x, range=gs$model[[comb]][gs$model[[comb]][,1]=="Sph",3], sill=1)
  }
  if(s=="Exp") {
    b_uu<-b$Exp[which(nmx==v[1], arr.ind=TRUE)]
    b_vv<-b$Exp[which(nmx==v[2], arr.ind=TRUE)]
    hll<-hll+sqrt(b_uu*b_vv)*Exp(x, range=gs$model[[comb]][gs$model[[comb]][,1]=="Exp",3], sill=1)
  }
} #end for s
allhulls[[comb]]<-hll
} #end for comb
}

return(list(b=b, nmx=nmx, hull=allhulls))
}

```

74

```

f_likfit<-function(g, model="spherical", ini.model=NULL, pars.sig, pars.phi, trend="cte", method="REML", print.pars=TRUE..
.., lines=FALSE, clr="red"){
#Run function likfit::gstat with a number of different parameters.
#g as geodata, pars.sig,pars.phi=c(middle, +-boundary, step)
#set lines=TRUE to enable drawing the models on a variogram plot (you have to check which device is the correct one)
#set model="unspecified" to obtain the model fitted by likfit in f_likfit()$models$...$cov.model
#Returns a list with vector logliks which are the log-likelihoods of the models in item models
#201006031315
r<-list()
best<-list()
pars.sig<-seq(pars.sig[1]-pars.sig[2],pars.sig[1]+pars.sig[2], pars.sig[3])
pars.phi<-seq(pars.phi[1]-pars.phi[2],pars.phi[1]+pars.phi[2], pars.phi[3])
for(sig in pars.sig){#for each sill
  for(phi in pars.phi){#for each range
    if(is.null(ini.model)){
      if(model=="unspecified"){
        r<-likfit(g, trend=trend, ini.cov.pars=c(sig, phi), lik.method=method, print.pars=print.pars)
      }else{
        r<-likfit(g, trend=trend, ini.cov.pars=c(sig, phi), cov.model=model, lik.method=method, print.pars=print.pars)..
        ..
      }
    } else {
      if(model=="unspecified"){
        r<-likfit(g, trend=trend, ini.cov.pars=ini.model, lik.method=method, print.pars=print.pars)
      }else{
        r<-likfit(g, trend=trend, ini.cov.pars=ini.model, cov.model=model, lik.method=method, print.pars=print.pars)
      }
    }
  }
}

```

```

    }
  }
  if(lines){ lines(r, col=clr) }
  best[[paste("s",sig,"p",phi,sep="")] ]<-r
} #end sig
} #end phi
logliks<-numeric()
for(i in names(best)){
  logliks[i]<-best[[i]]$loglik
}
return(list(logliks=logliks, models=best))
}

```

```

f_dowd<-function(cld, br=seq(0,8000,400)){
#Calculate the Dowd's robust estimate of variogram.
#Lark (2000) A comparison of some robust estimators of the variogram for use in soil survey, European Journal of Soil Sc..
..ience, 51, 137-157.
#cld: a variogram cloud from function variog(geodata, option="cloud")
#br: a vector of breaks
#Returns a variogram of estimator type "Dowd".
#NOTE that not all data items of class variogram are returned in the output properly which will probably cause problems ..
..whe using with other functions from geor
#201006031030
u<-numeric(); v<-numeric(); n<-numeric(); sd<-numeric()
for (i in 1:(length(br)-1)){
  u[i]<-br[i]+(br[i+1]-br[i])/2
  y<-cld$v[cld$u<br[i+1] & cld$u>br[i]]
  v[i]<-0.5*2.198*median(abs(y))^2
  n[i]<-length(y)
}
vg<-list(u=u, v=v, n=n, sd=sd, var.mark=var(cld$var.mark), estimator.type="Dowd", direction="omnidirectional", uvec=u)..
..
class(vg)<-"variogram"
return(vg)
}

```

```

hist.data.frame<-function(d, nr=2){
#Draw histograms of all numeric columns in data.frame d.
#nr: number of row in the resulting layout
#NOTE that dimensions are not checked.
#201006021715
layout(matrix(1:(nr*(ceiling(length(names(d)))/nr))), nrow=nr))
for(i in names(d)){if(is.numeric(d[,i])){ hist(d[,i], main=i) }}

```

```

}

f_trend<-function(x,y,z, ord=1, mode="residuals"){
#Detrending the data x,y,z.
#x,y,z: x,y, and z coordinates where x,y are meant to denote position and z the measured variable.
#ord: order of the polynomial surface to work with.
#if mode="expected", returns a vector of expected values of polynomial surface of order ord fitted through (x,y,z) at lo..
..cations (x,y)
#if mode="residuals", returns a vector of residuals (observed-expected)
#201006021715
n<-length(z)
if((n-length(y))!=0 || ((n-length(x))!=0)){ print("x,y,z must have the same length"); return() }
require(spatial)
surface<-surf.ls(ord,x,y,z) #fit the surface
detr<-numeric(n)
for(i in 1:n){ detr[i]<-trmat(surface, x[i], x[i], y[i], y[i], 1)$z }
if(mode=="residuals"){ return(z-detr) }else{
  if(mode=="expected"){ return(detr) } else { return() }
}
}
}

```

76

```

f_normal_score<-function(x){
#Perform normal score transformation.
#x: vector with data values
#Returns a list where first item ($nscore) is vector x transformed to its normal scores,
# second item ($trt) is the transformation table with columns 'orig' and 'norm' which can be used for backtransformation..
..
#Based on p.268 in Goovaerts (1999) Geostatistics for Natural Resources Evaluation, Oxford University Press, New York, U..
..SA.
#NOTE that normal score transform should be performed after detrending ( http://help.arcgis.com/en/arcgisdesktop/10.0/he..
..lp/index.html#//0031000000v000000.htm )
#no declustering implemented
#201006021600
n<-length(x)
pre<-data.frame(1:n, x)
pre<-pre[order(pre[,2]),]
pscore<-numeric(0)
for (k in 1:n){ pscore[k]<-(k/n)-(0.5/n) }
pre$pscore<-pscore; pre$trans<-qnorm(pscore)
trt<-data.frame(pre[,2], pre$trans); names(trt)<-c("orig","norm")
pre<-pre[order(pre[,1]),]
return(list(nscore=pre$trans, trt=trt))
}

```

```

f_normal_score_back<-function(r, trt=data.frame(orig=c(1,2),norm=c(1,-1))){
#Perform normal score back transformation according to specified transformation table.
#r: vector of normal scores
#trt: transformation table with columns 'orig' (original value) and 'norm' (normal score).
#Returns a backtransformed values of r according to the transformation table trt
#linear interpolation is performed between values
#NOTE that transformation out of range of trt$orig is not implemented!
#201006021600
  if(any(names(trt)== "orig") && any(names(trt)== "norm")){
    return(approx(x=trt$norm, y=trt$orig, xout=r)$y)
  }else{
    return(approx(x=trt[,2], y=trt[,1], xout=r)$y)
  }
}

"%p%"<-function(a,b){paste(a,b, sep="")} #operator facilitating pasting

as.geodata.except<-function(dta, coords.col=2:3, data.col, col="PID", val=c()){
#Create a geodata object but exclude specific rows in the input data.frame.
#dta: data.frame that would be normally used to create the geodata object by geOR::as.geodata(dta)
#data.col: same as data.col for geOR::as.geodata()
#col: column name in dta, values in this column will be evaluated by this function for exclusion
#val: vector of values of col, specifies which rows should be excluded
#Returns a geodata object created from dta with specified rows removed.
  d<-dta
  for(i in val){
    print(paste("excluding:",i))
    d<-d[d[,col]!=i,]
  }
  return(as.geodata(d, coords.col=coords.col, data.col=data.col))
}

fitting<-function(vgram, model="exponential", maxd, pars.sig=c(1), pars.phi=c(1), pars.nug=c(0), weights="npairs"){
#Fit variogram with different initial parameters.
#vgram: output from variog()
#pars.sig, pars.phi, pars.nug are vectors of values of sill, range and nugget, all combinations of these values will be ..
..used as initial parameters for the fitting procedure
#maxd: is for max.dist
#see help for variofit() for description of weights and other details.
#Returns a data.frame ordered according to the minimised weighted sum of squares showing the corresponding model paramet..
..es
#model parameter kappa not implemented

```



```

fit<-list()
for(s_i in pars.sig){ for(p_i in pars.phi){ for(n_i in pars.nug){
  fit[[paste("p",s_i,p_i,n_i,sep="_")]]<-variofit(vgram, ini=c(s_i, p_i), cov.model=model, nug=n_i, weights=weights, m..
  ..ax.dist=maxd)
}}
pars.comb<-character();sig<-numeric();phi<-numeric();tau<-numeric();minsq<-numeric()
for(i in names(fit)){
  pars.comb<-c(pars.comb, i)
  minsq<-c(minsq, fit[[i]][[5]])
  sig<-c(sig, fit[[i]][[2]][1])
  phi<-c(phi, fit[[i]][[2]][2])
  tau<-c(tau, fit[[i]][[1]][1])
}
rslt<-data.frame(pars.comb, minsq, sig, phi, tau)
return(rslt[order(rslt[,2]),])
}

hist.pdf.normal<-function(x=c(1,2), lwd=1, lty=1, col="black"){
#Draw the probability density function for X~N(mean(x), var(x))
#to the active graphical window (must be managed by the user).
#Can be used for adding such lines to histograms
#The histogram must be the probability/density/relative histogram to match properly.
#201004152336
x<-x[!is.na(x)] #remove NAs
m<-mean(x); s<-sd(x)
r<-max(m-min(x),max(x)-m)
if(r<1){ step<-0.001 }else{ if(r<10){ step<-0.01 }else{ step<-0.1 } }
a<-seq(m-4*r,m+4*r,step)
lines(a, dnorm(a, mean=m, sd = sd(x)), lwd = lwd, lty = lty, col = col)
}

f_skewness_desa<-function(x=c(1), help=FALSE){
#Calculates skewness of vector x, removes NA values first.
#Core of the function from: De Sá, J.P.M. (2007) Applied statistics using SPSS, STATISTICA, MATLAB and R, (2nd edition), ..
..Springer-Verlag, Berlin, D. Page 66
#201005182130
x<-x[!is.na(x)]; n<-length(x); y<-(x-mean(x))^3
return(n*sum(y)/((n-1)*(n-2)*sd(x)^3))
}

f_skewness<-function(x=c(1), help=FALSE){
#Calculate skewness of the vector x, remove NA values first.
#Formula for skewness from http://en.wikipedia.org/wiki/Skewness

```

```

#201005182130
y<-x[!is.na(x)]
m3<-0; m2<-0; mn<-mean(y); n<-length(y)
if(length(x)!=n){ print(paste(length(x)-n, "NA values ignored."))}
for (i in 1:n){ m3<-m3+(y[i]-mn)^3; m2<-m2+(y[i]-mn)^2 }
m3<-m3/n; m2<-m2/n; g<-m3/(m2^(3/2))
return(g)
}

f_pca<-function(x=matrix(c(1,2,3,4),2,2)){
#Return a list with two items. First is a matrix where columns
# are principal components of vectors in x, second item is a vector
# of eigenvalues of var(x).
#x: rows as replicates of different variables (columns)
#201005232115
e<-eigen(var(x))
y<-t(e$vectors)%*%t(x)
return(list(t(y),e$values))
}

```

## # regional\_stocks.r #

```
#estimation of element stocks in Davis Pond  
#HAS TO BE EXECUTED IN THE MAIN WORKSPACE (AFTER main.r)
```

```
area<-sum(ras.mask)*25^2 #Davis Pond area (37071250 m2)
```

```
#regional estimates in the upper layer using sample mean
```

```
rgn.up<-dta.orig[c("TC_UP", "TN_UP", "TP_UP")]
```

```
for(i in c("TC_UP", "TN_UP", "TP_UP")){
```

```
  conv<-ifelse(i == "TP_UP", 0.001, 1) #TP is in mg/kg, others are in g/kg, we will get kg/m3 after multiplying it by den..  
  ..sity [g/cm3] and this conversion factor
```

```
  rgn.up[i]<-conv*rgn.up[i]*dta.orig["DENS_UP"] #in kg/m3 at each sampling point
```

```
}
```

```
rgn.up.sum<-apply(rgn.up, 2, mean)*area*0.1 #the 0.1 is just the 10 cm layer
```

```
rgn.up.var<-apply(rgn.up, 2, var)*(area*0.1)^2 #variance  $D(cX) = c^2 D(X)$ 
```

```
rgn.up.se<-sqrt(rgn.up.var/139) #standard error of the mean in kg
```

```
#regional estimates in the lower layer using sample mean
```

```
rgn.lw<-dta.orig[c("TC_LW", "TN_LW", "TP_LW")]
```

```
for(i in c("TC_LW", "TN_LW", "TP_LW")){
```

```
  conv<-ifelse(i == "TP_LW", 0.001, 1) #TP is in mg/kg, others are in g/kg, we will get kg/m3 after multiplying it by den..  
  ..sity [g/cm3] and this conversion factor
```

```
  rgn.lw[i]<-conv*rgn.lw[i]*dta.orig["DENS_LW"] #in kg/m3 at each sampling point
```

```
}
```

```
rgn.lw.sum<-apply(rgn.lw, 2, mean)*area*0.1 #the 0.1 is just the 10 cm layer
```

```
rgn.lw.var<-apply(rgn.lw, 2, var)*(area*0.1)^2 #variance  $D(cX) = c^2 D(X)$ 
```

```
rgn.lw.se<-sqrt(rgn.lw.var/139) #standard error of the mean in kg
```

## # indicator\_variograms.r #

#indicator kriging in the lower layer

```
#set working directory, load packages and data
setwd("E:/cranfield/00_thesis/data/"); source("./rfunctions.r"); require(foreign); require(geoR)
d<-read.dbf("son.dbf"); d<-d[d$OUT!=1,]; d<-d[,which(names(d)!="OUT")]
```

#define functions that will facilitate the process

```
f_indicator_vg<-function(d, coords.col=1:2, data.col=3, tr, br=seq(0,8000,300), estimator="classical"){
  #returns indicator variogram using specified threshold 'tr'
  #d: data.frame or matrix containing coordinates and data columns, see ?variog for other details
  g<-as.geodata(d, coords.col=coords.col, data.col=data.col)
  g$data[g$data<tr]<-0; g$data[g$data>=tr]<-1
  return(variog(g, breaks=br, estimator.type=estimator))
}
```

```
plot_vgs<-function(vgs, maintext=NULL){
  #function for plotting the list of lists of variograms
  layout(matrix(1:(2*ceiling(length(names(vgs))/2)),ncol=2))
  for(i in names(vgs)){
    nw<-TRUE; pt<-1
    if(is.null(maintext)){mtx<-i}else{mtx<-""}
    for(j in names(vgs[[i]])){
      if(nw){
        limits<-c(0,0)
        for(m in names(vgs[[i]])){ limits[2]<-max(max(vgs[[i]][[m]]$v),limits[2]) } #search for ylimits
        par(mar=c(2,4,2,1))
        plot(vgs[[i]][[j]], pch=16, main=mtx, ylim=limits, xlab="", ylab="")
        nw<-FALSE
      }else{
        points(vgs[[i]][[j]]$u, vgs[[i]][[j]]$v, pch=pt)
        pt<-pt+1
      }
    }
    if(!is.null(maintext)){mtext(maintext[i][[1]], side=3, line=0.5, outer=F, cex=0.7)}
    mtext(expression(gamma), side=2, line=-1, outer=T, cex=0.9) #indicator variogram has no units
  }
}
```

```
plot_vgs_legend<-function(trs, newin=TRUE, maintext=NULL){
```

```

#function for plotting legend of the variograms based on thresholds in trs matrix
if(newwin){windows()}
par(mar=c(0,0,0,0))
plot(1:100,1:100, axes=FALSE, xlab="", ylab="", pch="")
legvec<-numeric(1+length(trs[,1]))
if(is.null(maintext)){ legvec[1]<-paste(dimnames(trs)[[2]], collapse="; ") } else { legvec[1]<- paste(as.character (mai..
..ntext[dimnames(trs)[[2]]]), collapse="; ")
}
for(i in 2:length(legvec)){legvec[i]<-paste(trs[i-1,], collapse="; ")}
legend("center",legend=legvec, pch=c(NA,16,1:(length(legvec)-1)), title="Thresholds for variables")
}

#end of function definition

vars<-c("PH_LW", "MOIST_LW", "DENS_LW", "ORGAN_LW", "TN_LW", "TC_LW", "TP_LW")
maintext<-c("(a) pH", "(b) MOIST", "(c) BD", "(d) OM", "(e) TP", "(f) TN", "(g) TC"); names(maintext)<-vars

#decide what thresholds to use
hist(d[vars])
trs<-matrix(NA, 4, length(vars), dimnames=list(NULL, vars))
trs[,"PH_LW"]<-c(6.25, 6.75, 7.25, 7.75); trs[,"MOIST_LW"]<-c(0.5, 0.6, 0.7, 0.8)
trs[,"DENS_LW"]<-c(0.15, 0.25, 0.4, 0.6); trs[,"ORGAN_LW"]<-c(0.2, 0.4, 0.6, 0.8)
trs[,"TP_LW"]<-c(500, 700, 900, 1100); trs[,"TN_LW"]<-c(5, 16, 15, 20); trs[,"TC_LW"]<-c(80, 160, 240, 320)

#construct variograms
vgs<-list()
for(i in vars){ for(j in trs[,i]){
  vgs[[i]][["tr"%p%j]]<-f_indicator_vg(d, 2:3, i, j, br=seq(0,4500,300))
}}

#plot the variograms and a legend
plot_vgs(vgs, maintext=maintext)
plot_vgs_legend(trs, newwin=FALSE, maintext=maintext)

#only ORGAN_LW for threshold 0.8 could be fitted
vg<-vgs[["ORGAN_LW"]][["tr0.8"]]
windows(); plot(vg)
md<-variofit(vg, ini.cov.pars=c(0.2,1000), cov.model="exponential", nugget=0.05, max.dist=3500, weights="npairs")
lines(md) #Exp(0.1295, 1381)+Nug(0.1244), minsQ=0.4091

```

## **Appendix H Maps**

Maps of the soil properties in 0–10 cm soil depth were produced in ArcMap (ESRI, 1999–2009) and are included after this page. Data and the maps can be also found on the enclosed CD.

# Davis Pond Freshwater Diversion, Louisiana, USA

Davis Pond ponding area has been receiving Mississippi River water since 2002.

Louisiana, USA



Data Source:  
Department of Oceanography & Coastal Sciences  
Louisiana State University  
Dr John White, jrwhite@lsu.edu  
ArcGIS Online maps - Imagery  
[www.openstreetmap.org](http://www.openstreetmap.org)  
[www.mapcruzin.com](http://www.mapcruzin.com)

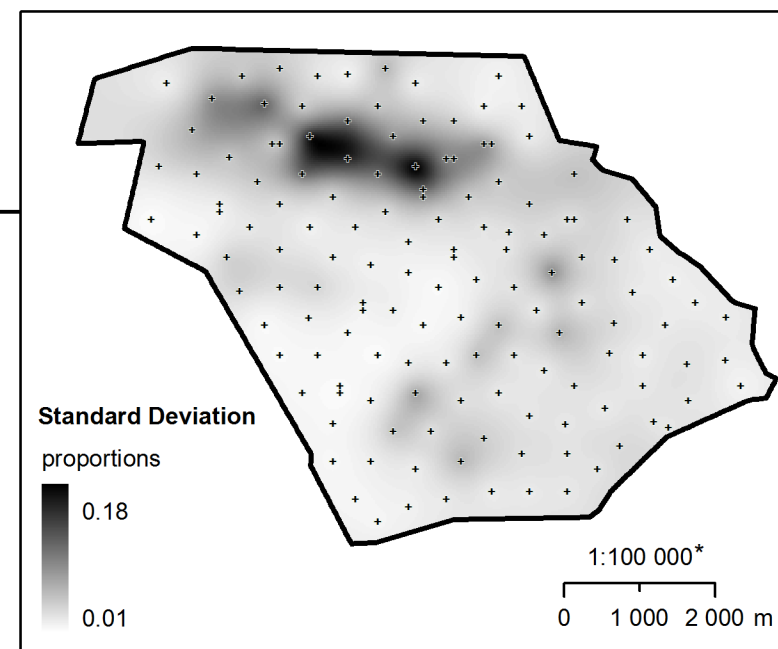
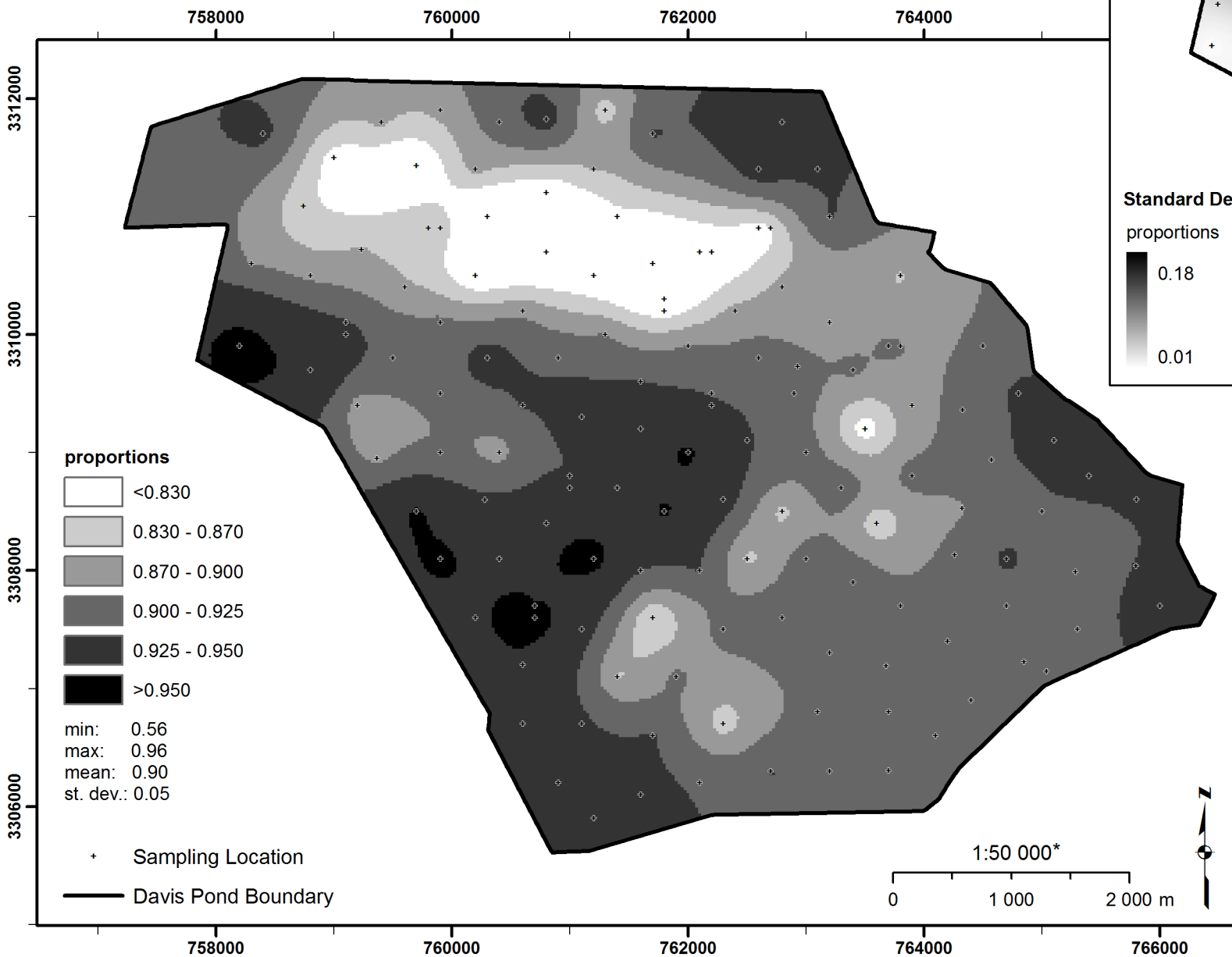
Further information:  
Kral, F. (2010) Mapping sediment properties  
in the Mississippi River Delta,  
MSc Thesis, Cranfield University.

Map ID: OVER  
Created: 2010-08-23  
Projection NAD\_1983\_UTM\_Zone\_15N  
EPSG: 26915

\*) when printed on A4 paper format

# Soil Moisture in Davis Pond

Moisture content (as proportions) in 0-10 cm soil depth.



Data Source:  
Department of Oceanography & Coastal Sciences  
Louisiana State University  
Dr John White, jrwhite@lsu.edu

Interpolation method:  
calculated as (0.9862 - 0.7772 density)

Further information:  
Kral, F. (2010) Mapping sediment properties  
in the Mississippi River Delta,  
MSc Thesis, Cranfield University.

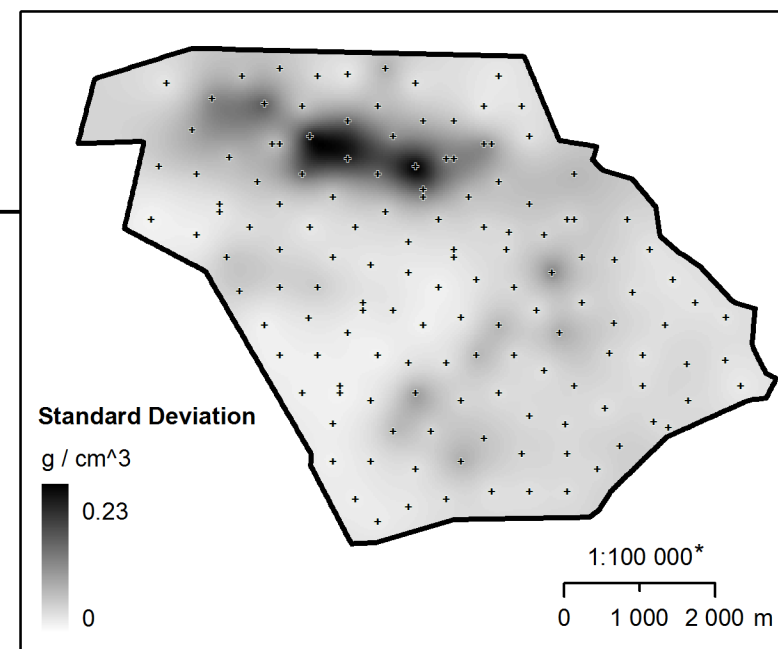
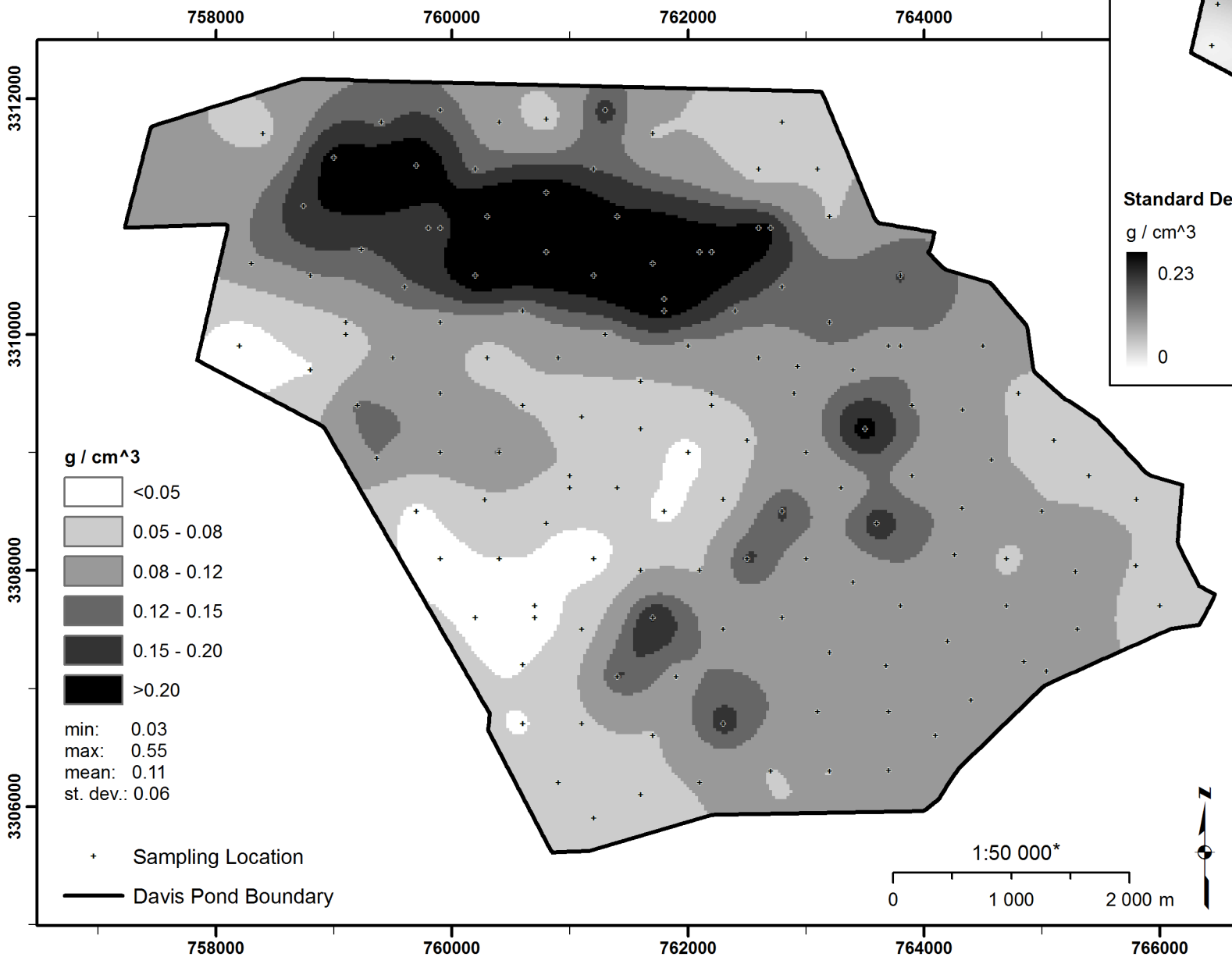
Map ID: MOIST\_UP\_ESTIM  
Created: 2010-08-23  
Projection NAD\_1983\_UTM\_Zone\_15N  
EPSG: 26915

\*) when printed on A4 paper format



# Soil Bulk Density in Davis Pond

Bulk density ( $\text{g cm}^{-3}$ ) in 0-10 cm soil depth.



Data Source:  
Department of Oceanography & Coastal Sciences  
Louisiana State University  
Dr John White, jrwhite@lsu.edu

Interpolation method:  
Box-Cox transformed with power -0.5  
ordinary kriging from sampling points  
model: exponential  
partial sill: 3.3056  
practical range: 2712 m  
nugget: 0.9694

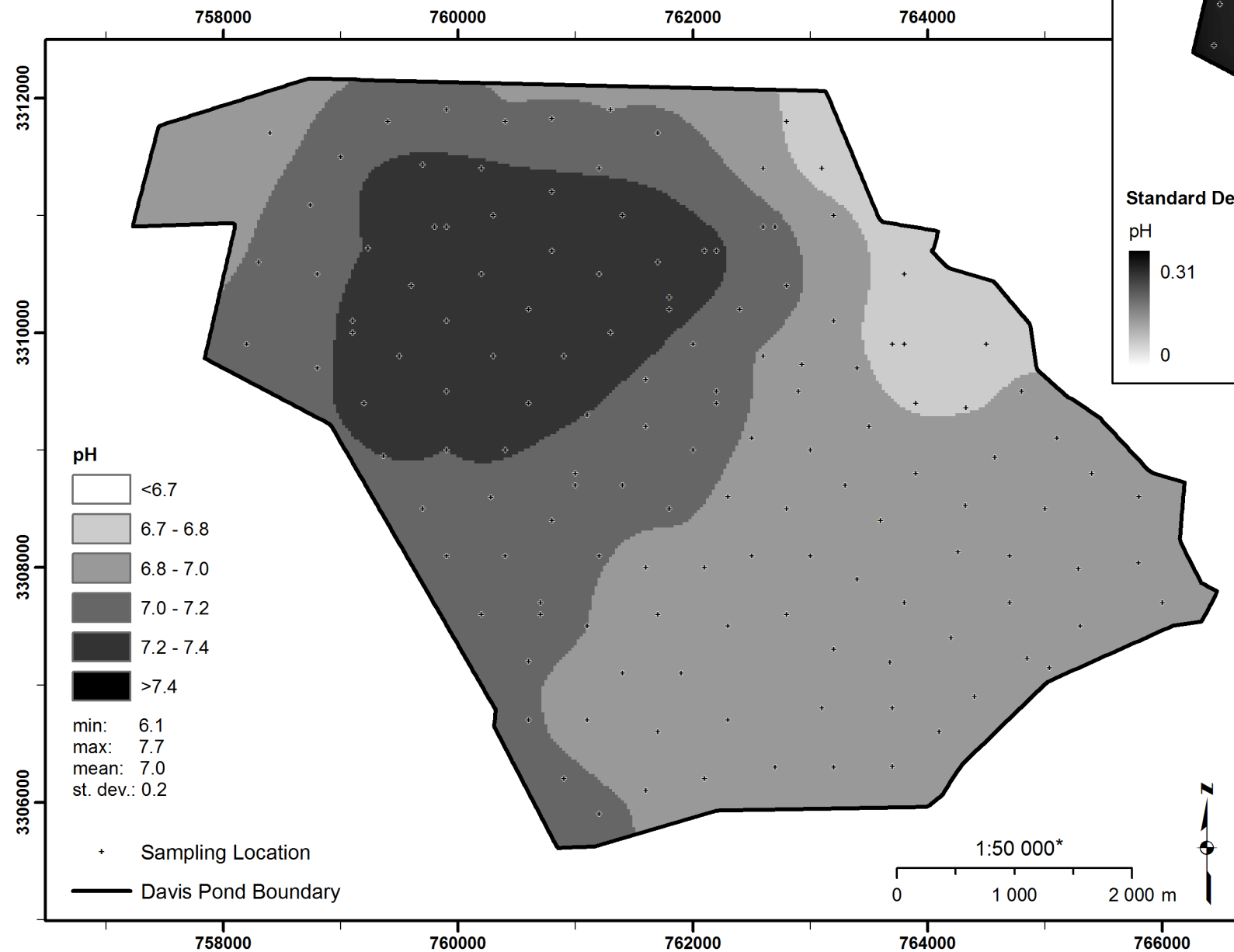
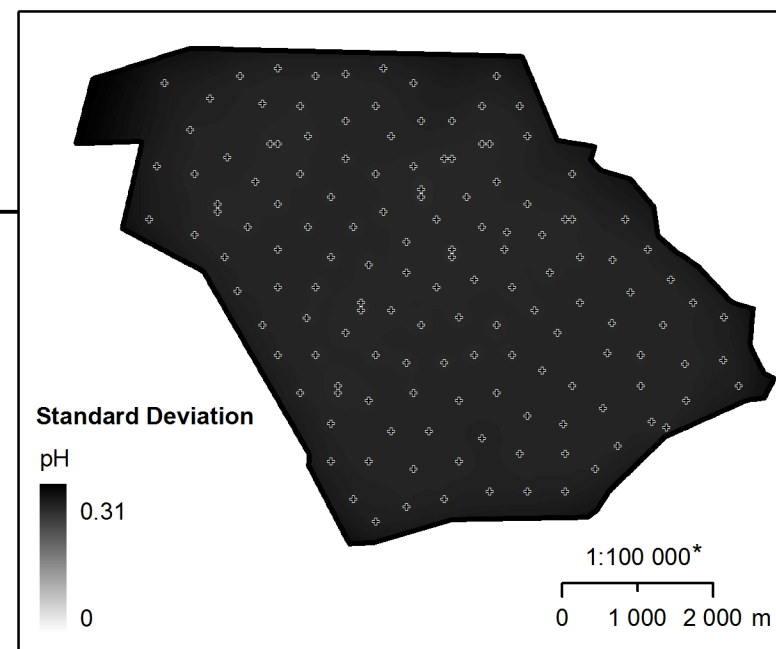
Further information:  
Kral, F. (2010) Mapping sediment properties  
in the Mississippi River Delta,  
MSc Thesis, Cranfield University.

Map ID: DENS\_UP\_ESTIM  
Created: 2010-08-23  
Projection NAD\_1983\_UTM\_Zone\_15N  
EPSG: 26915

\*) when printed on A4 paper format

# Soil pH in Davis Pond

Value of pH in 0-10 cm soil depth.



Data Source:  
Department of Oceanography & Coastal Sciences  
Louisiana State University  
Dr John White, jrwhite@lsu.edu

Interpolation method:  
ordinary kriging from sampling points  
model: spherical  
partial sill: 0.0544  
practical range: 4694 m  
nugget: 0.0573

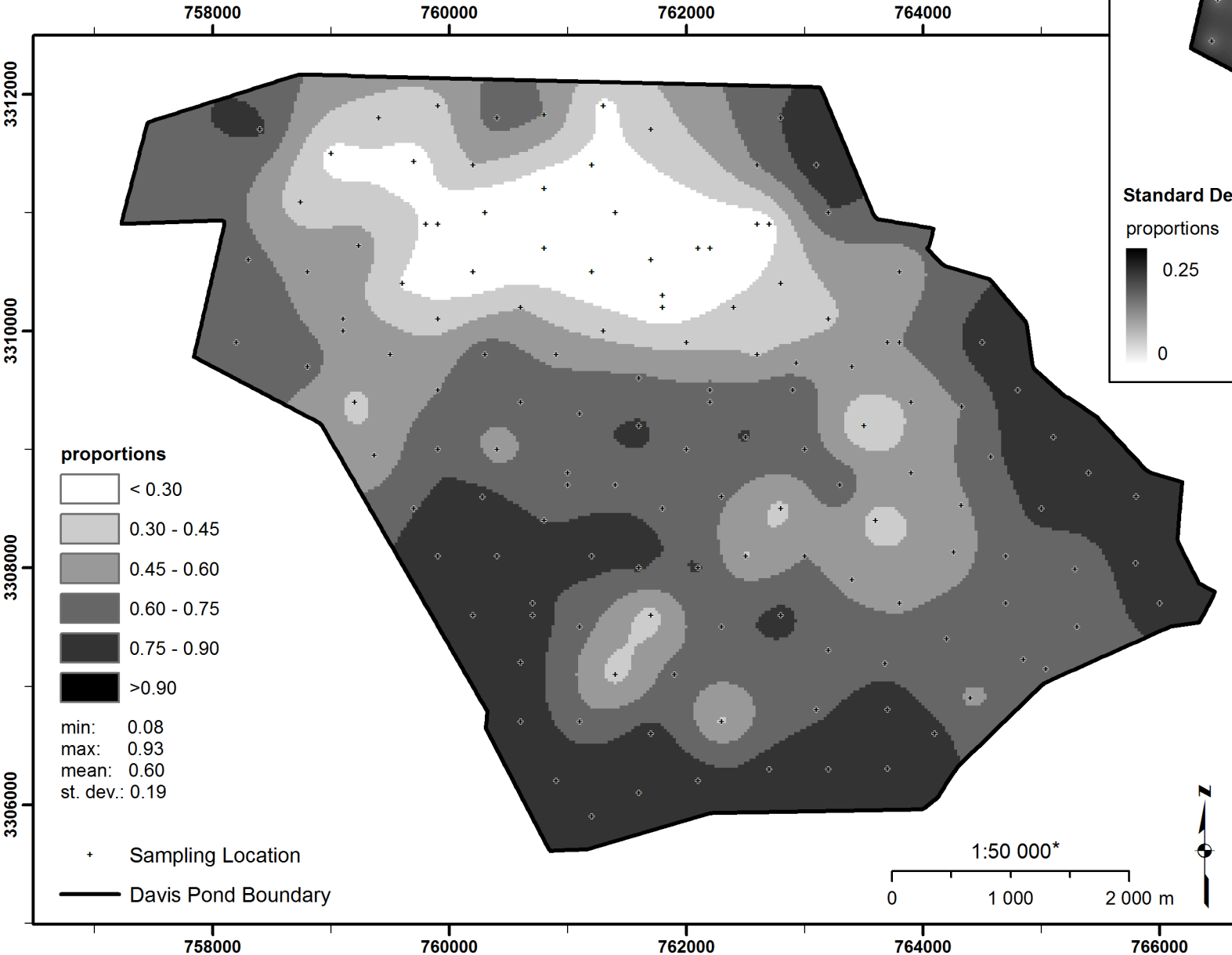
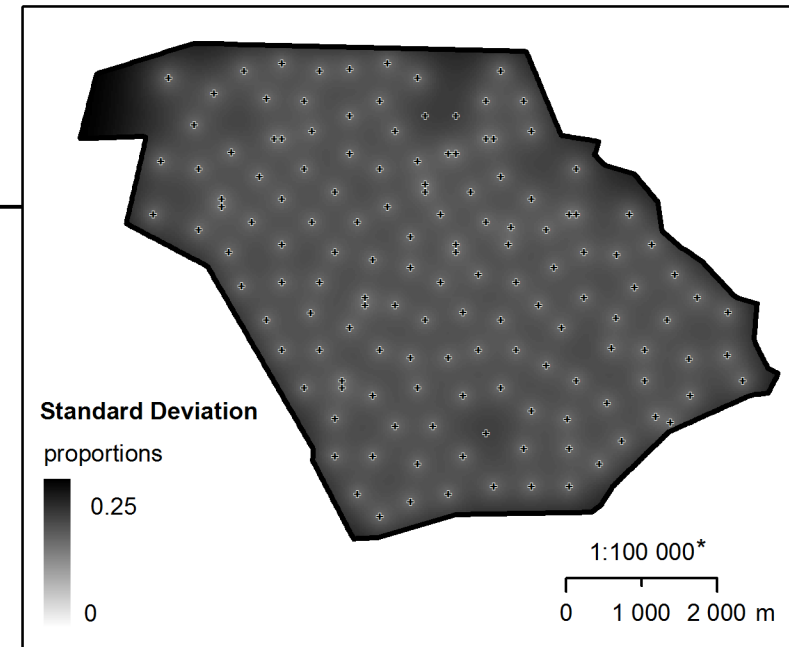
Further information:  
Kral, F. (2010) Mapping sediment properties  
in the Mississippi River Delta,  
MSc Thesis, Cranfield University.

Map ID: PH\_UP\_ESTIM  
Created: 2010-08-23  
Projection NAD\_1983\_UTM\_Zone\_15N  
EPSG: 26915

\*) when printed on A4 paper format

# Organic Matter in Davis Pond

Content of organic matter (as proportions) in 0-10 cm soil depth.



Data Source:  
Department of Oceanography & Coastal Sciences  
Louisiana State University  
Dr John White, jrwhite@lsu.edu

Interpolation method:  
ordinary kriging from sampling points  
model: exponential  
partial sill: 0.0563  
practical range: 3235 m  
nugget: 0.0113

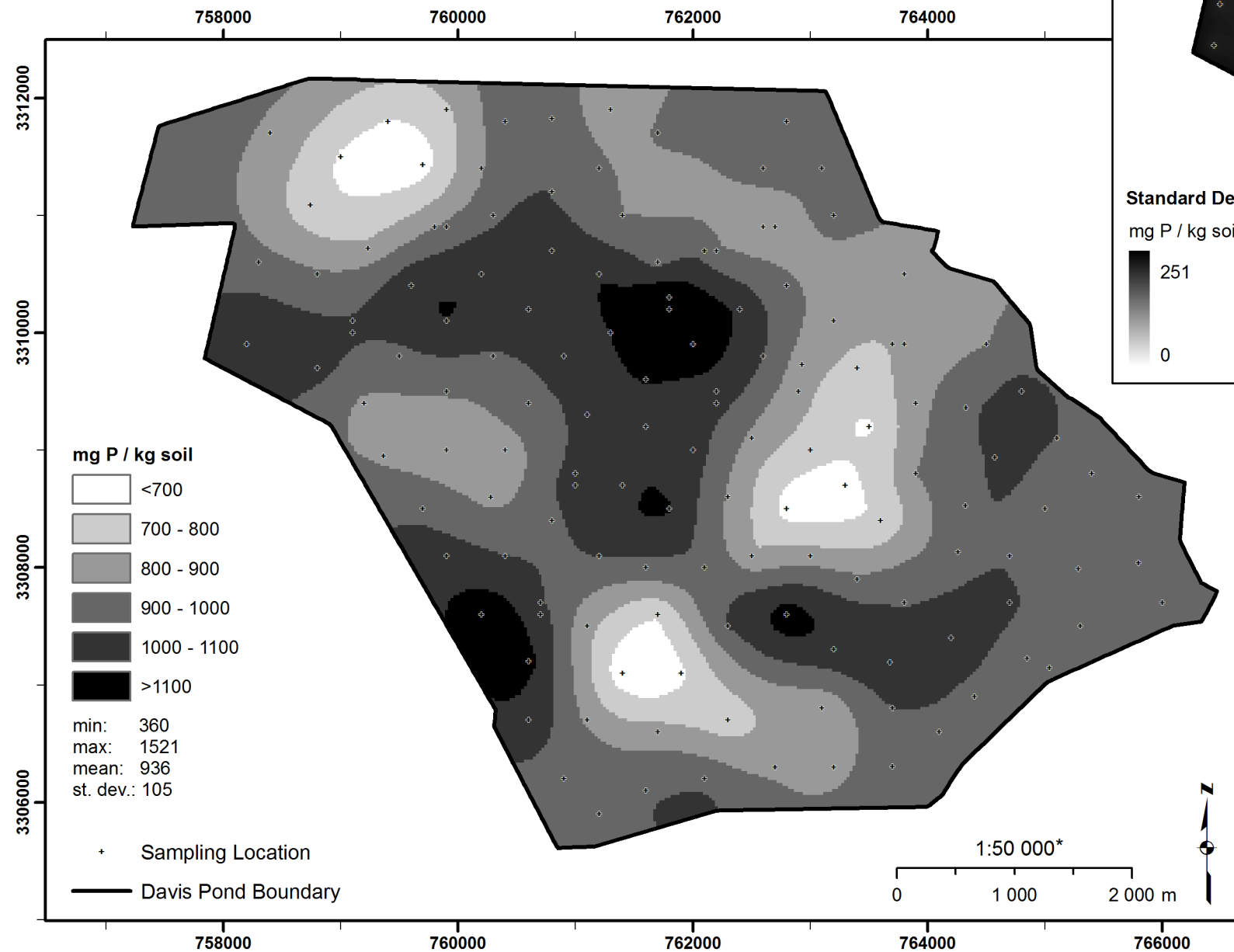
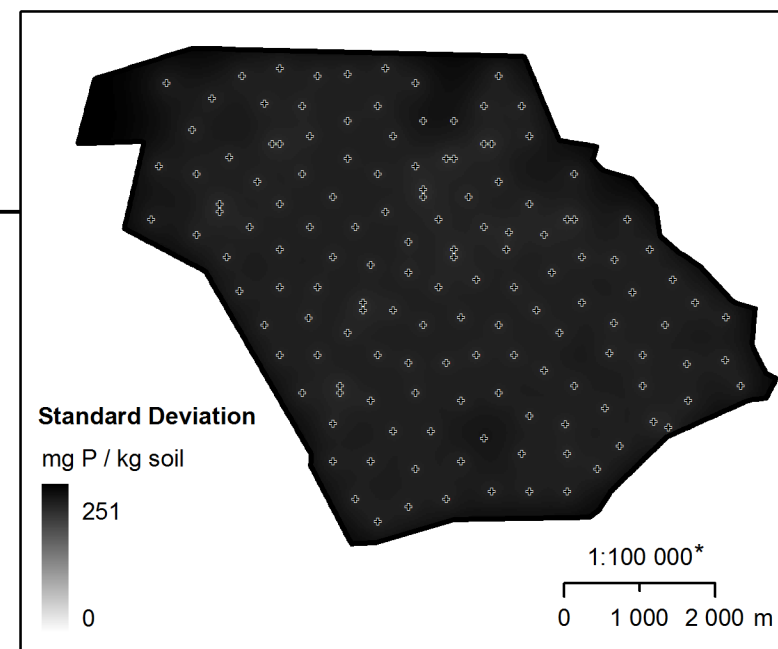
Further information:  
Kral, F. (2010) Mapping sediment properties  
in the Mississippi River Delta,  
MSc Thesis, Cranfield University.

Map ID: ORGAN\_UP\_ESTIM  
Created: 2010-08-23  
Projection NAD\_1983\_UTM\_Zone\_15N  
EPSG: 26915

\*) when printed on A4 paper format

# Total Phosphorus in Davis Pond

Content of total phosphorus (mg P kg<sup>-1</sup> soil) in 0-10 cm soil depth.



Data Source:  
Department of Oceanography & Coastal Sciences  
Louisiana State University  
Dr John White, jrwhite@lsu.edu

Interpolation method:  
ordinary kriging from sampling points  
model: spherical  
partial sill: 28839  
practical range: 1393 m  
nugget: 33037

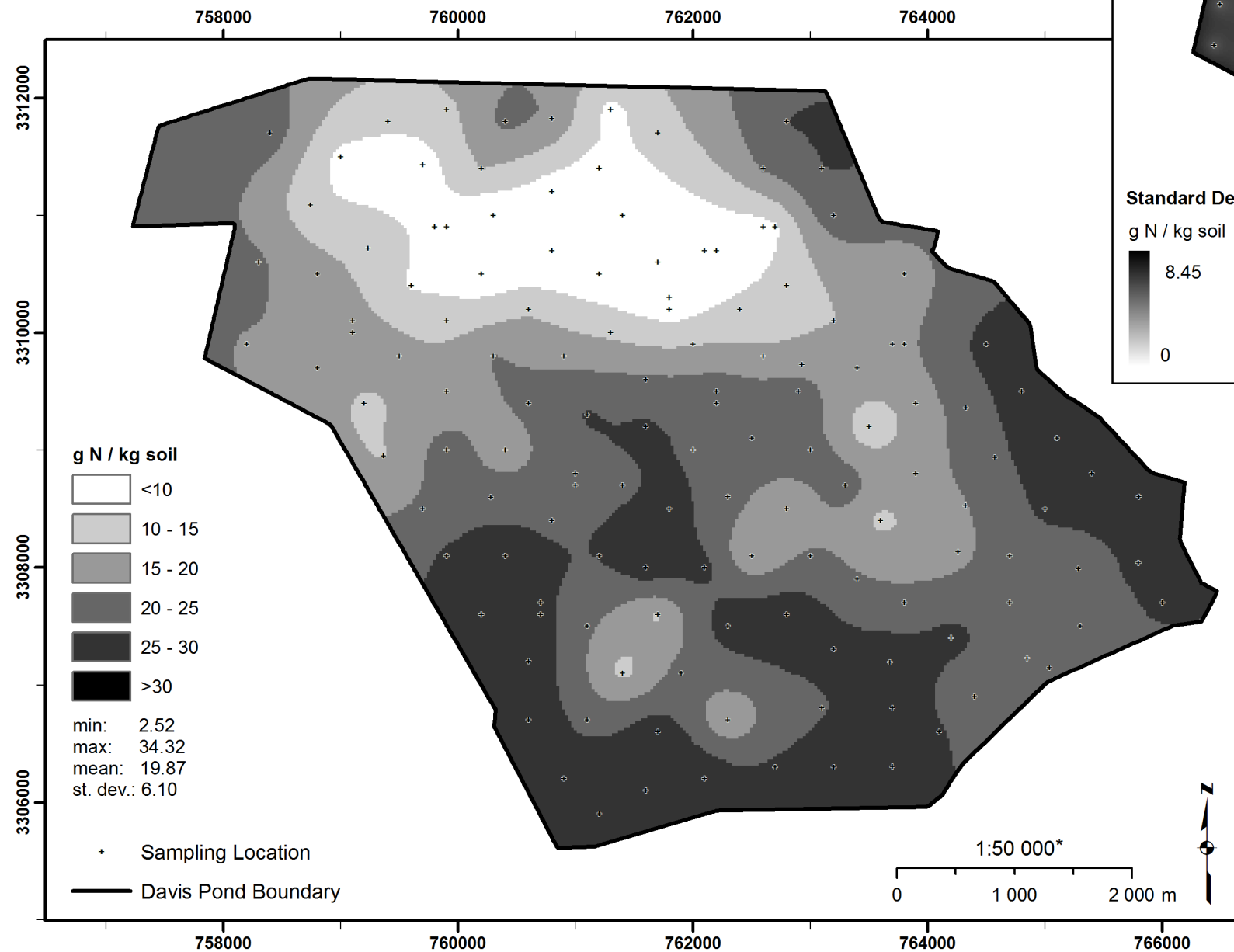
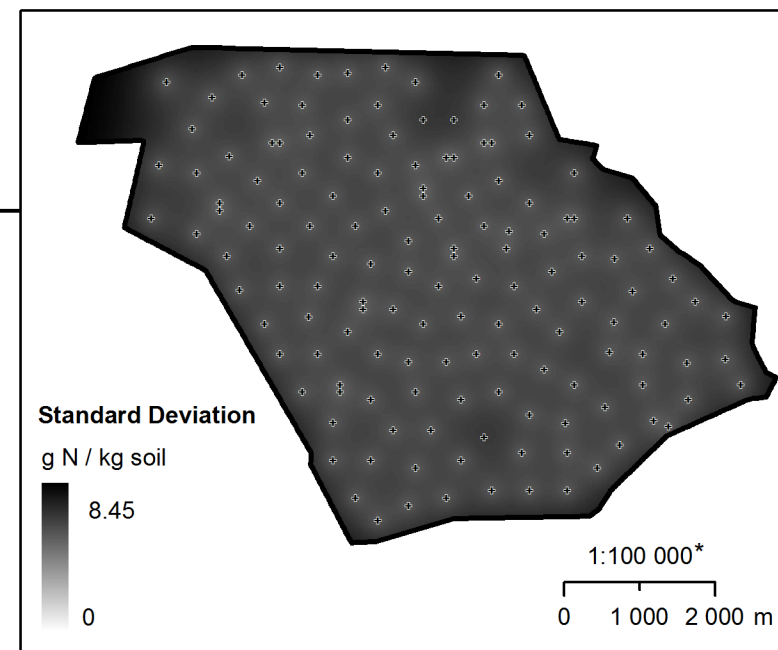
Further information:  
Kral, F. (2010) Mapping sediment properties  
in the Mississippi River Delta,  
MSc Thesis, Cranfield University.

Map ID: TP\_UP\_ESTIM  
Created: 2010-08-23  
Projection NAD\_1983\_UTM\_Zone\_15N  
EPSG: 26915

\*) when printed on A4 paper format

# Total Nitrogen in Davis Pond

Content of total nitrogen ( $\text{g N kg}^{-1}$  soil) in 0-10 cm soil depth.



Data Source:  
Department of Oceanography & Coastal Sciences  
Louisiana State University  
Dr John White, jrwhite@lsu.edu

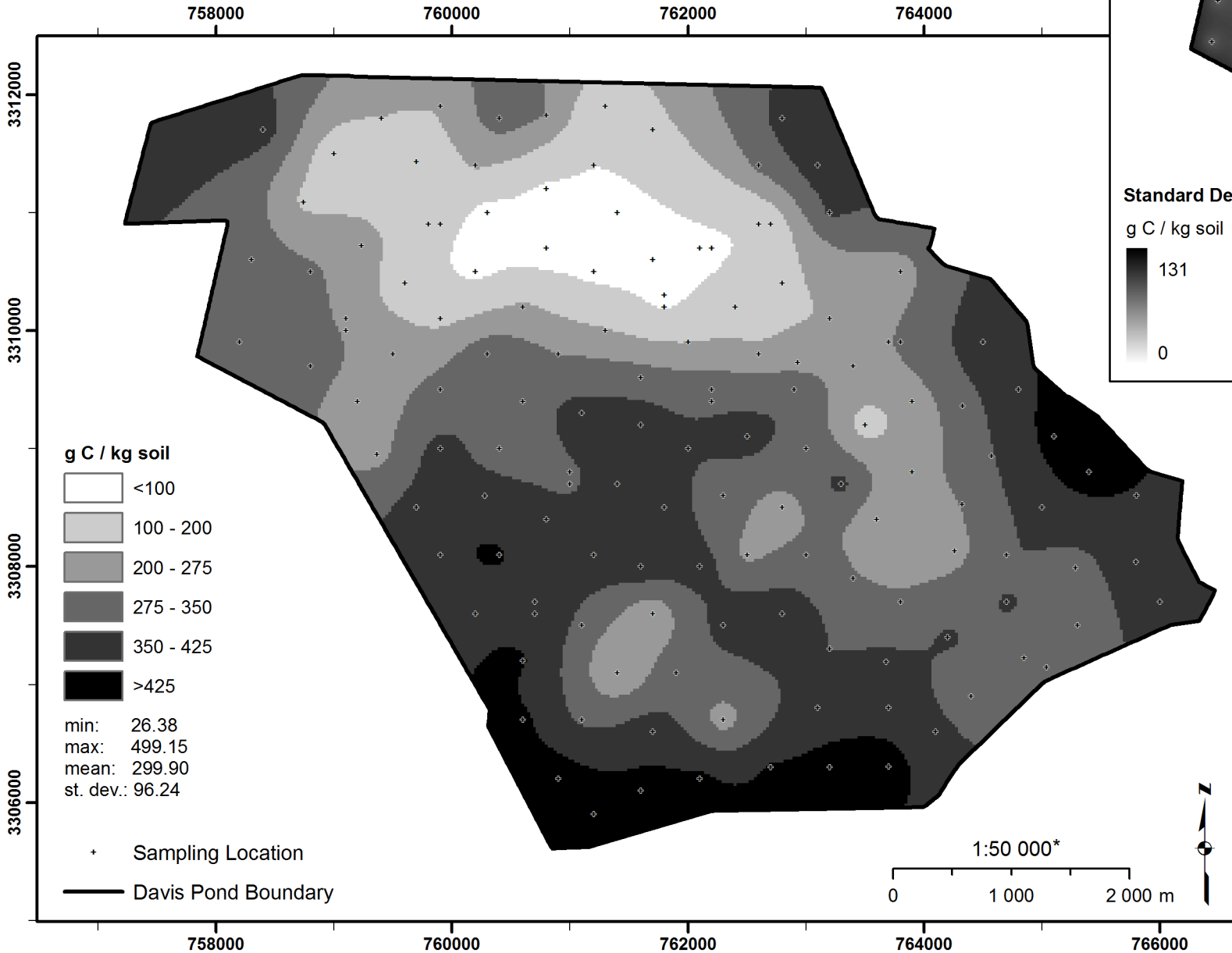
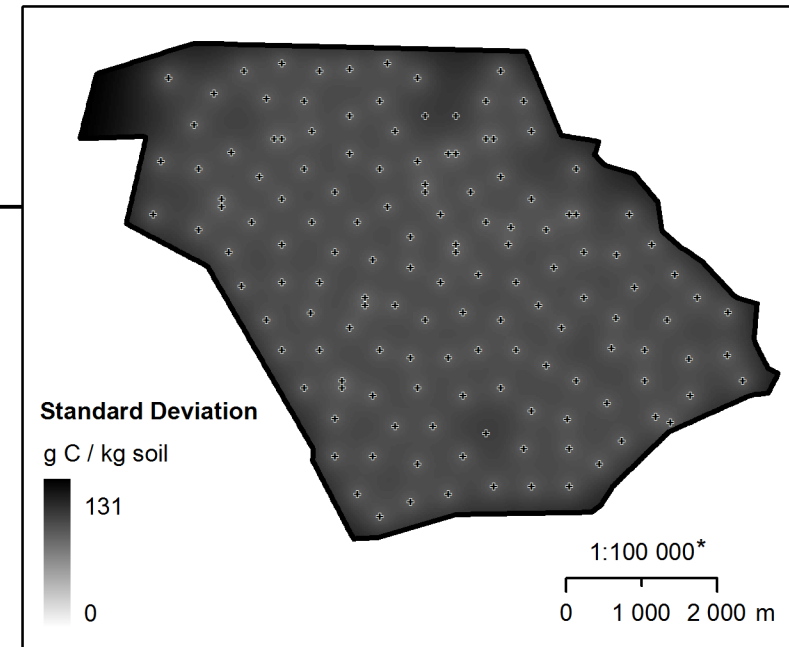
Interpolation method:  
ordinary kriging from sampling points  
model: exponential  
partial sill: 59.79  
practical range: 3280 m  
nugget: 18.07

Further information:  
Kral, F. (2010) Mapping sediment properties  
in the Mississippi River Delta,  
MSc Thesis, Cranfield University.

Map ID: TN\_UP\_ESTIM  
Created: 2010-08-23  
Projection NAD\_1983\_UTM\_Zone\_15N  
EPSG: 26915

# Total Carbon in Davis Pond

Content of total carbon (g C kg<sup>-1</sup> soil) in 0-10 cm soil depth.



Data Source:  
Department of Oceanography & Coastal Sciences  
Louisiana State University  
Dr John White, jrwhite@lsu.edu

Interpolation method:  
ordinary kriging from sampling points  
model: exponential  
partial sill: 15394  
practical range: 3707 m  
nugget: 4150

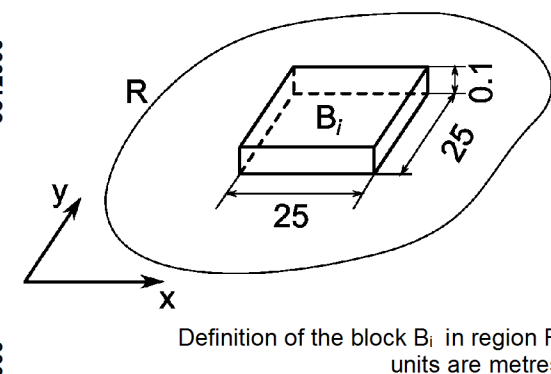
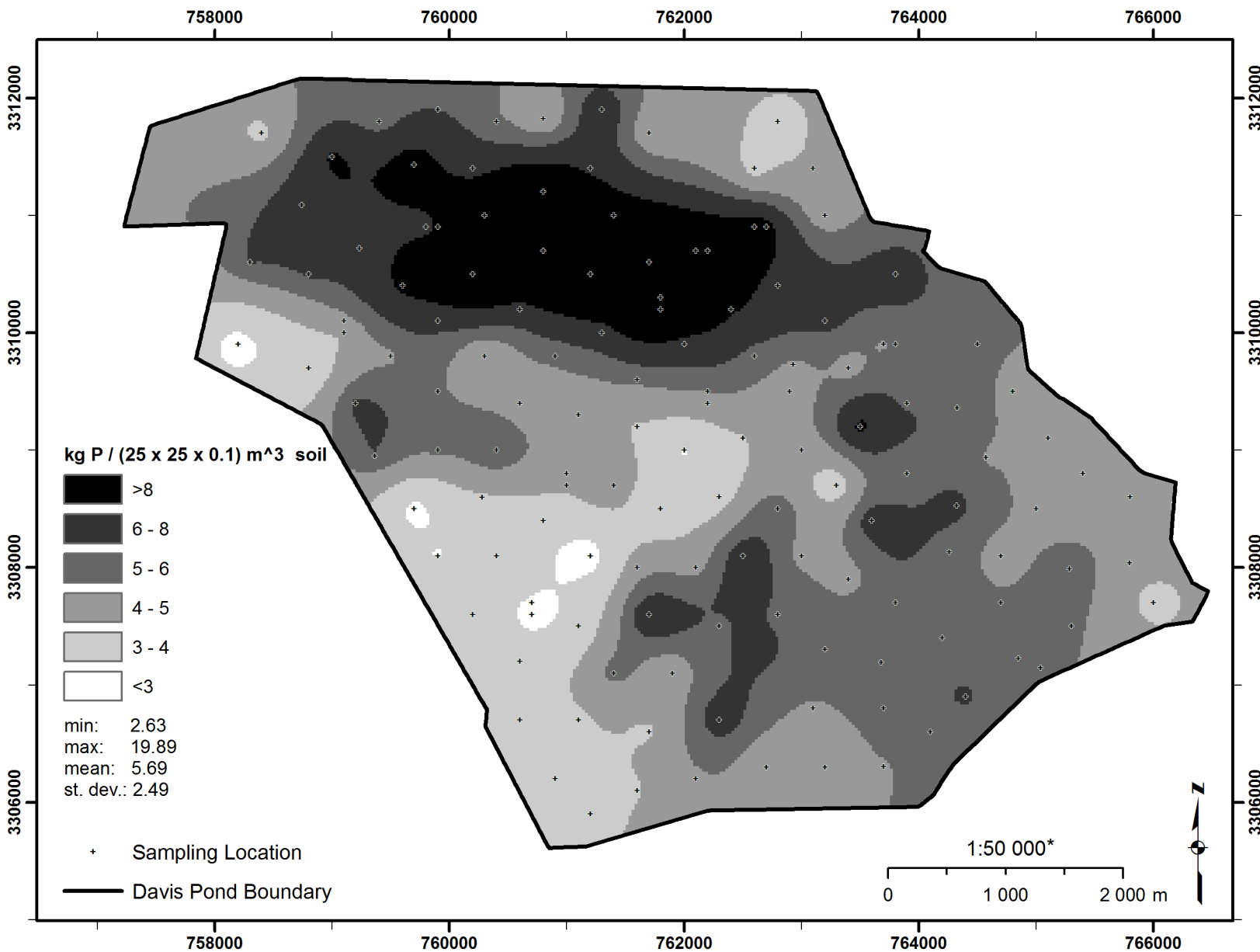
Further information:  
Kral, F. (2010) Mapping sediment properties  
in the Mississippi River Delta,  
MSc Thesis, Cranfield University.

Map ID: TC\_UP\_ESTIM  
Created: 2010-08-23  
Projection NAD\_1983\_UTM\_Zone\_15N  
EPSG: 26915

\*) when printed on A4 paper format

# Total Phosphorus per Volume in Topsoil in Davis Pond

Content of total phosphorus (kg) in 25 m x 25 m block in 0-10 cm soil depth.



Data Source:  
Department of Oceanography & Coastal Sciences  
Louisiana State University  
Dr John White, jrwhite@lsu.edu

One block (25 m x 25 m x 0.1 m)  
is 62.5 m<sup>3</sup> of soil.

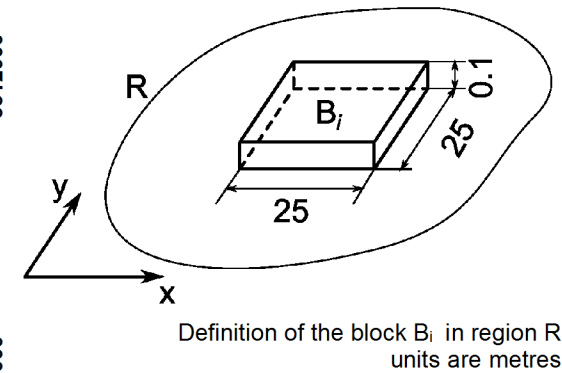
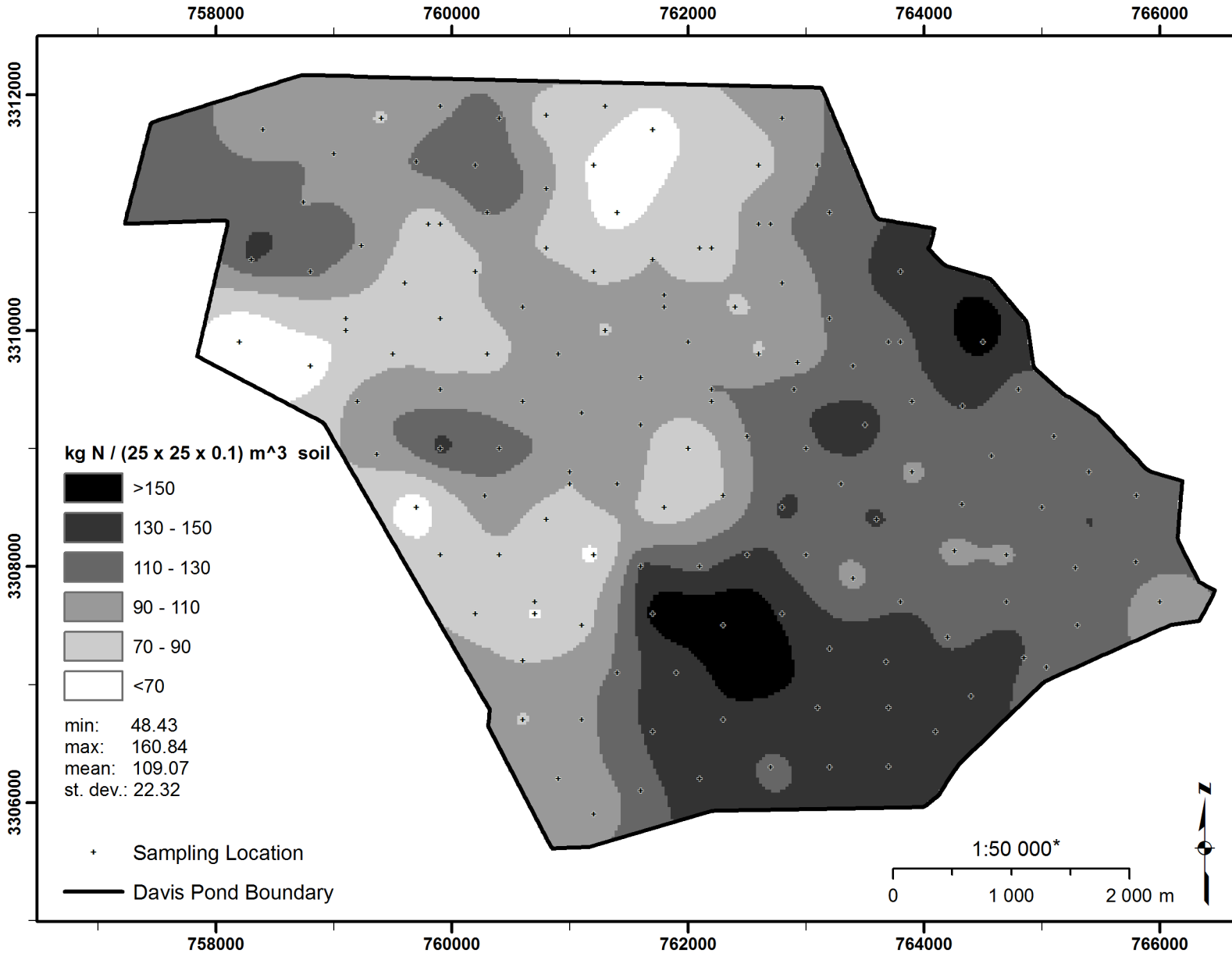
See appendix D,  
Derivation of Regional Stocks  
in Kral, F. (2010) Mapping sediment properties  
in the Mississippi River Delta,  
MSc Thesis, Cranfield University.

Map ID: TP\_UP\_BLOCK  
Created: 2010-08-23  
Projection NAD\_1983\_UTM\_Zone\_15N  
EPSG: 26915

\*) when printed on A4 paper format

# Total Nitrogen per Volume in Topsoil in Davis Pond

Content of total nitrogen (kg) in 25 m x 25 m block in 0-10 cm soil depth.



Data Source:  
Department of Oceanography & Coastal Sciences  
Louisiana State University  
Dr John White, jrwhite@lsu.edu

One block (25 m x 25 m x 0.1 m)  
is 62.5 m<sup>3</sup> of soil.

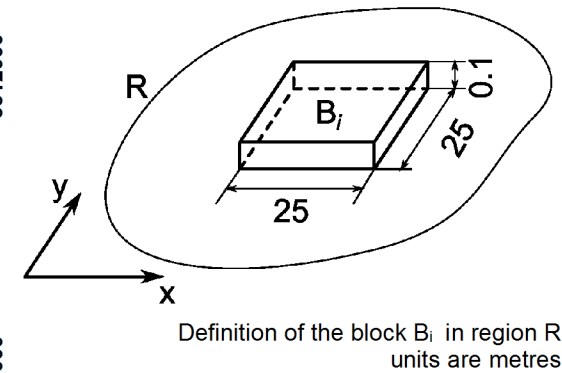
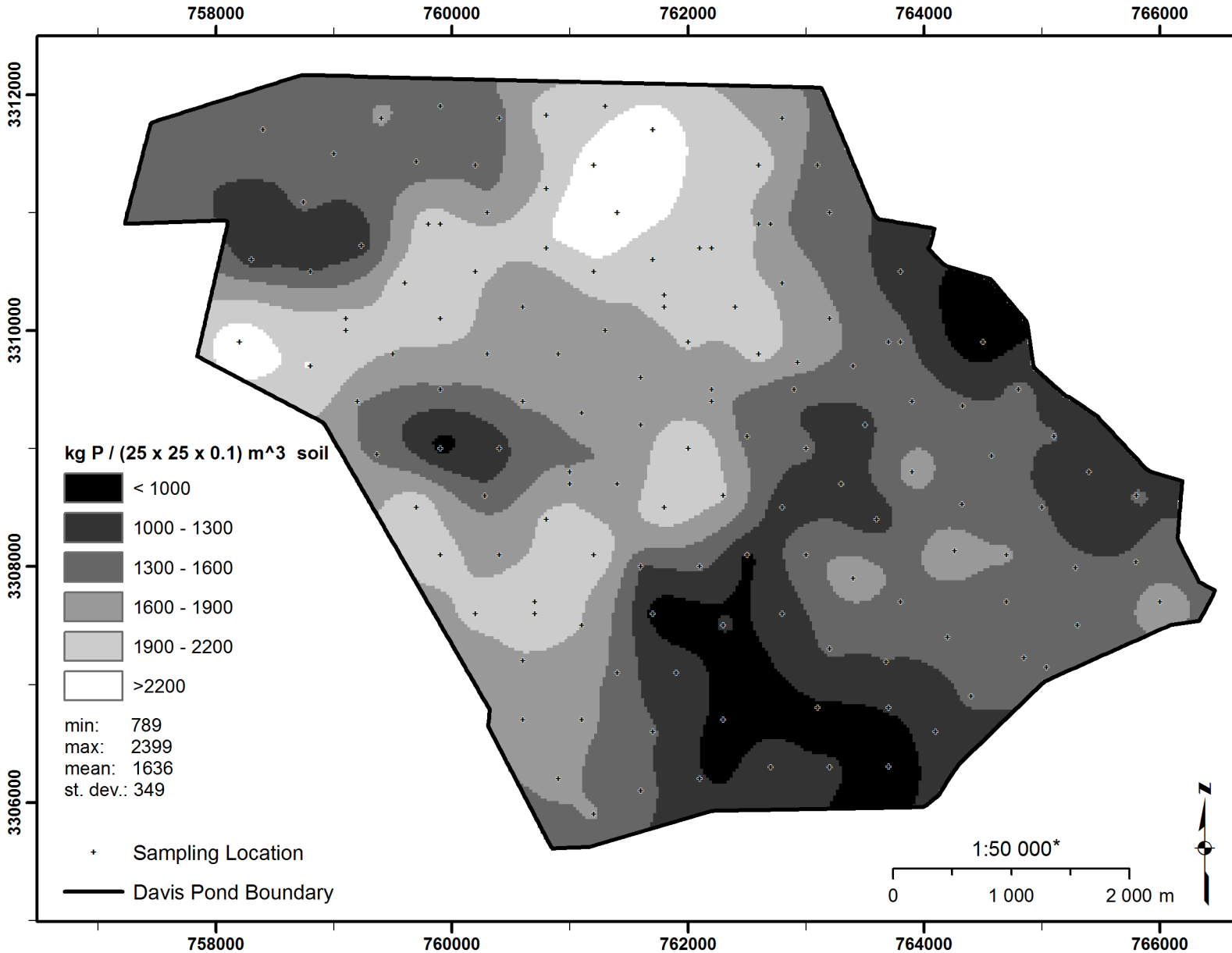
See appendix D,  
Derivation of Regional Stocks  
in Kral, F. (2010) Mapping sediment properties  
in the Mississippi River Delta,  
MSc Thesis, Cranfield University.

Map ID: TN\_UP\_BLOCK  
Created: 2010-08-23  
Projection NAD\_1983\_UTM\_Zone\_15N  
EPSG: 26915



# Total Carbon per Volume in Topsoil in Davis Pond

Content of total carbon (kg) in 25 m x 25 m block in 0-10 cm soil depth.



Data Source:  
Department of Oceanography & Coastal Sciences  
Louisiana State University  
Dr John White, jrwhite@lsu.edu

One block (25 m x 25 m x 0.1 m)  
is 62.5 m<sup>3</sup> of soil.

See appendix D,  
Derivation of Regional Stocks  
in Kral, F. (2010) Mapping sediment properties  
in the Mississippi River Delta,  
MSc Thesis, Cranfield University.

Map ID: TC\_UP\_BLOCK  
Created: 2010-08-23  
Projection NAD\_1983\_UTM\_Zone\_15N  
EPSG: 26915

\*) when printed on A4 paper format